To

The Editor

Earth Surface Dynamics

Date – 14.09.2020

[Sub: submission of revised manuscript #esurf-2020-37 and detailed comments on reviews]

Respected Prof. Glouagen,

First of all, I would like to convey our heart-felt thanks to you and the two reviewers Prof. S. Hergarten and Prof. A. Forte for their insightful reviews. The reviews have immensely helped us to improve the scientific quality and presentation of the manuscript. I further thank you for allowing additional time for submission of the revised manuscript considering my physical condition.

The revised manuscript has undergone major changes based on the suggestions of the reviewers. We have re-analyzed a significant part of the terrain morphometry and shifted a handful of field data/photographs to the main manuscript from the supplement. But the most important change in the revised manuscript is the incorporation of sediment chronology. Since the first submission, we obtained a handful of depositional ages of sediments from the Kishtwar valley using luminescence dating method. Luminescence dating, with its uncertainties and limitations, has long been used to determine sediment burial ages. We used OSL dating of quartz and IRSL dating of K-feldspars to obtain the chronology of sediment aggradation in the Kishtwar region. The ongoing fluvial incision post-dates the largest valley aggradation recorded in this region, therefore, we are able to constrain the upper age limit of fluvial bedrock incision. Bedrock incision rates since late Pleistocene are in agreement with long-term exhumation rates from the study area confirming protracted growth of the Himalayan interiors from million-year to millennial timescales. We affirm that the incorporation of bedrock incision rates do not alter our initial research finding, but strengthen our study with evidence of orogenic growth over geomorphic/millennial timescale.

Addition of field photographs on structural styles, geomorphic features and sediment archives, as well as incorporation of sediment chronology and incision rate estimates have resulted in an increase in no. of figures from 4 in the initial manuscript to 10 in the revised version. One table containing the details of luminescence dating samples is also added in the revised manuscript.

We revised the manuscript title to ‘Growth of the Lesser Himalayan Duplex and rapid fluvial incision modulate landscape morphology in tectonically-active Kishtwar Window in NW Himalayan interiors’.

With the addition of luminescence chronology in this manuscript, I would like to add Dr. Naveen Chauhan from PRL Ahmedabad as a co-author. He has been involved in luminescence dating along with me. The detailed list of changes and answers to the review comments are attached herewith.

Thanks again for considering our manuscript.

On behalf of the authors,

Saptarshi Dey

Answers to the review comments:

Reviewer 1 (Stefan Hergarten):

(Answers in blue font)

The problems concerning the quality of the manuscript occur at all levels. The structure is not really good at some points, e.g., parts of the discussion section read more like parts of an introduction, but the introductory part is already quite long. In general, too much of the reasoning relies on supplementary figures.

Thanks for your comments on the organization and arrangement of the manuscript. We also felt the same that parts of the manuscript is indeed a 'long read'. We revised and rechecked the possibilities of rearranging the text in introduction and discussion section. We reduced the redundant texts across these two sections and shortened the introduction. We are able to reduce some of the discussion part, which we believe we touched upon in the introduction. The supplementary figures are now incorporated in the main manuscript. They are largely clustered into 3 figures: - Figure 2 (structural styles and lithology), Figure 3 (Geomorphic features) and Figure 4 (Sediment archive stored along Chenab River).

The applied morphometric methods appear to be appropriate in total, but the description does not allow for a serious assessment whether the choice of the parameters is good or not. Bumps in the order of magnitude of 100 m in the river profile shown in Fig. 2 do not increase my trust in the analysis. Some information is missing, e.g., the width of the swaths. Beyond this, the different metrics (channel steepness, specific stream power, channel width) are a bit isolated, and following the reasoning how they are combined to the whole picture is not easy.

The morphometric analysis has been redone. The bumps in the river profile have been reduced and mostly removed by using smoothing with 20-pixel smoothing window (mentioned in the text). The swath widths are mentioned (3 km for stretch 1 and 2). All the morphometric analyses are now drafted in a single frame having same x-axis showing along-river distance (Fig.7). We hope that this revision will help us to visualize the variations in morphometric parameters and their significance in a much better way.

Beyond these aspects, there are also technical issues that should have been detected by the coauthors. There are several errors in the text (not only typos).

We rechecked the manuscript for typos and language/logical errors. We revised the entire text. The revised manuscript has been checked by a couple of skilled persons having higher proficiency in English language. We also had a thorough check with 'Grammarly'.

not all curves shown in Fig. 3 are explained.

The unexplained curves shown in figure 3 of the initial submission are now removed from the manuscript. In lieu of that, we provided field photos as a reference of changing valley morphology (Fig.3).

the two stretches shown in Fig. 2 b and c are not consistent with the marked regions in Fig. 2 a.

The two stretches are now marked in Fig.8a and the long-profiles are listed in Fig.8c and 8d. We guess the confusion is regarding the length and width of the stretch 2. All of us have to recognize that the stretch 2 (N-S traverse of the River) is basically parallel to the orogen or the proposed ramp structure. That is not the case with stretch 1. Stretch 1 is nearly perpendicular to the proposed ramp on which the duplex is growing. To estimate the orogen-perpendicular offset across the ramp, we used 'orthogonal projection of the orogen-perpendicular traverses of the River that can be seen on either side of the N-S traverse. That reasoning is now mentioned in the text in greater detail. For getting an idea of orogen-perpendicular width of the ramp (the steep segment), please refer to Fig.8a.

Even the first reference I checked randomly (Hack 1973) does not occur in the reference list.

We are sorry for the mistake. The reference list is now updated and thoroughly checked multiple times. In revision, a significant amount of vital references are added and some are removed.

From my point of view, a thorough rewriting is necessary.

We agree to your kind review comments and revised the whole text and the figures. In addition to the previously-shown morphometric analysis, in this revised version we have supplied a thorough understanding of the sediment aggradation in the valley and quantified bedrock incision rates using the sediment chronology based on luminescence dating method. This is the first attempt for assessment of late Pleistocene sediment deposition history in the entire middle Chenab valley. This addition helps us to compare long-term exhumation rates with millennial-scale fluvial incision rates and acts as a stand-alone metric for assessing the growth of the orogen-interior.

We would also like to refer you to go through some of the review comment answers for the second reviewer Prof. A. Forte. There are some more clarifications on the pertinent issues raised during review process.

Reviewer 2 (Adam Forte):

Line-by-line comments:

(Answers in blue font)

L35-47 – Without some sort of figure, this opening assumes a fair bit of knowledge on the part of the reader on the location and geometry of the major Himalayan structures. While many are passingly familiar with these, it might be advisable to include a simple cartoon illustrating these structures and there general location with respect to topography. Maybe add a panel to figure 1 that accomplishes this? At least referencing figure1 as is here could help, but not all of these structures are on here (MFT or STDS) and there are additional structures on Figure 1. Since much of the rest of paper hinges on which structures are active or not, not knowing where they are is kind of a detriment. Especially putting the LHD into structural context with these other structures seems crucial (and again, this can all be in a cartoon, not asking for a balanced cross section or anything). Other worthwhile question to consider which perhaps can put this issue in context, if this was any almost any other mountain range, would it be reasonable to expect a reader to know the relationships between the major local faults in an article published in a widely read, general geology journal like ESurf? You could cite fig S1 / S2 here, but I would argue that the knowledge of this information is sufficiently important to the main point of the paper that such a figure should be in the main text.

Thank you for pointing this out. At the first go, we were hesitant to put a conceptual sketch as Fig.1b. Now, with your comment, we added a general sketch of cross-section of NW Himalaya as Fig.1b. A detailed balanced cross-section is also there in the supplement S2. The overview of Himalayan orogen is drafted in supplement Fig.S1.

L216-217 – You need to explain a little bit more about how you're doing your basin wide statistics. It's not clear from this description, and the representation of it in Figure 3 is confusing (i.e. where are the basin boundaries, etc?).

More details of basinwide calculations are now added in line # 274-279. The whole analysis has been redone. We preferred to show the variation in elevation, topographic relief, annual rainfall data and basin wide mean ksn for the entire Chenab drainage (area shown in Fig.1a). That is drafted in Fig.5. The basin boundaries are also plotted. We hope that the figure is clear enough to distinguish the variations in regional scale as well as in smaller segments such as the KW.

L246-248 – RE the specific stream power calculation (1) you should state here in your methods that you assume constant discharge (not relegate it to the caption of Table 1) and perhaps more importantly (2) you need to justify that a constant discharge is applicable here. On figure 3, this is traversing >160 km of river distance and potentially traversing some large gradients in precipitation. As a worst case, you should be able to use the available TRMM data for the region to estimate discharge (this is simple with TopoToolbox that you are already using as you can calculate flow accumulation with a precipitation raster is an optional input). Is there any discharge data in the region

to compare this to? Perhaps you have good reason to assume constant discharge, but until that is shown in the paper, it's hard to know how to interpret the SSP data (or whether it should be believed at all).

We agree to your concern and now added the statement that we used uniform discharge for SSP calculation in the main text (line #370-373). The reasoning behind assuming a constant discharge has been derived by looking at the TRMM data (as suggested by you). Please refer to Fig.5c and 5e. The interior of the Jammu-Kashmir Himalaya has no orographic barrier and receives more-or-less uniform rainfall <1.5 m/y. That is why we had put the term 'discharge-normalized' in the first place.

L256-265 – Part 1 : Your measurements are your measurements, so you'll need to make do with what you've got, but it is worth discussing/addressing why you only collected 8-10 per location as this is ~1/2 to 1/3 of the number of measurements thought to be needed to be robust (e.g. Niedzielski, T., Migon, P., Placek, A., 2009. A minimum sample size required from Schmidt hammer measurements. Earth Surface Processes and Landforms 34, 1713–1725. https://doi.org/10.1002/esp.1851). Perhaps it would be worthwhile considering pooling results from units/lithologies you consider to be similar and to get a larger N and seeing how those compare to the small N individual sites (i.e. if you have 5 sites all in the same unit with 10 measurements each, look at the statistics of the aggregate population of 50 values and see how those compare to the statistics of each of the 5 measurement sites). Such an analysis might help to alleviate some concerns, but there will remain lingering issues with a small N for each site. Similarly reporting of the raw values in a supplemental table and considering the standard deviation on the means when you're using them would be warranted (i.e. are the apparent differences in mean rebound values in Figure 3 'real'? how much of those differences would disappear or be less extreme if you considered the uncertainty?). Whether you follow my specific recommendations here or not, there needs to be more transparency with regards to these values and how reliable they may (or may not) be.

Thanks for recommending the nice article on Schmidt hammer experiment. We agree to the fact that our measurement-per site is lower than what would be statistically-meaningful. That is partly due to the awful fact that I have not been allowed by the army to have a pit-stop for more than 10-15 minutes at a single site. Neither was I allowed to roam off-road. In that stipulated time, I had to do whatever I could, including observation, photography, sample procurement and taking hardness measurements. Thankfully, they allowed more time where I took luminescence samples. I understand that this reasoning sounds weak and weird, but that much difficulty is expected in Kashmir.

Therefore, I followed your suggestion of pooling all the results from same litho-units together and calculated the mean ± 1σ for that population. Raw measurements are listed in Supplementary Table ST1. I have removed the data taken close to fractures and also removed the data from the tributary

Maru River. These steps resulted in reduction in total no. of sites from 96 to 75 as we removed biased data. The recalculated R values are plotted along the long-profile in Fig.7e.

L256-265 – Part 2: In general, a lot more detail is required to interpret your Schmidt hammer data. Later you describe significant fabrics in the rocks in the field (plus some nice field photos in the supplement). How did you consider this when taking your Schmidt hammer readings? Were you consistent with taking readings parallel or perpendicular to fabrics? Generally, where did you take these readings? Were they in the active channels? On the banks? Were the measured faces wet (which can bias readings)? Did you evenly space your measurements? Did you avoid fractures (which can bias readings)? Did you try to measure near fractures (which can bias readings)? There is a rich literature on concerns related to Schmidt hammer readings, like the Niedzielski paper above, but Aydin, A., Basu, A., 2005. The Schmidt hammer in rock material characterization. Engineering Geology 81, 1–14. https://doi.org/10.1016/j.enggeo.2005.06.006 is a good source for why knowing the answers to at least some of the questions posed above are relevant to interpreting your results.

All the measurements were done perpendicular to the bedding/foliation planes of dry rocks along road-cut section. No data is taken from riverbanks. Sentences mentioning these facts are drafted in line #389-396. The R values reported in the revised version were taken away from visible fractures. We tested the hardness values of fractured surfaces; they are lower by ~20 units in R-value than non-fractured ones.

L319-322 – The knickpoints might be easier to visualize if you included a chi (integral of drainage area) vs elevation plot as a companion to the long-profile.

Post-smoothing of the long-profile using a 20-pixel moving window identifying the knickpoints was easier. To be sure, we ran the ‘knickpointfinder’ tool in Topotoolbox with a threshold ‘dz’ value of 30m. That confirmed our hand-picked knickpoints in Fig.7a. For your reference chi vs. elevation plot is drafted in supplement Fig.S4.

L338-339 – More discussion / consideration of the influence of dams and reservoirs on your width measurements might be warranted in your methods (it wasn’t clear until now that there were dams on the profile).

We agree to the fact that the dams and reservoirs have altered the ‘natural’ channel width. Both the reservoirs expectedly have wider channels due to damming. One might argue that the dams were made on pre-existing geological structures which had gentler channel slopes in the upstream. But, we have very little or rather no access to the dam sites to confirm this. Considering the channel width downstream from the dams, there should exist a control of the water release from the dam. To eradicate that bias, we used the satellite image from summer monsoon months when these dams are

open due to higher discharge caused by glacial melting and monsoon precipitation. Therefore, the channel width we showcase is expectedly the highest of the year.

However, there is more external control on channel width. In some parts, let's say, downstream from the point K2 and K3 (cf. Fig.7a and 7b), the channel width are lower because of formation of epigenetic gorge. The issue of epigenetic gorge formation is discussed in section 5.1.3. and 5.3.

L342-343 – Similar to the comments earlier with regards to the SSP calculation, it is worth considering how the widths you measure compare to drainage area / discharge. This also gets to the constant discharge assumption, i.e. what is the change in drainage area along the portion of the river you're examining? Obviously your width measurements are not varying smoothly as a function of drainage area, but this is an important contributor to channel width that appears to be largely ignored.

Agreed. But, if we look at the aspect of change in drainage area, the most obvious change in drainage area occurs when the tributary Maru R. joins the Chenab R. now, if we look in the channel width before and after the joining of the tributary, we see no significant change in channel width. In fact, that is our argument that there is some other (tectonic) control on channel width. Where, there is no tectonic control, let's say, from ~70km-15 km of the long-profile, we see monotonous increase in channel width with increasing drainage area.

L354 – But assuming a constant discharge right? That's what Table 1 indicates.

Revised accordingly.

L384- An alternative / complimentary approach might be thinking about patterns in cosmogenic erosion rates with topography. At least based on a quick browsing of the OCTOPUS database (https://earth.uow.edu.au/) there are no cosmo basins directly in your area, but there are some not that far away (Olen et al, 2016, Munack, 2014, Dortch 2011). There is good evidence of relationships between erosion rates and ksn (e.g. Kirby, E., Whipple, K.X., 2012. Expression of active tectonics in erosional landscapes. Journal of Structural Geology 44, 54–75.) so you could explore what an aggregate of ksn vs E data in the surrounding regions imply for your area (need to consider complicating factors like precip and rock type when transporting relationships and restrict your analysis to locally equilibriated basins, but maybe at least another option you could consider). These would also be more on a complimentary timescale compared to thermochron, which might be giving you a longer term average.

Stefanie in her paper (Olen et al., 2016) emphasized on the power-law scaling relationship between topographic metric and erosion rates. The power-law equation stands as-

$$Ksn = a * (\text{erosion rate})^{b}$$

For the pan-Himalayan dataset, the paper predicts a = 215 and b= 0.3. If we incorporate the high ksn values (>500) obtained from KW and the surroundings, we obtain absurdly-high predicted erosion-rate for the study area (e ~ 15-16 mm/y). That tells us the fact that this power-law fit probably can't explain the true relationship of erosion vs. ksn values. Both, Rasmus and me are also preparing one manuscript on paleo erosion rates vs. topographic steepness in the nearby Dhauladhar Range. We hardly find the power-law scaling to be true there.

But, now we have an additional constraint on landscape change over geomorphic timescales. We obtained a handful of OSL-IRSL ages from aggraded sediment sequence stored above the bedrock straths in the Kishtwar valley. We demonstrate the sediment bodies in Fig.4, Fig.9. Details of sediment aggradation and their relationship with fluvial bedrock incision are drafted in section 3.3. methods of luminescence dating of transiently-stored sediments in and around Kishtwar, section 4.3.results of luminescence chronology, section 5.2. discussion on sediment aggradation in Chenab valley and section 5.3. discussion on drainage reorganization and strath terrace formation along Chenab River. Based on the stratigraphic relationship of the deposits and the underlying bedrock straths, we calculated fluvial bedrock incision rates over millennial timescales. Our estimates are in agreement with long-term exhumation rates. But, as we are able to come up with bedrock incision rates since 80 ky, we believe that the issue of mismatch in timescale is addressed.

L452 – Are these cooling ages on any of your figures / maps? It might help for spatial context. Could probably add them to Figure 4 without cluttering too much.

AFT cooling ages (Kumar et al., 1995) are shown in Fig.1a in revised version.

L492 – Worth considering how consistent your observations are with other studies focused on the surface / geomorphic expression of a growing duplex. The paper from Adams et al, 2016 (Adams, B.A., Whipple, K.X., Hodges, K.V., Heimsath, A.M., 2016. In situ development of high-elevation, low-relief landscapes via duplex deformation in the Eastern Himalayan hinterland, Bhutan. Journal of Geophysical Research: Earth Surface 121, 294–319. https://doi.org/10.1002/2015JF003508) might be a relevant one to consider. Similarly, you are ultimately arguing for motion over a series of ramps and flats. You may want to think about the role that lateral advection could play in the observed topographic patterns (e.g. Eizenhöfer, P.R., McQuarrie, N., Shelef, E., Ehlers, T.A., 2019. Landscape Response to Lateral Advection in Convergent Orogens Over Geologic Time Scales. J. Geophys. Res. Earth Surf. 124, 2056–2078. https://doi.org/10.1029/2019JF005100). In general, need to think / talk much more about how your observations lead to the model you propose, because at present, this is not clear at all.

Thanks for recommending the paper by Adams et al., (2016). I went through it and on the basis of that, I can draw a few initial comments. Some of the findings of Adams et al. are in agreement with

our data. We also observe a physiographic transition at the western margin of the KW, exposing the LH duplex. However, the low-relief landscape they propose to be sitting on a blind duplex at the stoss side of the transition, doesn't seem to fit in our context. The low-relief zone we have in the frontal Higher Himalaya show no sign of gorge formation and very limited fluvial bedrock incision. Therefore, we may argue that the duplex is limited within the KW. The duplex in KW is exposed to the surface and show structural variations (detected by changes in orientation). The observed steepening and narrowing of channel correlate well with segments of steep bedrock orientation. We argue that the steepening of river reflects the differential uplift along river triggered by existing ramp-flat geometry of the basal decollement. Unless the growth of the duplex is continuous, the topographic response would have been much subdued. For example, we may refer to the topographic metrics at the frontal MCT brittle fault zone. The MCT is no longer active, and that's why the morphometric parameters are subdued. To continue more on the paper by Adams et al., the structural architecture of the Bhutanese Himalaya is distinctly different from the NW Himalaya. That is why we compared our findings with studies from NW Himalaya (Nennewitz et al., 2018; Gavillot et al., 2018; Thiede et al., 2017).

In connection to your opinion on the role of lateral advection in topographic build-up, I would like to show the regional map of topographic relief and basinwide ksn distribution (Fig.5b,5d). In this study, we have no evidence of a lateral ramp in KW. The bedrock orientations shown in Fig. 8a attests to that. In the nearby Dhauladhar Range (DR) (SE of the KW), Thiede et al., (2017) proposed a frontal ramp beneath the Dhauladhar uplifting the topography. Now these two rapidly-uplifting zones have along-strike difference in the distance from the mountain front. Now referring to the topographic relief as well as the ksn map, we see that these two zones (KW and the Dhauladhar) are connected by a ~50-kn wide N-S trending zone of high relief and steepness. At this moment, we don't have structural data from this proposed link segment, but, by looking at the regional topographic pattern we would argue that, lateral ramp, if any, would be this one. But, at this moment, we have no data to comment anything on impact or evidence of lateral advection on KW.

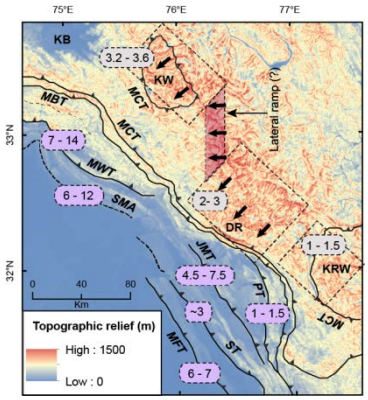

Figure showing distribution of topographic relief in far western Himalaya. Quaternary exhumation rates are shown in grey and Pleistocene-Holocene shortening rates on active faults shown in purple-colored boxes. The proposed lateral ramp is shaded by transparent-red color.

Figure 2 – In a, what is the jagged blue line floating above the profile? Is it fluvial relief? A blow up the profile? There's no mention of it in the caption. In general, applying some amount of smoothing to the profile (and its derivatives) would be appropriate as it is hard to see the signals you're trying to highlight with the noise from the DEM superimposed.

The longitudinal profile has been revised. Smoothing has been performed with 20-pixel smoothing window. That removed the noise (Figure 6, 7a).

Additions/ changes in the manuscript:

Revised title:

Growth of the Lesser Himalayan Duplex and rapid fluvial incision modulate landscape morphology in tectonically-active Kishtwar Window in NW Himalayan interiors

Revised abstract:

The Kishtwar Window (KW) of the NW Himalaya exposes the north-western termination of the orogen-parallel anticlinal stack of thrust nappes, known as the Lesser Himalayan Duplex. However, its exact tectonic deformation pattern, geographic extent and activity are still debated. Here we combine morphometric analyses with structural data, field evidence and chronological constraints to describe the spatial pattern of internal deformation of the duplex. We agree with previous findings that the variations in the geometry of the basal décollement, the Main Himalayan Thrust (MHT) is important; however, the observed topography and neotectonic deformation can be explained only with additional internal faulting within the duplex. We recognize two significant steep stream segments/ knickzones, one in the center of the window, and a second one along its western margin, which we relate to fault-ramps emerging from the MHT. The larger of the knickzones corresponds to highly-fractured and folded rocks at the base of the steep stream segment suggesting internal deformation of the duplex, possibly linked to surface-breaking thrust fault-ramp at the core of the duplex. The second steepened knickzone coincides with the western margin of the window and is identified by a narrow channel through a comparatively weaker bedrock gorge. Luminescence dating of sediments overlying the bedrock strath provides the upper limit of terrace abandonment. We deduced a minimum of 3.1-3.5 mm/y fluvial bedrock incision on the MHT-fault ramp which is in overall agreement with long-term exhumation rates from the KW. Summarizing our findings, we favor a structural and active tectonic control on the growth of the duplex even over geomorphic timescales.

Line # 58-60: text replaced '~~and not contributing to the growth and total shortening of the Himalaya since at least late Pleistocene~~' with 'over millennial timescales'.

Line # 77-78: added sentence- While most of the published cross-sections of the Himalayan orogen today recognize the duplex (Webb et al., 2011; Mitra et al., 2010; DeCelles et al., 2001), usually very little or no data is available whether the duplex is active over millennial timescales, and potentially a source of major Holocene earthquakes.

Line # 139-140: Added text- '4. Can we obtain new constraints on deformation over millennial timescales? Do millennial-scale fluvial incision rates support long-term exhumation rates?'

Line # 146: removed text- '~~data by using hand-held rebound hammer~~'.

Line # 147-156: Added sentence- 'We used basinwide steepness indices and specific stream power calculation (derived from channel gradient and channel width) as a proxy of the fluvial incision. And, lastly but most importantly, we are able to constrain the fluvial bedrock incision rates by using depositional ages of aggraded sediments along Chenab River.'

Line # 160-162: Added sentence- 'Our new estimates on the bedrock incision rate agree with Quaternary exhumation rates from the KW, which mean consistent active growth of the duplex over million-year to millennial timescales.'

Line #159: Changed section header to –'2.Geological background and field observations'.

Line # 204-250: Sentences added on field observations with reference to field photographs in Fig.2, Fig.3 and Fig.4.

The Higher Himalayan sequence dips steeply away from the duplex (~65° towards west) (Fig.2a). The frontal horses of the LH duplex expose internally-folded greenschist facies rocks. Although at the western margin of the duplex, the quartzites stand sub-vertically (Fig.2b), the general dip amount reduces as we move from west to east for the next ~10-15 km up to the core of the KW. Near the core of the KW, we observed highly-deformed (folded and multiply-fractured) quartzite and granites at the core of the KW (Fig.2d, 2e). We also observed deformed quartz veins of at least two generations, as well as macroscopic white mica. Here, the river is also very steep and narrow; the rock units are also steeply-dipping towards the east (~55-65°) and are nearly isoclinal and strongly deformed at places (Fig.2f). Towards the eastern edge of the window, however, the quartzites dip much gently towards the east (~20-30°) and much lesser folding and faulting have been recognized in the field (Fig.2g).

The valley profile near the town of Padder at the eastern margin of the KW is U-shaped (Fig.3a). At the core of the KW, the Chenab River maintains narrow channel width and a steep gradient (Fig.3b). The E-W traverse of the Chenab River through the KW is devoid of any significant sediment storage. However, along the N-S traverse parallel to the western margin of the KW, beneath the Kishtwar surface, ~150-170m thick sedimentary deposits are transiently-stored over the steeply-dipping Higher Himalayan bedrock (Fig.3c). The height of the Kishtwar surface from the Chenab River is ~450m, which means ~280m of bedrock incision by the river since the formation of the Kishtwar surface. Along the N-S traverse of the River, epigenetic gorges are formed as a result of damming of paleo-channel by hillslope debris flow, followed by establishment of a newer channel path (Ouimet et al., 2008; Kothyari and Juyal, 2014). One example of such epigenetic gorge formation near the town of Drabshalla is shown in Fig.3d. Downstream from the town of Drabshalla, the River maintains narrow channel width (< 25 m) and flows through a gorge having sub-vertical valley-walls (Fig.3e). The tributaries originating in the Higher Himalayan domain form one major knickpoint close to the confluence with the trunk stream (Fig.3f). We have identified at least three strath surface levels above

the present-day river channel, viz., T1 (280±5 m), T2 (170-175 m) and T3 (~120±5 m), respectively (Fig.3g). The first study on sediment aggradation in Middle Chenab valley (transect from Kishtwar to Doda town) was published by Norin (1926). He argued the sediment aggradation in and around the Kishtwar town is largely contributed by fluvioglacial sediments and the U-shaped valley morphology is a marker of past glacial occupancy. We partially agree to the findings of Norin (1926) and Ul Haq et al., (2019) as we observe ~100m thick fluvioglacial sediment cover unconformably overlying the Higher Himalayan bedrock (Fig.4b). The fluvioglacial sediments included alternate layers of pebble conglomerate and coarse-medium sand (Fig.4c). The pebbles are moderately rounded and polished suggesting significant fluvial transport. Our field observations suggest that the fluvioglacial sediments have been succeeded by a significant volume of hillslope debris (Fig.4c). The thickness of the debris-flow deposits is variable. The hillslope debris units contain mostly coarse-grained, highly-angular, poorly-sorted quartzite clasts from the frontal horses of the Lesser Himalayan Duplex. The hillslope debris units also contain a few fine-grain sediment layers trapped in between two coarse-grained debris layers (Fig.4e). The town of Kishtwar is situated on this debris flow deposit.

Line # 258-261: Added sentence- 'We compiled the topographic relief over a circular moving window of 4 km diameter (Fig.5b) and the rainfall distribution of the Chenab region (Fig.5c). The rainfall distribution is adapted from 12-year-averaged annual rainfall data from TRMM database (Bookhagen and Burbank, 2006).'

Line # 262-295: Text reorganized- section on Basin-wide normalized steepness indices revised as section 3.1.1.

Line # 274-285: Text added- 'Stream-specific ksn values in and around the KW are drafted in Supplementary Fig.S3. The catchments were delineated by using a maximum threshold of 200 sq. km, so that the basins we pick are smaller in size. The stream-specific k_{sn} values were rasterized in ArcGIS and were extrapolated to the respective catchments using the zonal statistics toolbox. Basinwide mean k_{sn} values for the delineated watersheds are portrayed in Fig.5d.Basinwide mean k_{sn} values are plotted using a 500 km^2 threshold catchment area (Fig. 2d).

A 50-km-wide swath profile along line AB (cf.Fig.5a) show variation in elevation, mean annual rainfall and mean k_{sn} values in the area (Fig.2e).'

Line # 279-283: Text removed- '~~The slope breaks, known as the knickpoints (sometimes referred to as knickzones if it is manifested by a series of rapids instead of a single sharp break in profile), were allocated by comparing the change of slope along the distance-elevation plot (Fig.2a). The threshold 'dz' value (projected stream offset across a knickpoint) for this study is 30m.~~'

Line # 286-295: Text removed.

Line # 282: Change in section number to 3.1.2. Drainage network extraction.

Line # 286: Added text-‘(250 m smoothing window)’.

Line # 305-319: Added text- ‘Identification of the knickpoints/ knickzones and their relationship with the rock-types as well as with existing structures are necessary to understand the causal mechanism of the respective knickpoints/ knickzones. Knickpoints/(zones) can be generated by lithological, tectonic and structural control. Lithological knickpoints are stationary and anchored at the transition from the soft-to-hard substrate. The tectonic knickpoints originate at the active tectonic boundary and migrate upstream with time. Structural variations, such as ramp-flat geometry of any emerging thrust may cause a quasistatic knickpoint at the transition of the flat-to-ramp of the fault. In such cases, the ramp segment is characterized by higher steepness than the flat segment and often the ramp is characterized by a sequence of rapids, forming a wide knickzone, instead of a single knickpoint.

Longitudinal profile of the Chenab River show oversteepening across the KW (Fig.6), therefore, we focused on that segment (marked by red rectangle, cf. Fig.6) for further analysis. Longitudinal profile of the selected segment is shown in Fig.7a.’

Line # 339: Altered text- ‘~~50~~’ replaced by ‘100’.

Line # 340: Altered text- ‘~~Twenty~~’ replaced by ‘Ten’.

Line # 359-360: added sentence- ‘Variations in channel gradient and ksn values along the longitudinal profile of the selected stretch are shown in Fig.7c and 7d, respectively.’

Line # 370-372: Added sentence- ‘With the available TRMM data, we argue that the rainfall distribution in the study area is almost uniformly low (<1.5 m/y) (Fig.5c and 5e) and therefore we assumed a uniform discharge (Q) for SSP calculation.’

Line # 387: changed number- from ‘~~96~~’ to ‘74’. (Removed data from tributary valleys, data from sites having irregular fractures)

Line # 389-396: Added sentences- ‘All the measurements were taken perpendicular to the bedding/ foliation plane and no measurements are from wet surfaces or surfaces showing fractures. Each reading was taken at least 0.5m apart from the previous one. Average rock strength data collected from each of the test locations are plotted against the longitudinal river profile and channel width data in Fig.7e. Our data from individual sites are smaller in number than what is preferred for checking the statistical robustness of Schmidt hammer data (Niedzielski et al., 2009). Therefore, we combined the data from all sites representing similar lithology and portrayed the mean ±standard deviation for the same.’

Line # 397-465: Added method section on '**3.3. luminescence dating of transiently-stored sediments in and around Kishtwar**'

Added text- 'Luminescence dating of Quaternary fluvial sediments is a globally accepted method for constraining the timing of deposition of sediments in a drainage system (Olley et al., 1998; Wallinga et al., 2001; Cunningham and Wallinga, 2012). Although there exists a few persistent problems in luminescence dating of the Himalayan sediments (including poor sensitivity of quartz and numerous cases of heterogeneous bleaching of the luminescence signal), studies over the past couple of decades have also provided a good control on Himalayan sedimentary chronology by using luminescence dating with quartz (Optically stimulated luminescence, OSL) and feldspar (Infra-red stimulated luminescence, IRSL). Earlier studies have reported sediment aggradation over the Higher Himalayan bedrocks in the Kishtwar valley (Norin, 1926; Ul Haq et al., 2019).

The samples for luminescence dating were collected in galvanized iron pipes. The pipes were opened in subdued red light (wavelength ~650 nm). The outer ~3 cm of sediment from both the ends of the pipe were removed to omit possibility of exposure of sample to daylight during collection. The removed portion was used for moisture content estimation and determination of Uranium (U), Thorium (Th) and Potassium (K) concentrations. The interior unexposed portion of sample was further processed to obtain quartz and feldspar using standard procedures (e.g. Aitken, 1998). The portion was treated with sufficient quantity of 1N HCl and 30% H2O2 to remove carbonates and organic materials respectively. The sediments were then oven dried at 45□C and sieved to obtain a size fraction of 90-150 μm. The quartz and feldspar was separated using Frantz isodynamic separator at a magnetic field of ~10,000 gauss and collected separately. Obtained quartz grains were etched with 40% HF for 80 minutes to remove alpha irradiated outer layer (~10 μm) followed by 37% HCl treatment for 20 minutes to dissolve fluorides formed during previous step. The isodynamic separation procedure was repeated to remove any broken feldspar grain. However, even after repeating the last step for 2 times, we were unable to completely eliminate the feldspar contamination from the most of the samples.

Samples K02 and K11 procured from the fine-grain layers of ~1-1.5m thickness, trapped within coarse, angular and poorly-sorted thick layers of clasts (identified as hillslope debris) were used for OSL (Optically stimulated luminescence) dating using Double SAR (Single Aliquot Regenerative) protocol (IRSL wash before OSL measurement) for equivalent dose estimation (Roberts, 2007). The test doses were set for 75 Gy, 225 Gy and 450 Gy, respectively (Fig.5). The aliquots were considered for ED estimation only if: (i) recycling ratio was within 1±0.1, (ii) ED error was less than 20%, (iii) test dose error was less than 10%, and (iv) recuperation was below 5% of the natural. For samples K16 and K17 (fluvial sand trapped above the T3 strath surface) the feldspar contamination was negligible. Therefore, OSL SAR protocol was tried with test doses of 50 Gy, 100 Gy and 150 Gy,

respectively. Samples K16 and K17 returned highly scattered equivalent dose (De) estimates (over-dispersion > 30%) (cf. Table 2) and thus, both of them have been interpreted by minimum age model (Bailey and Arnold, 2006). Sample K18 (from silty clay layer found above the T1 strath surface in the wind gap of Maru River) was saturated and hence, we also provided the minimum age estimate for the same. The sample was exhausted after we performed OSL measurements, therefore, we couldn't proceed towards feldspar dating with sample K18.

OSL dating for the three samples procured from the fluvio-glacial sediments showed saturation; therefore, we tried for IRSL (Infra-red stimulated luminescence) dating of feldspar for those three samples (K07-K09) using standard post infrared (pIR-IR) protocol (Buylaert et al., 2013), in which, the preheat temperature was 320°C for 60s. The samples were first stimulated at 50°C with IR diodes for 100s followed by IR stimulation at 290°C and a violet-blue luminescence emission (395 ± 50 nm) was detected by PMT through the combination of optical filters, Corning 7-59 (4 mm) and BG-39 (2 mm). However, the samples showed significant saturation possibly due to improper bleaching of Post-IR IRSL signal, however the IRSL signal is not saturated suggesting it to be better bleached. We encountered significant IRSL signal while testing the luminescence of hand-picked individual quartz grains suggesting a presence of feldspar inclusion within the quartz. We tried leaching with 40% HF for three times, which exhausted most of the separated quartz sample. Hence, we had to proceed with standard IR protocol (Preusser, F., 2003) using K-feldspar. The initial test dose for the samples was set for 150 Gy and the rest of the runs were set for 375 Gy and 750 Gy, respectively (Fig.5). Fading correction tests were done for two samples K07 and K09 and the fading correction factors have been calculated using conventional methods after Huntley and Lamothe, (2001). The over-dispersion values are less than 30% (cf. Table 2) and hence, Central Age Model (CAM) has been used for estimation of equivalent dose (De) (Bailey and Arnold, 2006) instead of RMM-based De estimation as prescribed by Chauhan and Singhvi, (2011), useful for samples having higher over-dispersion.

The dose rate was estimated using online software DRAC (Durcan et al., 2015) from the data of Uranium (U), Thorium (Th) and Potassium (K) measured using ICP-MS and XRF (Table 2) in IISER Kolkata. The estimation of moisture content was done by using the fractional difference of saturated vs. unsaturated sample weight. Shine curve, dose growth curve and radial plots for De estimation obtained from analysis of three representative samples: K07 (IRSL), K11 (OSL D-SAR) and K17 (OSL SAR) are shown in Supplementary Fig.S3.'

Line # 494-495: Added text- 'and therefore, they are ignored while plotting the regional rock strength values in Fig.7e.'

Line # 495-501: Revised text with new results 'The dominant Rampur quartzites in the KW, as well as the granitic intrusives in the eastern part of the KW, shows very high R values of 51±4 and 58±2, respectively (Fig.7e). Compared to the high R values in the KW, the Higher Himalayan migmatites

near the KT (western margin of the KW) show moderate strength (R: 49±5)whereas, the HHCS units show lower strength (R: 39±3). The rock strength increases (R: 44±2) within the Haimanta Formation until it reaches the MCT shear zone. The R-value in the frontal Lesser Himalaya is moderate (R: 41±2).'

Line # 502-516: Text removed from this section and merged with section 2: Geological background and field findings.

Line # 548-554: Text removed.

Line # 561-577: Section added on '**4.3. Luminescence chronology**'

Added text- 'The results for the luminescence chronology experiment are listed in Table 2 and the shine curve, dose growth curve and De estimation plots for different samples are provided in the supplementary Fig.S3. Sample K07, K08 and K09 yield IRSL ages of 104.5±5.9 ky, 114.4±6.3 ky, and 119.2±6.8 ky, respectively. Fading corrections done for samples K07 and K09 yield the correction factors (g%) of 0.89 and 1.11 respectively. The sample K08 has not been treated for fading correction, but for easier understanding, we have assumed a constant sedimentation rate between the samples K07 and K09 and extrapolated the 'fading-corrected' age for K08. The oldest sample K09 (132±7 ky) (fading-corrected IRSL age) is succeeded by samples K08 (126±6 ky) and K07 (113±6 ky) respectively (Fig.4c). The initial IRSL ages (before fading-correction) therefore may be regarded as minimum age estimate for the fluvioglacial sediment sequence. The finer fraction of the hillslope debris overlying the fluvio-glacial deposits yield OSL ages of 81.1±4.6 ky (K02) and 85±5 ky (K11) (Fig.4d, 4e). OSL samples taken from sparsely-preserved sediment layers above the T3 strath surface shows heterogeneous bleaching and hence we provide a minimum age of 22.8±2.1 ky (sample K16) and 20.5±1.0 ky (sample K17). One sample taken above T1 strath level is saturated and shows a minimum age of 52.1±2.8 ky (sample K18) (Table 2).'

Line # 588-590: added text – 'In this section, we discuss how we combined terrain morphometry and Quaternary dating of sediments to evaluate ongoing deformation in the interior of the NW Himalaya.'

Line # 590- 597: text removed.

Line # 598-599: Revised text.' Apatite fission-track cooling ages at the center of the LH duplex and along the western margin of the KW are younger (~2-3 Ma) as compared to the surrounding Higher Himalaya,'

Line # 603- 605: text removed.

Line # 607-609: Added sentence- 'With additional chronological constraints from late Quaternary sedimentary deposits, we predict rapid fluvial bedrock incision in the Himalayan interiors.'

Line # 678-685: Sub-section added on '**5.1.3. Knickpoint marking epigenetic gorge**'

Added text- 'Epigenetic gorges are common geomorphic features in the high-mountain landscape (Ouimet et al., 2008). Epigenetic gorges form when channels of a drainage system are buried by sediment aggradation and during subsequent re-incision, a new river channel is incised. The N-S traverse of the Chenab River is largely affected by hillslope sediment flux from the steep eastern flank. The knickpoint K3 situated near the village of Janwas, mark one such instance of epigenetic gorge where the paleo-valley has been filled initially by fluvioglacial sediments and the channel abandonment was caused by hillslope debris flow ~80 ky (Fig.4b, 4c).'

Line # 686-694: Section added on '**5.2. Sediment aggradation in the Chenab valley**'

Added text – 'The luminescence chronology of the transiently-stored sediments in the Chenab valley point towards protracted sediment aggradation since the onset of the last glacial-interglacial cycle till ~80 ky. Fluvioglacial outwash sediments range from ~110-130 ky, whereas the hillslope debris range from ~90 to ~80 ky (cf. Fig.4). The obtained chronology of the sediment deposits match well with the relative stratigraphic order of the sedimentary units, and therefore, we believe the obtained ages are reliable. The deeply-incised fluvial network as we observe today require net fluvial incision and formation of bedrock strath surfaces sometime after ~80 ky before present.'

Line # 696-717: Section added – '**5.3. Drainage reorganization and strath terrace formation along Chenab River**'

Added text – 'Hillslope debris flow characterized by white quartzite blocks of different sizes and shapes can only originate from the high-relief frontal horses of the Lesser Himalayan Duplex exposed in the eastern flanks of the valley. These hillslope debris overlies the fluvioglacial sediments stored beneath the Kishtwar surface (Fig.9a, 9c). We argue that the hillslope debris flow intervened in the paleo-drainage of the Chenab River, which might have been flowing through an easterly path than now (Fig.9). The Maru River, coming from the north-western corner of our study area, was also joining the Chenab River at a different location (Fig.9). Our argument is supported by field observation of the thick silt-clay layer in the proposed paleo-valley of the Maru River (Fig.9a, 9c). OSL sample (K18) from the silt-clay layer is saturated and hence only provides the minimum age of 52±3 ky. We suggest that the hillslope sediment flux has ceased the flow of the Chenab River and also propagated through the wind-gap of the Maru River. The decline in depositional energy has resulted in a reduction of grain-size. Post-hillslope debris flow episode, the Chenab River also diverted to a new path. The new course of the Chenab River upstream from the confluence with the Maru River is defined by a very narrow channel flowing through the Higher Himalayan bedrock gorge (Fig.9). Downstream from the confluence, we identified at least three levels of strath terraces lying at heights of ~280-290m (T1), ~170m (T2), and ~120m (T3), respectively (Fig.4g, 10a). Our

field observation suggests that the formation of the straths is at least ~52 ky-old. The luminescence chronology samples in this study belong to the ~150-170m-thick soft sediments that are stored stratigraphically-up from the T1 strath level. Our field observations and chronological estimates suggest that the renewed path of the Chenab River must have been formed post the hillslope debris flow ~80-90 ky but before 52 ky.'

Line # 718-738: Added section on '**5.4. Rapid bedrock incision along Chenab River**'

Added text- 'Considering the rate of excavation of softer sediments to be at least an order of magnitude higher than the rate of bedrock incision (Ouimet et al., 2008; Kothyari and Juyal, 2013), we calculated the minimum bedrock incision rate using the height of the T1 strath (~280±5 m) and the average age of the sediments from the Hillslope debris flow deposit. It yields a minimum bedrock incision rate of ~3.1-3.5 mm/y over the last 80-90 ky. Considering the saturated OSL sample from the paleo-valley, we estimated the maximum bedrock incision since 52 ky to be 5.1-5.5 mm/y. Similarly, using the minimum age estimate of the T3 terrace abandonment, we deduce a maximum bedrock incision rate of ~5.7-6.1 mm/y since ~21 ky (Fig.10b).

Many studies have used dated strath surfaces to quantify rock uplift rates in the Himalaya (Wesnousky et al., 1999; Lave and Avouac, 2000; Mukul et al., 2007; Thakur et al., 2014). Assuming the channel hypsometry to be constant during the incision period, we may infer the minimum fluvial incision reflects regional rock uplift caused by movement of rocks over the ramp of the MHT at a rate of ~3.1-3.5 mm/y. This minimum uplift rate estimate is in agreement with long-term exhumation rates of 3.2-3.6 mm/y deduced from the KW (Gavillot et al., 2018). The inferred uplift rate can be translated to a shortening rate by using a simple trigonometric function. Our field findings suggest that the larger ramp on the MHT (MCR-1) have an average near-surface dip of ~60˚. Considering a similar geometry for MCR-2, we obtained a minimum shortening rate of 1.8-2.0 mm/y. On the other hand, considering the minimum ages of T3 terrace abandonment, we obtained maximum uplift rates ~5.5-6.0 mm/y, which would translate into a shortening rate of ~3.2-3.5 mm/y since ~21 ky.'

Line # 740-746: Revised text- ' The young AFT-cooling ages by the pioneering work of Kumar et al., (1995) showcased a rapid exhumation of the KW (AFT ages: ~1-3 My) compared to the surroundings (AFT age: 6-12 My). The exhumation rates proposed by Gavillot et al. (2018) are based on using a geothermal gradient of 35-40˚C/km in Dodson's equation assuming a 1-D model (Dodson, 1973). Unfortunately, a proper thermal modeling of the region is lacking, therefore, regional correlation with the proposed cooling ages and exhumation rates have large uncertainties.'

Line # 776-779: Added text- 'We don't have any direct field evidence of surface-breaking faults, which could be linked to the MCR-2. However, a rapid fluvial incision along the western margin of

KW and an increase in morphometric parameter values (k_{sn}, channel gradient, topographic relief, etc.) probably justify the existence of MCR-2.'

Line #805-822: revised text.

'Nennewitz et al., (2018) have proposed that the million-year-timescale shortening achieved in the interior of the Himalaya near the Sutlej-Beas area in the eastern Himachal Pradesh is caused by accentuated rock uplift over a ramp at a mid-crustal depth of ~ 8-25 km on the MHT. In contrast, studies from the Dhauladhar Range in the north-western Himalaya hints the presence of deep-seated crustal ramp on the MBT and yielded a shortening rate of 3±0.5 mm/y across the MBT over the last 8 My and absence of mid-crustal ramp (Deeken et al., 2011; Thiede et al., 2017). The work by Gavillot et al. (2018) favors the existence of at least two mid-crustal ramps beneath the KW (Supplementary Fig.S2). Their suggestion is in agreement with very young AFT cooling ages (1-3 Ma) (Kumar et al., 1995) in the window (Fig.1a) and the findings of this study. These studies altogether point out the along-strike variation in the location of the rapidly-uplifting crustal ramp with respect to the southern Himalayan front. The crustal ramp in the nearby Kangra recess is located beneath the Dhauladhar Range at the main Himalayan front, whereas, in the Himalayan transects situated towards the east and west of Kangra recess, the ramps are located ~100km inside from the MBT. Topographic relief and basinwide mean k_{sn} distribution (Fig.5) hint towards the existence of a lateral ramp in between the Kangra and the Jammu-Kashmir Himalayan transects. However, at this moment, we have no conclusive data in support of this claim.'

Line # 798-806: Modifications in conclusion.

Added text-

'5. Luminescence chronology of the transiently-stored sediments along the Chenab River suggests that the valley had been overfilled with sediments of fluvio-glacial origin as well as with hillslope debris flow. Massive sediment aggradation during ~130-80 ky led to drainage re-organization and bedrock incision leaving behind a set of strath surfaces.

6. The late Quaternary bedrock incision rates on the mid-crustal ramp beneath the western margin of the KW are high 3.1-3.6 mm/y. We argue that this rapid fluvial incision can potentially be linked to the accommodation of crustal shortening along a mid-crustal ramp of the basal decollement of the Himalaya. Our results indicate a minimum shortening rate of ~1.8-2.1 mm/y being accommodated along the N-S traverse of the Chenab River.'

Reference list: Added references-

Aitken, M. J. (1992). Optical dating. Quaternary Science Reviews, 11(1-2), 127-131.

Bailey, R. M., & Arnold, L. J. (2006). Statistical modelling of single grain quartz De distributions and an assessment of procedures for estimating burial dose. Quaternary Science Reviews, 25(19-20), 2475-2502.

Bookhagen, B., & Burbank, D. W. (2006). Topography, relief, and TRMM-derived rainfall variations along the Himalaya. Geophysical Research Letters, 33(8).

Buylaert, J.P., Murray, A.S., Gebhardt, A.C., Sohbati, R., Ohlendorf, C., Thiel, C., Wastegård, S., Zolitschka, B. and Team, T.P.S., 2013. Luminescence dating of the PASADO core 5022-1D from Laguna Potrok Aike (Argentina) using IRSL signals from feldspar. Quaternary Science Reviews, 71, pp.70-80.

Chauhan, N., & Singhvi, A. (2011). Distribution in SAR palaeodoses due to spatial heterogeniety of natural beta dose. Geochronometria, 38(3), 190-198.

Cunningham, A. C., & Wallinga, J. (2012). Realizing the potential of fluvial archives using robust OSL chronologies. Quaternary Geochronology, 12, 98-106.

Dey, S., Kaushal, R. K., & Jain, V. (2019). Spatiotemporal variability of neotectonic activity along the Southern Himalayan front: A geomorphic perspective. Journal of Geodynamics, 129, 237-246.

Dodson, M. H. (1973). Closure temperature in cooling geochronological and petrological systems. Contributions to Mineralogy and Petrology, 40(3), 259-274.

Hack, J. T. (1973). Stream-profile analysis and stream-gradient index. Journal of Research of the us Geological Survey, 1(4), 421-429.

Huntley, D. J., & Lamothe, M. (2001). Ubiquity of anomalous fading in K-feldspars and the measurement and correction for it in optical dating. Canadian Journal of Earth Sciences, 38(7), 1093-1106.

Kothyari, G. C., & Juyal, N. (2013). Implications of fossil valleys and associated epigenetic gorges in parts of Central Himalaya. Current Science, 383-388.

Niedzielski, T., Migoń, P., & Placek, A. (2009). A minimum sample size required from Schmidt hammer measurements. Earth Surface Processes and Landforms: The Journal of the British Geomorphological Research Group, 34(13), 1713-1725.

Norin, E. (1926). The relief chronology of the Chenab valley. Geografiska Annaler, 8(4), 284-300.

Olley, J., Caitcheon, G., & Murray, A. (1998). The distribution of apparent dose as determined by optically stimulated luminescence in small aliquots of fluvial quartz: implications for dating young sediments. Quaternary Science Reviews, 17(11), 1033-1040.

Ouimet, W. B., Whipple, K. X., Crosby, B. T., Johnson, J. P., & Schildgen, T. F. (2008). Epigenetic gorges in fluvial landscapes. Earth Surface Processes and Landforms: The Journal of the British Geomorphological Research Group, 33(13), 1993-2009.

Preusser, F. (2003). IRSL dating of K-rich feldspars using the SAR protocol: comparison with independent age control. Ancient tL, 21(1), 17-23.

Roberts, H. M. (2007). Assessing the effectiveness of the double-SAR protocol in isolating a luminescence signal dominated by quartz. Radiation measurements, 42(10), 1627-1636.

Wallinga, J., Murray, A. S., Duller, G. A., & Törnqvist, T. E. (2001). Testing optically stimulated luminescence dating of sand-sized quartz and feldspar from fluvial deposits. Earth and Planetary Science Letters, 193(3-4), 617-630.

1

~~Structural variations in basal decollement and internal deformation~~Growth of the Lesser Himalayan Duplex and rapid fluvial incision ~~trigger~~ modulate landscape morphology in tectonically-active Kishtwar Window in NW Himalayan interiors

Saptarshi Dey[1], Rasmus Thiede[2], Arindam Biswas[3], Naveen Chauhan[4], Pritha Chakravarti[1], and Vikrant Jain[1]

[1]*Earth Science Discipline, IIT Gandhinagar, Gandhinagar-382355, India.*

[2]*Institute of Geosciences, Christian Albrechts University of Kiel, Kiel-24118, Germany.*

[3] *Department of Applied Geology, IIT-ISM Dhanbad, Jharkhand-826004, India.*

[4] *Atomic Molecular and Optical Physics Division, Physical Research Laboratory, Ahmedabad.*

Corresponding author

Saptarshi Dey

saptarshi.dey@iitgn.ac.in

Abstract

The Kishtwar Window (KW) of the NW Himalaya exposes the north-western termination of the orogen-parallel anticlinal stack of thrust nappes, ~~termed~~ known as the Lesser Himalayan Duplex. ~~and its evolution portrays rapid exhumation at least over the last 2-3 Myr.~~ However, its exact tectonic deformation pattern, geographic extent and activity are still debated.~~speculations remain if it still actively deforming.~~ Here we combine morphometric analyses with structural ~~and~~ data, field evidence~~s~~ and chronological constraints to describe the spatial pattern of internal deformation of the duplex. We ~~suggest~~ agree with previous findings that the variations in the

geometry of the basal décollement, the Main Himalayan Thrust (MHT) is important; however, the observed topography and neotectonic deformation can be explained only with additional ~~and~~ internal faulting within the duplex ~~define the observed neotectonic deformation~~. We recognize two significant steep stream segments/ knickzones, one in the center of the window, and a second one along its western margin, which we relate to fault-ramps emerging from the MHT. The larger of the knickzones corresponds to~~, in the core of the window, show an increase in the angle of foliations towards downstream. H~~highly-fractured and folded rocks at the base of the steep stream segment~~,~~ suggesting internal deformation of the duplex, possibly linked to surface-breaking thrust fault-ramp at the core of the duplex. The second steepened knickzone coincides with the western margin of the window and is identified by a narrow channel through a comparatively weaker bedrock gorge. Luminescence dating of sediments overlying the bedrock strath provides the upper limit of terrace abandonment. We deduced a minimum of 3.1-3.5 mm/y fluvial bedrock incision on the MHT-fault ramp which is in overall agreement with long-term exhumation rates from the KW. Summarizing our findings, we favor a structural and active tectonic control on the growth of the duplex even over geomorphic timescales. ~~Corroborating with previous studies, we suggest that the differential uplift and growth of the duplex is linked to several flat-ramp structures along the MHT.~~

Keywords

Steepness index, knickzone, rock strength, Lesser Himalayan Duplex, Main Himalayan Thrust.

1. Introduction

Protracted convergence between the Indian and the Eurasian plate resulted into the growth and evolution of the Himalayan orogen and temporally in-sequence formation of the Southern Tibetan Detachment System (STDS), the Main Central Thrust (MCT), the Main Boundary Thrust (MBT) and the Main Frontal Thrust (MFT) towards the south (Yin and Harrison, 2000; Yin, 2006; Mukherjee, 2013). All these fault-zones emerge from a low-angle basal decollement, viz. the Main Himalayan Thrust (MHT) which forms the base of the Himalayan orogenic wedge (Ni and Barazangi, 1984; Nabelek et al., 2009; Avouac et al., 2016). The MHT was probably established in the late Miocene (Vannay et al., 2004).

The majority of scientists have favored that the late Pleistocene-Holocene shortening ~~of the Himalaya~~ is mostly accommodated within the southern ~~margin~~ fringe of the Himalayan wedge, i.e., the Sub-Himalaya (morphotectonic segment in between the MBT and the MFT) (Wesnousky et al., 1999; Lave and Avouac, 2000; Burgess et al., 2012; Thakur et al., 2014; Mukherjee, 2015; Vassalo et al., 2015; Dey et al., 2016; Dey et al., ~~2018~~2019). ~~The statement above~~This implies that the northerly thrusts, i.e., the MBT and the brittle faults exposed in the vicinity of the southern margin of the Higher Himalaya, are considered inactive ~~and not contributing to the growth and total shortening of the Himalaya since at least late Pleistocene~~over millennial timescales. However, in recent years, several studies that focused on the low-Temperature thermochronologic~~al~~ data and thermal modeling of the interiors of the NW Himalaya have raised questions on ~~the statement above~~this. The recent studies suggested that 10-15% of the total Quaternary shortening has been accommodated within the interiors of the Himalaya as out-of-sequence deformation~~, i.e., in hanging wall of the MBT or other structures~~ (Thiede et al., 2004; Deeken et al., 2011; Thiede et al., 2017; Gavillot et al., 2018) (Supplementary Fig. S1). Earlier, out-of-sequence deformation of the Himalayan wedge has been

explained by two end-member models- (a) the reactivation of the MCT (Wobus et al., 2003), or, (b) enhanced rock uplift over a major ramp on the MHT (Bollinger et al., 2006; Herman et al., 2010; Robert et al., 2009). Landscape evolution models, structural analysis and thermochronologic~~al~~ data from the interior of the Himalaya favor that the Lesser Himalaya has formed a duplex at the base of the southern Himalayan front by sustained internal deformation since late Miocene (Decelles et al., 2001; Mitra et al., 2010; Robinson and Martin, 2014). The growth of the duplex resulted in~~to~~ the uplift of the Higher Himalaya ~~forming~~ and established the major topographic and orographic barrier ~~of the orogen~~as seen today. The Kishtwar Window (KW) in the NW Himalaya represents the north-western termination of the Lesser Himalayan Duplex (LHD). While most of the published cross-sections of the Himalayan orogen today recognize the duplex (Webb et al., 2011; Mitra et al., 2010; DeCelles et al., 2001), usually very little or no data is available whether the duplex is active over millennial timescales, and potentially a source of major Holocene earthquakes.~~on how the deformation is spatially as well as temporally distributed. And most importantly, whether the duplex is active over timescales shorter than a million year.~~

The pioneering low-temperature thermochron study by Kumar et al. (1995) portrayed the first orogen-perpendicular sampling traverse extending from the south-western margin of the Kishtwar tectonic Window crossing the Zanskar Range. More recent studies link the evolution of the KW to the growth of the LHD (Gavillot et al., 2018). Along its margin, it is surrounded by the Miocene MCT shear zone along the base of the High Himalayan Crystalline Sequence (HHCS~~), ~~). ~~locally~~ Locally, the bounding fault zone is named ~~as~~ the Kishtwar Thrust (KT). Thermochronological constraints suggest higher rates of exhumation within the ~~window~~ KW (3.2-3.6 mm/y) (Gavillot et al., 2018~~), ~~). Their findings ~~corroborating~~ corroborate well with

similar thermochron-based ~~findings~~ Quaternary exhumation rates published from the of the Kullu-Rampur window in eastern Himachal Pradesh~~along the Beas (Stübner et al., (2018) and Sutlej valley~~ (Jain et al., 2000; Vannay et al., 2004; Thiede et al., 2004; Stübner et al., 2018)~~ over the Quaternary timescale~~. In contrast, geodetic shortening rates~~,~~ lack spatial resolution and only capture inter-seismic deformation (Banerjee and Burgmann, 2002; Kundu et al., 2014), and there exists no chronological data to provide information on ongoing tectonic activity in the interiors of the Himalaya over intermediate timescales. Therefore, to understand the 10^3-10^4-year timescale neotectonic evolution, either we have to have geological field evidence, chronologically-constrained geomorphic markers or at least have a rigorous morphometric analysis of potential study areas, such as the KW.

~~Documenting over-steepened longitudinal river profiles along the southern margin of the Higher Himalaya was pioneered by Seeber and Gornitz (1983), who related that to Quaternary internal deformation and recent uplift. They used longitudinal stream profiles and stream-length index and identified unadjusted and steep stream segments at the transition from the Lesser to the Higher Himalaya along sixteen major Himalayan rivers, including the Chenab river passing through the Kishtwar-Jammu region. Similarly, a study by Nennewitz et al., (2018) also portrayed morphometric indices (basinwide steepness indices and topographic relief) across a large part of the NW Himalaya. Though the resolution of the analyses was coarse, the first-order results encourage us to explore the large drainage networks over the prospect study areas in much more detail and with a terrain data having finer resolution than 30m SRTM DEM used before.~~

~~Another pivotal question on the Himalayan wedge kinematics is about the structural pattern of the basal decollement. Based on the large-scale basinwide morphometric analysis,~~

~~Nennewitz et al., (2018) have proposed that the million-year-timescale shortening achieved in the interior of the Himalaya near the Sutlej-Beas area in the eastern Himachal Pradesh is caused by accentuated rock uplift over a ramp at a mid-crustal depth of ~ 8-25 km on the MHT. In contrast, studies from the Dhauladhar Range in the northwestern Himalaya hints the presence of deep-seated crustal ramp on the MBT and yielded a shortening rate of 3±0.5 mm/y across the MBT over the last 8 My and absence of mid-crustal ramp (Thiede et al., 2017). However, it is still unclear whether this proposed ramp on the MHT is laterally continuous or is interrupted in the far-western sectors of the Ravi-Chamba region in the western Himachal Pradesh and Jammu region. Gavillot et al. (2018) recently presented an orogen-perpendicular balanced cross-section of the Chenab region extending ~160 km inside the MFT, which favors the existence of mid-crustal ramp beneath the KW. Their suggestion is in agreement with very young AFT cooling ages (1-3 Ma) (Kumar et al., 1995) in the window and previous documentation of structural deformation styles described in DiPietro and Pogue (2004), Yin (2006) and Searle et al., (2007). Previous work, however, lacks field evidence, as well as details about of active deformation. The thermochronological control is also restricted to very limited stretches along the Chenab River and hardly covers the entire KW. Therefore, the interpretation of deformation pattern based on exhumation rates is not very well constrained. However, the high Quaternary exhumation rates from the KW motivated us to study the KW and the surroundings in detail.~~

In this study, we will focus on a few long-standing questions on Himalayan neotectonic evolution, which are-

1. What is the spatial extent of neotectonic deformation, if any, in the interiors of the Himalaya?

2. What is the role of the Lesser Himalayan duplex in defining the morphology of the Himalayan interiors?

3. How reliably ~~we~~ can we infer about sub-surface structural variations of the orogenic wedge by analyzing the terrain morphology?

4. Can we obtain new constraints on deformation over millennial timescales? Do millennial-scale fluvial incision rates support long-term exhumation rates?

To address these questions, we adopted a combination of methods such as morphometric analysis using high-resolution digital elevation models, field observation on rock type, structural variations as well as rock strength data ~~collection~~ and~~,~~ analysis of satellite images to determine channel width and assessing the spatial distribution and relative differences ~~of~~ in the late Quaternary deformation of the KW and surroundings (Fig.1). ~~Our aim was~~We aimed to test if the landscape morphology can be explained by changes in the geometry of the basal decollement. We used basinwide steepness indices and specific stream power calculation (derived from channel gradient and channel width) as a proxy of the fluvial incision. ~~We have used 12.5m ALOS PALSAR DEM and LANDSAT satellite imagery for various morphometric analyses such as longitudinal stream profiles, basinwide normalized steepness indices and channel width measurement. We calculated specific stream power of selected stretches within the study area and used it as a proxy of fluvial incision. We combined the results with field observation, field-collected data on bedrock structural styles and rock strength data by using hand-held rebound hammer to investigate the spatial distribution of neotectonic deformation in the vicinity of the KW.~~ And, lastly but most importantly, we calculated the fluvial bedrock incision rates by using depositional ages of aggraded sediments along the Chenab River. In this study, we show that the regional distribution of faulting is concentrated in the core ~~of the window~~ and along the western

158 margin of the window. We propose that active faulting within the LH Duplex is controlling the
159 ongoing deformation in the Himalayan interior and driving the uplift of Higher Himalaya in its
160 hanging wall. Our new estimates on the bedrock incision rate agree with Quaternary exhumation
161 rates from the KW, which mean consistent active growth of the duplex over million-year to
162 millennial timescales. ~~With this study, we put new insights on the structural variations within the~~
163 ~~NW Himalayan interiors and spatial distribution of neotectonic evolution of the Himalayan~~
164 ~~orogen over the geomorphic timescale of 10^4-10^5 years.~~

165

166 **2. Geological background and field observations**

167 The orogenic growth of the Himalaya is defined by overall in-sequence development of
168 the orogen-scale fault systems which broadly define the morphotectonic sectors of the orogen
169 (Fig. 1b). Notable among those sectors, the Higher Himalaya is bordered by the MCT in the
170 south and is comprised of high-grade metasediments (Haimanta Formation), Higher Himalayan
171 Crystalline Sequence (HHCS), and Ordovician granite intrusives (Yin and Harrison, 2000). The
172 Low-grade metasediments (quartzites, phyllites, schists, slates) of the Proterozoic Lesser
173 Himalayan sequence are exposed between the MCT in the north and MBT in the south. The
174 Lesser Himalayan domain is narrow (4-15 km) in the NW Himalaya except where it is exposed
175 within tectonic windows (Kishtwar window, Kullu-Rampur window etc.) (Steck, 2003). The
176 Sub-Himalayan fold-and-thrust belt lying to the south of the MBT is tectonically the most active
177 sector since the late Quaternary (Thakur et al., 2014; Vignon et al., 2016).

178 Near the southwest corner of our study area, Proterozoic low-grade Lesser Himalayan
179 metasediments are thrust over the Tertiary Sub-Himalayan sediments along the MBT (Wadia,

1934; Thakur, 1992). Near the Chenab region, Apatite U-Th/He ages suggest that cooling and exhumation related to faulting along the MBT thrust sheet initiated before ~5 ± 3 Myr (Kumar et al., 1995). Geomorphic data obtained across the MBT in Kashmir Himalaya suggest that MBT has not been reactivated for the last 14-17 ky (Vassallo et al., 2015). In the NW Himalaya, the Lesser Himalayan sequence (LHS) exposed between the MBT and the MCT is characterized by a < 10 km-wide zone of sheared schists, slates, quartzites, phyllites and Proterozoic intrusive granite bodies (Bhatia and Bhatia, 1973; Thakur, 1992; Steck, 2003). The LHS is bounded by the MCT shear zone in the hanging wall. The MCT hanging wall forms highly deformed nappe exposing lower and higher Haimantas, which are related to the Higher Himalayan Crystalline Sequence (HHCS) (Fig.2a) (Bhatia and Bhatia, 1973; Thakur, 1992; Yin and Harrison, 2000; Searle et al., 2007). Nearly 40 km NE of the frontal MCT shear zone, the MCT fault zone is re-exposed in the vicinity of KW and is called the Kishtwar Thrust (KT) (Ul Haq et al., 2019) (Fig. 1a, 2b). Within the KW, Lesser Himalayan Rampur quartzites (Fig.2c), low-grade mica schists and phyllites along with the granite intrusives are exposed (Steck, 2003; DiPietro and Pogue, 2004; Yin, 2006; Gavillot et al., 2018).KW exposes a stack of LHS nappes in the footwall of the MCT (in this case, KT) which is related to the Lesser Himalayan Duplex (LHD), characteristic of the central Himalaya (Decelles et al., 2001). Regionally balanced cross-sections (DiPietro and Pogue, 2004; Searle et al., 2007; Gavillot et al., 2018) suggest that the Himalayan wedge is bounded at the base by a low-angle décollement, namely as the MHT. Sub-surface structural formations beneath the KW is not well-constrained. A recent study by Gavillot et al. (2018) propose the existence of two mid-crustal ramp segments beneath the KW, viz., MCR-1 and MCR-2 (Fig. S2). Based on thermochronological constraints, Gavillot et al. (2018) and Kumar et

al.~~,~~ (1995)~~,~~ proposed that the core as well as the western margin of the window ~~-~~exhumed with rates ~ 3.2-3.6 mm/y during the Quaternary, at a higher rate when compared to the surroundings.

The Higher Himalayan sequence dips steeply away from the duplex (~65° towards west) (Fig.2a). The frontal horses of the LH duplex expose internally-folded greenschist facies rocks. Although at the western margin of the duplex, the quartzites stand sub-vertically (Fig.2b), the general dip amount reduces as we move from west to east for the next ~10-15 km up to the core of the KW. Near the core of the KW, we observed highly-deformed (folded and multiply-fractured) quartzite and granites at the core of the KW (Fig.2d, 2e). We also observed deformed quartz veins of at least two generations, as well as macroscopic white mica. Here, the River is also very steep and narrow; the rock units are also steeply-dipping towards the east (~55-65°) and are nearly isoclinal and strongly deformed at places (Fig.2f). Towards the eastern edge of the window, however, the quartzites dip much gently towards the east (~20-30°), and much lesser folding and faulting have been recognized in the field (Fig.2g).

The broad, 'U-shaped' valley profile near the town of Padder at the eastern margin of the KW is in contrast with the interior of the window (Fig.3a). At the core of the KW, the Chenab River maintains a narrow channel width and a steep gradient (Fig.3b). The E-W traverse of the Chenab River through the KW is devoid of any significant sediment storage. However, along the N-S traverse parallel to the western margin of the KW, beneath the Kishtwar surface, ~150-170m thick sedimentary deposits are transiently-stored over the steeply-dipping Higher Himalayan bedrock (Fig.3c). The height of the Kishtwar surface from the Chenab River is ~450m, which means ~280m of bedrock incision by the River since the formation of the Kishtwar surface. Along the N-S traverse of the River, epigenetic gorges are formed as a result of the damming of paleo-channel by the hillslope debris flow, followed by the establishment of a newer channel

path (Ouimet et al., 2008; Kothyari and Juyal, 2013). One example of such epigenetic gorge formation near the town of Drabshalla is shown in Fig.3d. Downstream from the town of Drabshalla, the River maintains narrow channel width (< 25 m) and flows through a gorge having sub-vertical valley-walls (Fig.3e). The tributaries originating from the Higher Himalayan domain form one major knickpoint close to the confluence with the trunk stream (Fig.3f). We have identified at least three strath surface levels above the present-day river channel, viz., T1 (280±5 m), T2 (170-175 m) and T3 (~120±5 m), respectively (Fig.3g). The first study on sediment aggradation in the middle Chenab valley (transect from Kishtwar to Doda town) was published by Norin (1926). He argued the sediment aggradation in and around the Kishtwar town is largely contributed by fluvioglacial sediments and the U-shaped valley morphology is a marker of past glacial occupancy. In general, we agree with the findings of Norin (1926) and Ul Haq et al., (2019) as we observe ~100m thick late Pleistocene fluvioglacial sediment cover unconformably overlying the Higher Himalayan bedrock, most likely to be paleo-strath surface (Fig.4b). At the same time, we do not agree with the interpretation of surface-breaking faults near Kishtwar town by Ul Haq et al. (2019). We inspected the proposed fault locations in detail and didn't find any indication of fault movement, including offset, broken and rotated clasts, fault gouges etc. on the proposed fault planes. Therefore, we refute the existence of such surface-breaking faults. The fluvioglacial sediments included alternate layers of pebble conglomerate and coarse-medium sand (Fig.4c). The pebbles are moderately rounded and polished suggesting significant fluvial transport. Our field observations suggest that the fluvioglacial sediments have been succeeded by a significant volume of hillslope debris (Fig.4c). The thickness of the debris-flow deposits is variable. The hillslope debris units contain mostly coarse-grained, highly-angular, poorly-sorted quartzite clasts from the frontal horses of the Lesser Himalayan Duplex.

The hillslope debris units also contain a few fine-grain sediment layers trapped in between two coarse-grained debris layers (Fig.4e). The town of Kishtwar is situated on this debris flow deposit.

3. Methods of morphometric analysis and field data collection

3.1.Morphometry

For conducting the morphometric analysis, we have used 12.5m ALOS-PALSAR DEM data (high resolution terrain-corrected) (Fig.5a). This DEM data has lesser issues with artifacts and noises than 30m SRTM data, which fails to capture the drainage network properly in areas populated by narrow channel gorges. We compiled the topographic relief over a circular moving window of 4 km diameter (Fig.5b) and the rainfall distribution of the Chenab region (Fig.5c). The rainfall distribution is adapted from 12-year-averaged annual rainfall data from TRMM database (Bookhagen and Burbank, 2006).

3.1.1. Basinwide normalized steepness indices

Global observations across a broad spectrum of tectonic and climatic regimes have revealed a power-law scaling between the local river gradient and upstream contributing area:

$$S = k_s . A^{-\theta} \quad (1)$$

where S is the stream gradient (m/m), k_s is the steepness index ($m^{2\theta}$), A is the upstream drainage area (m^2), and θ is the concavity index (Flint, 1974; Whipple and Tucker, 1999). Normalized steepness-index values (k_{sn}) are steepness indices calculated using a reference concavity value (θ_{ref}), which is useful to compare steepness-indices of different river systems (Wobus et al., 2006). We extracted the k_{sn} values in the study area using the ArcGIS and

MATLAB-supported Topographic Analysis Toolkit (Forte and Whipple, 2019) following the procedure of Wobus et al. (2006). We performed an automated k_{sn} extraction using a critical area of 10^6 m^2 for assigning the channel head, a smoothing window of 500 m, a θ_{ref} of 0.45, and an auto-k_{sn} window of 250 m for calculating k_{sn} values. Stream-specific ksn values in and around the KW are drafted in Supplementary Fig.S3. The catchments were delineated by using a maximum threshold of 200 sq. km, so that the basins we pick are smaller in size. The stream-specific k_{sn} values were rasterized in ArcGIS and were extrapolated to the respective catchments using the zonal statistics toolbox. Basinwide mean k_{sn} values for the delineated watersheds are portrayed in Fig.5d.~~The slope-breaks, known as the knickpoints (sometimes referred to as knickzones if it is manifested by a series of rapids instead of a single sharp break in profile), were allocated by comparing the change of slope along the distance-elevation plot (Fig.2a). The threshold 'dz' value (projected stream offset across a knickpoint) for this study is 30m.~~ Basinwide mean k_{sn} values are plotted using a ~~1000~~500 km^2 threshold catchment area (Fig. ~~3a~~2d).

A 50-km-wide swath profile along line AB (cf.Fig.5a) show variation in elevation, mean annual rainfall and mean k_{sn} values in the area (Fig.2e).

~~Identification of the knickpoints/ knickzones and their relationship with the rock types as well as with existing structures are necessary to understand the causal mechanism of the respective knickpoints/ knickzones. Knickpoints/(zones) can be generated by lithological, tectonic and structural control. Lithological knickpoints are stationary and anchored at the transition from the soft-to-hard substrate. The tectonic knickpoints originate at the active tectonic boundary and migrate upstream with time. Structural variations, such as ramp-flat geometry of any emerging thrust may cause a quasistatic knickpoint at the transition of the flat-to-ramp of the~~

~~fault. In such cases, the ramp segment is characterized by higher steepness than the flat segment and often the ramp is characterized by a sequence of rapids, forming a wide knickzone, instead of a single knickpoint.~~

3.1.2. Drainage network extraction

The drainage network and the longitudinal stream profiles were extracted using the Topographic Analysis Kit toolbox (Forte and Whipple, 2019). An equivalent of ~~10~~20-pixel smoothing of the raw DEM (250 m smoothing window) data has been applied to remove noises from the DEM (Fig.6). The longitudinal stream profile of the Chenab trunk stream was processed with the Topotoolbox 'Knickpointfinder' tool (Schwanghart and Scherler, 2014). Several jumps/ kinks in the longitudinal profile are seen and those are marked as knickpoints (Fig.~~2a~~6). A 30m tolerance threshold was applied to extract only the major knickpoints. Results from knickpointfinder tool were rechecked with chi vs. elevation distribution (Supplementary Fig.S4). Identification of the knickpoints/ knickzones and their relationship with the rock-types as well as with existing structures are necessary to understand the causal mechanism of the respective knickpoints/ knickzones. Knickpoints/(zones) can be generated by lithological, tectonic and structural control. Lithological knickpoints are stationary and anchored at the transition from the soft-to-hard substrate. The tectonic knickpoints originate at the active tectonic boundary and migrate upstream with time. Structural variations, such as ramp-flat geometry of any emerging thrust may cause a quasistatic knickpoint at the transition of the flat-to-ramp of the fault. In such cases, the ramp segment is characterized by higher steepness than the flat segment and often the ramp is characterized by a sequence of rapids, forming a wide knickzone, instead of a single knickpoint.

Longitudinal profile of the entire Himalayan traverse of the Chenab River show oversteepening across the KW (Fig.6), therefore, we focused on that segment (marked by red rectangle, cf. Fig.6) for further analysis. Longitudinal profile of the selected segment is shown in Fig.7a.

3.1.3. ~~Basinwide normalized steepness indices~~

~~Global observations across a broad spectrum of tectonic and climatic regimes have revealed a power-law scaling between the local river gradient and upstream contributing area:~~

$$S = k_s . A^{-\theta} \quad (1)$$

~~where S is the stream gradient (m/m), k_s is the steepness index ($m^{2\theta}$), A is the upstream drainage area (m^2), and θ is the concavity index (Flint, 1974; Whipple and Tucker, 1999). Normalized steepness index values (k_{sn}) are steepness indices calculated using a reference concavity value (θ_{ref}), which is useful to compare steepness indices of different river systems (Wobus et al., 2006). We extracted the k_{sn} values in the study area using the ArcGIS and MATLAB-supported Topographic Analysis Toolkit (Forte and Whipple, 2019) following the procedure of Wobus et al. (2006). We performed an automated k_{sn} extraction using a critical area of 10^6 m^2 for assigning the channel head, a smoothing window of 500 m, a θ_{ref} of 0.45, and an auto k_{sn} window of 250 m for calculating k_{sn} values. The slope breaks, known as the knickpoints (sometimes referred to as knickzones if it is manifested by a series of rapids instead of a single sharp break in profile), were allocated by comparing the change of slope along the distance-elevation plot (Fig.2a). The threshold 'dz' value (projected stream offset across a knickpoint) for this study is 30m. Basinwide mean k_{sn} values are plotted using a 1000 km^2 threshold catchment area (Fig. 3a).~~

~~Identification of the knickpoints/ knickzones and their relationship with the rock types as well as with existing structures are necessary to understand the causal mechanism of the respective knickpoints/ knickzones. Knickpoints/(zones) can be generated by lithological, tectonic and structural control. Lithological knickpoints are stationary and anchored at the transition from the soft-to-hard substrate. The tectonic knickpoints originate at the active tectonic boundary and migrate upstream with time. Structural variations, such as ramp-flat geometry of any emerging thrust may cause a quasistatic knickpoint at the transition of the flat-to-ramp of the fault. In such cases, the ramp segment is characterized by higher steepness than the flat segment and often the ramp is characterized by a sequence of rapids, forming a wide knickzone, instead of a single knickpoint.~~

3.1.4. Channel Width

Channel width is a parameter of assessment of lateral erosion/incision through bedrocks of equivalent strength (Finnegan et al., 2005; Turowski, 2009). The channel width of the Chenab trunk stream within the elevation range of 600 to 2200 m above the MSL was derived by manual selection and digitization of the channel banks using the Google Earth Digital Globe imagery (http://www.digitalglobe.com/) of minimum 3.2 m spatial resolution. We used the shortest distance between the two banks as the channel width and~~. We~~ rejected areas having largely unparallel channel-banks as that would bias the result. We used a ~~50~~ 100 m step between two consecutive points for channel width determination. ~~Twenty~~ Ten point-averaged channel width data along with elevation of the riverbed is shown in Fig.7b.

Variations in channel gradient and k_{sn} values along the longitudinal profile of the selected stretch are shown in Fig.7c and 7d, respectively.

3.1.5. Specific stream power (SSP) calculation

Specific stream power has often been used as a proxy of fluvial incision or differential uplift along the channel (Royden and Perron, 2013; Whipple and Tucker, 1999). Areas of higher uplift/incision are characterized by a transient increase in the specific stream power. Channel slope and channel width data were used to analyze the corresponding changes in the specific stream power (SSP) from upstream of the gorge area to the gorge reaches (Bagnold, 1966). The SSP (ω) was estimated using the following equation –

$$\omega = \gamma . Q . s / w \qquad \text{(Eq. 1)}$$

Where, γ - unit weight of water, Q – water discharge, s – energy slope considered equivalent to the channel slope; w – channel width. With the available TRMM data, we argue that the rainfall distribution in the study area is almost uniformly low (<1.5 m/y) (Fig.5c and 5e) and therefore, we assumed a uniform discharge (Q) for SSP calculation. SSP data from selected stretches (stretch 1 and stretch 2, cf. Fig.8a) are shown in Table 1.

3.2. Field data collection

3.2.1. Structural data

We measured the strike and dip of the foliations and bedding planes of the Lesser and Higher Himalayan rocks using the Freiberg clinometer compass. We took at least five measurements at every location, and the average has been reported in Fig. ~~4a~~8a. Field photos in Fig.2 ~~support~~ document the observed variations in the structural styles.

3.2.2. Rock strength data

Recording rock strength data in the field is essential to understand the role of variable rock-type and rock-strength in changes in morphology. It provides us vital insights on the genesis of knickpoints, whether they are lithologically-controlled or not. It also helps to

understand the variations in channel steepness across rocks of similar lithological strength. We systematically measured the rock strength of the major geologic units using a hand-held rebound hammer. Repeated measurements (8-10 measurements at each of the ~~96~~ 75 locations throughout the study area) were conducted to measure the variability of rock-strength within the major lithologic units. All the measurements were taken perpendicular to the bedding/ foliation plane, and no measurements are from wet surfaces or surfaces showing fractures. Each reading was taken at least 0.5m apart from the previous one. Average rock strength data collected from each of the test locations are plotted against the longitudinal river profile and channel width data in Fig.7e. Our data from individual sites are smaller in number than what is preferred for checking the statistical robustness of Schmidt hammer data (Niedzielski et al., 2009). Therefore, we combined the data from all sites representing similar lithology and portrayed the mean ±standard deviation for the same.

3.3. Luminescence dating of transiently-stored sediments in and around Kishtwar

Luminescence dating of Quaternary fluvial sediments is a globally accepted method for constraining the timing of deposition of sediments in a drainage system (Aitken, 1992; Olley et al., 1998; Wallinga et al., 2001; Cunningham and Wallinga, 2012). Although there exists a few persistent problems in luminescence dating of the Himalayan sediments (including low sensitivity of quartz and numerous cases of heterogeneous bleaching of the luminescence signal), studies over the past couple of decades have also provided an adequate control on Himalayan sedimentary chronology by using luminescence dating with quartz (Optically stimulated luminescence, OSL) and feldspar (Infra-red stimulated luminescence, IRSL). Earlier studies have reported sediment aggradation over the Higher Himalayan bedrocks in the Kishtwar valley (Norin, 1926; Ul Haq et al., 2019).

The samples for luminescence dating were collected in galvanized iron pipes. The pipes were opened in subdued red light (wavelength ~650 nm). The outer ~3 cm of sediment from both the ends of the pipe were removed to omit the possibility of exposure of the sample to daylight during collection. The removed portion was used for moisture content estimation and determination of Uranium (U), Thorium (Th), and Potassium (K) concentrations. The unexposed interior portion of the sample was further processed to obtain quartz and feldspar using standard procedures (e.g., Aitken, 1998). The portion was treated with a sufficient quantity of 1N HCl and 30% H_2O_2 to remove carbonates and organic materials, respectively. The sediments were then oven-dried at 45°C and sieved to obtain a size fraction of 90-150 μm. The quartz and feldspar were separated using Frantz isodynamic separator at a magnetic field of ~10,000 gauss and collected separately. Obtained quartz grains were etched with 40% HF for 80 minutes to remove alpha irradiated outer layer (~10 μm), followed by 37% HCl treatment for 20 minutes to dissolve fluorides formed during the previous step. The isodynamic separation procedure was repeated to remove any broken feldspar grain. However, even after repeating the last step twice, we were unable to eliminate the feldspar contamination from most of the samples thoroughly. Those samples are not suitable for OSL SAR protocol.

Samples K02 and K11 procured from the fine-grain layers of ~1-1.5m thickness, trapped within coarse, angular and poorly-sorted thick layers of clasts (identified as hillslope debris) were used for OSL (Optically stimulated luminescence) dating using Double SAR (Single Aliquot Regenerative) protocol (IRSL wash before OSL measurement) for equivalent dose estimation (Roberts, 2007). The test doses were set for 75 Gy, 225 Gy, and 450 Gy, respectively (Fig.5). The aliquots were considered for ED estimation only if: (i) recycling ratio was within 1±0.1, (ii) ED error was less than 20%, (iii) test dose error was less than 10%, and (iv)

recuperation was below 5% of the natural. For samples K16 and K17 (fluvial sand trapped above the T3 strath surface), the feldspar contamination was negligible. Therefore, the OSL SAR protocol was tried with test doses of 50 Gy, 100 Gy, and 150 Gy, respectively. Samples K16 and K17 returned highly scattered equivalent dose (De) estimates (over-dispersion > 30%) (cf. Table 2), and thus, both of them have been interpreted by the minimum age model (Bailey and Arnold, 2006). Sample K18 (from the silty clay layer found above the T1 strath surface in the wind gap of Maru River) (cf. Fig.9b) was saturated, and hence, we also provided the minimum age estimate for the same. The sample was exhausted after we performed OSL measurements. Therefore, we couldn't proceed towards feldspar dating with sample K18.

OSL dating for the three samples procured from the fluvio-glacial sediments showed saturation; therefore, we tried for IRSL (Infra-red stimulated luminescence) dating of feldspar for those three samples (K07-K09) using standard post infrared (pIR-IR) protocol (Buylaert et al., 2013), in which, the preheat temperature was 320°C for 60s. The samples were first stimulated at 50°C with IR diodes for 100s followed by IR stimulation at 290°C, and a violet-blue luminescence emission (395 ± 50 nm) was detected by PMT through the combination of optical filters, Corning 7-59 (4 mm) and BG-39 (2 mm). However, the samples showed significant saturation, possibly due to improper bleaching of the Post-IR IRSL signal. The IRSL signal is not saturated, suggesting it to be better bleached. We encountered a significant IRSL signal while testing the luminescence of hand-picked individual quartz grains, indicating a presence of feldspar inclusion within the quartz. We tried leaching with 40% HF for three times, which exhausted most of the separated quartz sample. Hence, we had to proceed with standard IR protocol (Preusser, F., 2003) using K-feldspar. The initial test dose for the samples was set for 150 Gy, and the rest of the runs were set for 375 Gy and 750 Gy, respectively (Fig.5). Fading

correction tests were done for two samples (K07 and K09), and the fading correction factors have been calculated using conventional methods after Huntley and Lamothe (2001). The over-dispersion values are less than 30% (cf. Table 2). Hence, Central Age Model (CAM) has been used for estimation of equivalent dose (De) (Bailey and Arnold, 2006) instead of RMM-based De estimation as prescribed by Chauhan and Singhvi (2011), useful for samples having higher over-dispersion.

The dose rate was estimated using online software DRAC (Durcan et al., 2015) from the data of Uranium (U), Thorium (Th) and Potassium (K) measured using ICP-MS and XRF (Table 2) in IISER Kolkata. The estimation of moisture content was done by using the fractional difference between the saturated vs. unsaturated sample weight. Shine curve, dose growth curve, and radial plots for De estimation obtained from the analysis of three representative samples: K07 (IRSL), K11 (OSL D-SAR) and K17 (OSL SAR) are shown in Supplementary Fig.S5.

4. Results

4.1.Field observations and measurements

The Chenab River has deeply incised the KW (Fig. ~~2a and 3c~~3a). The LH metasediments exposed within the KW are mainly composed of Rampur Quartzites (Fig.2b,2d) and phyllites~~.~~ with occasional schists in between. (Steck, 2003; Gavillot et al., 2018). The LHD has been suggested to be an asymmetric antiformal stack with a steeper western flank (dip: 70°/west) (Fig.~~4a~~8a). The KW is surrounded by rock units related to the Higher Himalayan high-grade metasedimentary sequence (HHCS), mainly garnet-bearing mica schists and gneisses (Fig.2a). Higher Himalayan rocks close to the western edge of the KW form a syncline with a southwest-

verging MCT at its' base. The KT, southern structural boundary of the window margin, accommodating the differential exhumation between the window ~~internal~~ and the surroundings – and it is expressed as highly deformed sub-vertical shear bands (Fig.2b).

Along the traverse of the Chenab River through the window and further downstream, two prominent stretches of ~20 and ~25-30 km length have been identified where the channel gradients are high (Fig.7c), and we observed a sequence of rapids (~~f~~Fig. ~~S5~~Fig.3a,3e). These steep segments are also characterized by a very narrow channel width (< 30m) (~~fig.~~Fig. ~~S8~~7b). These two steepened segments define knickzone rather than a single knickpoint. We refer to the knickzone at the core of the window as K1 and the one downstream from the KW as K2 (Fig.6, 7). The knickzones are hosted over bedrock gorges, and field evidence confirms that none of them (downstream from the eastern edge of the KW) are related to damming by landslides or other mass movements. The east~~ern~~ margin of the KW is characterized by a broad 'U-shaped' valley filled with thick sand layers and coarser fluvioglacial sediments. The ~~river~~ River incises through this Late Pleistocene fill at present (~~*f*~~*Fig.* ~~S4~~Fig.3a).

The rock strength data taken along the Chenab River shows large variations ~~(R-value ranging from 28 to 62)~~ across different ~~morphotectonic segments~~rock types (Fig.7e). Within the KW, Lesser Himalayan phyllites and schists have low R values (30-35); however, the low-strength schists and phyllites are sparsely present and therefore, they were ignored while plotting the regional rock strength values in Fig.7e. The dominant Rampur quartzites in the KW, as well as the granitic intrusives in the eastern part of the KW, shows very high R values of ~~-~~ 51±4 and 58±2, respectively (Fig.7e). Compared to the high R values in the KW, the Higher Himalayan ~~rocks~~ migmatites near the KT (western margin of the KW) show ~~low~~ moderate strength (R: ~~35-45~~49±5)~~-~~ whereas, the HHCS units show lower strength (R: 39±3)~~till the point L2 (*Fig. 3b*)~~. The

rock strength increases (R: ~~45-50~~44±2) within the Haimanta Formation until it reaches the MCT shear zone. The R-value in the frontal Lesser Himalaya is moderate (R: ~~40-45~~41±2).

~~The Higher Himalayan sequence dips steeply away from the duplex (~65° towards west) (fFig. S10). The frontal horses of the LH duplex expose internally folded greenschist facies rocks. Although at the western margin of the duplex, the quartzites stand sub-vertically, the general dip amount reduces as we move from west to east for the next ~10-15 km (*Fig. 4a*). Near the core of the KW, we observed deformed quartz veins of at least two generations, as well as macroscopic white mica. Near the core of the window, where the rRiver is also very steep and narrow, the rock units are also steeply-dipping towards the east (~60-65°) and are extremely nearly isoclinal and vigorously deformed at places (*fig. S14, S15*). Towards the eastern edge of the window, however, the quartzites dip much gently towards the east (~25-30°) and much lesser folding and faulting have been recognized in the field.~~

~~The E-W traverse of the Chenab river is completely devoid of any sediment storage. However, along the N-S traverse parallel to the western margin of the KW, The town of Kishtwar is situated on this debris flow deposit (fFig. S17). Along the N-S traverse of the Chenab, we have observed at least two epigenetic gorges lying along the main channel (fFig. S18). The active channel has incised the Higher Himalayan bedrock and formed strath surfaces.~~

4.2. Results from morphometric analysis

4.2.1. Steep stream segments and associated knickpoints

The longitudinal stream profile along the Chenab River does not portray a typical adjusted concave-up profile across the Himalaya (Fig. ~~2a~~6,7a). We observed breaks in slope and concavity at least at six occasions within a ~~150~~ 170 km traverse upstream from the MBT (point A, cf. Fig.1a) (Fig.7a). These breaks are defined as knickpoints or knickzones, depending on

their type characteristics. The slope breaks represent the upstream reaches of the steep stream segments. The basinwide steepness indices span from ~30- >~~750~~ 550 $m^{0.9}$ across the study area (Fig. ~~3a~~5d). We assigned a threshold value of k_{sn}>~~650~~ 550 for the steepest watersheds/ stream segments. Along the traverse, the major knickpoints are L1 (~1770m), K1 (~1700m), K2 (~1150m), K3 (~950m), ~~and~~ L2 (~~800m~~750m) and D1 (~700m) respectively (Fig.~~2a~~7a).

Already Nennewitz et al.~~,~~ (2018) had proposed a high basin-averaged k_{sn} value of > 300 in the KW. Here in this study, we worked with a much-detailed DEM ~~and~~ for stream-specific k_{sn} allocation (~~f~~Fig. ~~S3~~Fig.5d), as well as a basinwide steepness calculation with smaller watersheds. Our results corroborate with the earlier findings~~, but predicts the zone of interest in greater detail~~. It is important to note that by setting a higher tolerance level in the 'knickpointfinder' tool in Topotoolbox, we have managed to remove most of the DEM artifacts from consideration (Schwanghart and Scherler, 2014).

4.2.2. Channel width and valley morphology

The channel width of the Chenab river is on average low (30-60m) within the core of the KW (Fig. ~~3b~~7b), and the low channel width continues till the Chenab River flows N-S along the western margin of the KW. However, there are a few exceptions; upstream from the knickpoint L1 in the Padder valley (in which the town of Padder is located), the channel widens (width ~80-100m), and the channel gradient is low (Fig. 3a,~~2a~~7b,7c). The second instance of a ~~wider~~ broader channel is seen upstream from knickpoint K2, where there is a reservoir for the Dul-Hasti dam (Fig.7b~~fig. S7~~). Downstream from K2 within the Higher Himalaya, the channel width ranges from 50-70 m. However, towards the lower stretches of the N-S traverse, the width is even lower (16-52m). The river width increases to 100-200m as Chenab River takes a westward path after that. The river width increases beyond 300m until it leaves the crystalline rocks in the hanging

wall of the MCT and enters the Lesser Himalaya in the hanging wall of the MBT across the Baglihar dam. Within the frontal LH, the channel width is again lowered (50-80 m).

~~We have also drawn topographic swath profiles across the Chenab River, which represents the shape of the valley at four different morphotectonic domains (*Fig.3c*). While section 1 representing the upstream segment of the MCT hanging wall (E-W traverse of the rRiver) shows an 'open' 'V-shaped' profile, the shape of the valley at location 2 across the N-S traverse of the rRiver shows an acute 'V-shaped' channel morphology. The similar strongly-incised channel is seen at the core of the KW (location 3) and location 4 in the Padder valley, where the valley becomes 'U-shaped.'~~

4.2.3. Changes in specific stream power (SSP)

Discharge-normalized SSP data calculated from the upstream stretches and the knickzones, K1 and K2, show a ~~major~~ significant increase in SSP within the steep knickzones. The rise in SSP from upstream to the knickzones K1 and K2 ~~are~~ is 4.44 and 5.02 times, respectively (Table 1). Such a high increase in SSP is aided by the steepening of channel gradient and narrowing of the channel ~~bed~~.

4.3. Luminescence chronology

The results for the luminescence chronology experiment are listed in Table 2 and the shine curve, dose growth curve and De estimation plots for different samples are provided in the supplementary Fig.S3. Sample K07, K08 and K09 yield IRSL ages of 104.5±5.9 ky, 114.4±6.3 ky, and 119.2±6.8 ky, respectively. Fading corrections done for samples K07 and K09 yield the correction factors (g%) of 0.89 and 1.11, respectively. The sample K08 has not been treated for fading correction. Still, for easier understanding, we have assumed a constant sedimentation rate between the samples K07 and K09 and extrapolated the 'fading-corrected' age for K08. The

oldest sample K09 (132±7 ky) (fading-corrected IRSL age) is succeeded by samples K08 (126±6 ky) and K07 (113±6 ky), respectively (Fig.4c). The initial IRSL ages (before fading-correction), therefore, may be regarded as a minimum age estimate for the fluvioglacial sediment sequence. The finer fraction of the hillslope debris overlying the fluvioglacial deposits yields OSL ages of 81.1±4.6 ky (K02) and 85±5 ky (K11) (Fig.4d, 4e). OSL samples taken from sparsely-preserved sediment layers above the T3 strath surface show heterogeneous bleaching, and hence we provide a minimum age of 22.8±2.1 ky (sample K16) and 20.5±1.0 ky (sample K17). One sample taken above the T1 strath level is saturated and shows a minimum age of 52.1±2.8 ky (sample K18) (Table 2).

5. Discussions

Morphometric parameters are widely used as indicators of active tectonics and transient topography (Hack, 1973; Kirby and Whipple, 2012; Seeber and Gornitz ~~,~~ (1983~~)~~). Many studies have used morphometry as a proxy for understanding the spatial distribution of active deformation across ~~certain~~ specific segments of the Himalayan front (Malik and Mohanty, 2007; van der Beek et al., 2016; Nennewitz et al., 2018; Kaushal et al., 2017). More importantly, some studies have integrated morphometric analysis with rigorous chronological constraints to assess the spatial and temporal variability in deformation within the Sub-Himalaya (Lave and Avouac, 2000; Thakur et al., 2014; Vassalo et al., 2015; Dey et al., 2016; Srivastava et al., 2018). In this section, we discuss how we combined terrain morphometry and Quaternary dating of sediments to evaluate ongoing deformation in the interior of the NW Himalaya.~~All these studies have shown that morphometric indicators can also be used for a qualitative estimate of changes in~~

~~uplift rate or spatial variations of deformation, even in the Sub-Himalayan domain where the rivers are often alluviated due to high sediment load (Malik and Mohanty, 2007). Therefore, using morphometric indices to examine some prospect areas and using their relative difference as a proxy of relative changes in faulting and differential uplift as well as connecting these regions with nearby regions having chronological constraints on short-intermediate timescale deformation, is a potent option, when applied carefully.~~

~~The KW exhibits younger~~ Apatite fission-track cooling ages at the center of the LH duplex and along the western margin of the KW are younger (~2-3 Ma) as compared to the surrounding Higher Himalaya. Young AFT cooling ages have been interpreted as the result of rapid exhumation of the LH duplex over million-year timescale (Kumar et al., 1995; Gavillot et al., 2018). However, to date, we lack any estimate of deformation on the 10^3-10^5-year timescale. ~~With the existing AFT data and assuming that no major changes of the deformation regime have taken place since the Quaternary, we may well use it for calibration of morphometric proxies and interpolate these estimates to regions, where no thermochronological constraint exists.~~ Thus, we have come up with a detailed morphometric analysis of the terrain and structural data to decipher the spatial distribution of faulting and fault patterns. With additional chronological constraints from late Quaternary sedimentary deposits, we predict rapid fluvial bedrock incision in the Himalayan interiors.

5.1. Knickpoints and their genesis

Already Seeber and Gornitz (1983) showed that the Chenab River is characterized by a zone of steep channel gradient in the vicinity of the KW. Thiede and Ehlers (2013) demonstrated a strong correlation between steeped longitudinal river profiles and young thermochronological

cooling ages, suggesting ~~recent~~ focused rock uplift and rapid Quaternary exhumation along many major rivers draining the southern Himalayan front. Although, it is still an open debate whether uplift and growth of the LHD are triggered solely by slip over the crustal ramp of the MHT or additional out-of-sequence surface-breaking faults are augmenting it (Avouac et al., 2001; Herman et al., 2010; Elliot et al., 2016; Whipple et at., 2016).

The longitudinal profile of the lower Chenab traverse (below ~2000 m above MSL) is punctuated by two prominent stretches of knickpoint zones (Fig.~~2a~~7a). Below we will discuss the potential cause of formation of those major knickpoints in the context of detailed field observation, of existing field-collected structural and lithological data, geomorphic features, rock strength, and channel width information (*Fig.3b*).

5.1.1. Lithologically-controlled knickpoints

The Himalayan traverse of the Chenab River is characterized by large variations in substrate lithology and rock strength (Fig.~~1~~7a~~, Fig.2a~~). These variations have inflicted their 'marks' on the river profile. An instance of soft-to-hard substrate transition happens across the knickpoint L1, lying downstream from the Padder valley, at the eastern edge of the KW (Fig.~~2a~~3a, 7). Across L1, the ~~river~~ River enters the LH bedrock gorge (R value> ~~50~~55) after exiting the Padder valley filled with unconsolidated fluvioglacial sediments (Fig.3a~~fig. S4~~). A similar soft-to-hard substrate transition is observed upstream from the MCT shear zone. The corresponding knickpoint L2 represents a change in lithological formation from the sheared and deformed Higher Himalayan crystalline (R value~35-40) to deep-seated Haimantas (R value~40-50) (Fig.7a). There is no field evidence, such as fault splays or ramps, in support of L2 to be a structurally-controlled one.

5.1.2. Tectonically-controlled knickpoints

Compiling previously-published data on regional tectonogeomorphic attributes (Gavillot et al., 2018) with detailed field documentation of structural styles and tectonic features, we have deciphered the role of rock-uplift and variable structural styles in the interiors of the NW Himalaya. We have found at least two instances where knickpoints are not related to change in substrate, nor are they artificially altered.

The knickzone K1 (~1700 m above MSL) represents the upstream reach of a steepened stream segment of run-length ~18-20 km. The upstream and downstream side of K1 is characterized by a change in the orientation (dip angle) of the foliation of the LH bedrock (Fig.2f, 2g~~Fig. 4a~~). Across K1, the dip amount of the foliation planes change from ~25-30° to ~60-65° (both cases dip towards east). K1 also reflects a narrowing of the channel width (Fig. ~~3b~~7b) and an increase in channel gradient (Fig.7c) and ksn value (Fig.7d). ~~The steep segment exhibits a narrower channel through the core of the LH duplex.~~ Near the end of the steep segment, we observed intensely-deformed (folded and fractured) LH rocks (Fig.2d, 2e~~fig. S14~~). We explain this as evidence of faulting within the LH duplex and the steep stream segment represents the ramp of the fault or fault zone between two duplex nappes (Fig.8d). K1, therefore reflects the transition from flat to ramp of the existing structure soled to the basal decollement. The steep segment represents a drop of ~420m of the Chenab River across a run-length of ~20 km (Fig.8c). In addition to this, we may comment that the schists and phyllites within the Lesser Himalayan sequence probably act as the basal planes of the thrust nappes.

On the other hand, the other knickpoint K2 nearly coincides with the exposure of the KT (Fig.~~2a~~7a). K2 cannot be a lithologically-controlled knickpoint as it reflects no significant change in substrate hardness, at least not a soft-to-hard substrate transition. LH quartzites (R value: 51±4) and HH migmatites (R value: 49±5) have similar rock hardness (cf. Fig.7e).

However, in the longitudinal profile, K2 does not represent a sharp slope break because the downstream segment runs parallel for ~25-30 km and not perpendicular to the orientation of all major structures of the orogen, including the KT. Therefore, we performed an orthogonal projection of the E-W trending traverses of the Chenab River and tried to estimate an orogen-perpendicular drop of the Chenab across K2 (Fig. ~~2c~~8d). The truncated profile across K2 shows a drop of ~230m of the channel across an orogen-perpendicular run-length of ~5 km. The orogen-parallel stretch of the ~~river~~ River exhibits narrow channel width (<30-35m) through ~~a moderately~~moderately hard HH bedrock (R-value: 35-45). The tributaries within this stretch form significant knickpoint at the confluence with the trunk stream (Fig. 3f~~fig. S6~~). These pieces of evidence hint towards a rapid uplift of the HH rocks ~~near~~ along the western margin of the KT and are possibly related to the presence of another crustal ramp emerging from the MHT (Fig.~~4b~~8b).

Both the knickzones, K1 and K2 portray transiently-high specific stream power values (Table 1), which we relate to the fact that the knickzones are undergoing much rapid fluvial incision than the rest of the study area. If we consider the fluvial incision as a proxy of relative uplift (assuming a steady-state), we may well say that the knickzones define the spatial extent of the areas undergoing differential uplift caused by movement on the fault ramps.

5.1.3. Knickpoint marking epigenetic gorge

Epigenetic gorges are common geomorphic features in the high-mountain landscape (Ouimet et al., 2008). Epigenetic gorges form when channels of a drainage system are buried by sediment aggradation and during subsequent re-incision, a new river channel is incised. The N-S traverse of the Chenab River is largely affected by hillslope sediment flux from the steep eastern flank. The knickpoint K3 situated near the village of Janwas, mark one such instance of

685 epigenetic gorge where the paleo-valley has been filled initially by fluvioglacial sediments and
686 the channel abandonment was caused by hillslope debris flow ~80 ky (Fig.4b, 4c).

687 **5.2. Sediment aggradation in the Chenab valley**

688 The luminescence chronology of the transiently-stored sediments in the Chenab valley
689 point towards protracted sediment aggradation since the onset of the last glacial-interglacial
690 cycle till ~80 ky. Fluvioglacial outwash sediments range from ~110-130 ky, whereas the
691 hillslope debris range from ~90 to ~80 ky (cf. Fig.4). The obtained chronology of the sediment
692 deposits match well with the relative stratigraphic order of the sedimentary units, and therefore,
693 we believe the obtained ages are reliable. The deeply-incised fluvial network as we observe
694 today require net fluvial incision and formation of bedrock strath surfaces sometime after ~80 ky
695 before present.

696

697 **5.3. Drainage re-organization and strath terrace formation along Chenab River**

698 Hillslope debris flow characterized by white quartzite blocks of different sizes and shapes
699 can only originate from the high-relief frontal horses of the Lesser Himalayan Duplex exposed in
700 the eastern flanks of the valley. These hillslope debris overlies the fluvioglacial sediments stored
701 beneath the Kishtwar surface (Fig.9a, 9c). We argue that the hillslope debris flow intervened in
702 the paleo-drainage of the Chenab River, which might have been flowing through an easterly path
703 than now (Fig.9). The Maru River, coming from the north-western corner of our study area, was
704 also joining the Chenab River at a different location (Fig.9). Our argument is supported by field
705 observation of the thick silt-clay layer in the proposed paleo-valley of the Maru River (Fig.9a,
706 9c). OSL sample (K18) from the silt-clay layer is saturated and hence only provides the
707 minimum age of 52±3 ky. We suggest that the hillslope sediment flux has ceased the flow of the

Chenab River and also propagated through the wind-gap of the Maru River. The decline in depositional energy has resulted in a reduction of grain-size. Post-hillslope debris flow episode, the Chenab River also diverted to a new path. The new course of the Chenab River upstream from the confluence with the Maru River is defined by a very narrow channel flowing through the Higher Himalayan bedrock gorge (Fig.9). Downstream from the confluence, we identified at least three levels of strath terraces lying at heights of ~280-290m (T1), ~170m (T2), and ~120m (T3), respectively (Fig.4g, 10a). Our field observation suggests that the formation of the straths is at least ~52 ky-old. The luminescence chronology samples in this study belong to the ~150-170m-thick soft sediments that are stored stratigraphically-up from the T1 strath level. Our field observations and chronological estimates suggest that the renewed path of the Chenab River must have been formed post the hillslope debris flow ~80-90 ky but before 52 ky.

5. 4. Rapid bedrock incision along Chenab River

Considering the rate of excavation of softer sediments to be at least an order of magnitude higher than the rate of bedrock incision (Ouimet et al., 2008; Kothyari and Juyal, 2013), we calculated the minimum bedrock incision rate using the height of the T1 strath (~280±5 m) and the average age of the sediments from the Hillslope debris flow deposit. It yields a minimum bedrock incision rate of ~3.1-3.5 mm/y over the last 80-90 ky. Considering the saturated OSL sample from the paleo-valley, we estimated the maximum bedrock incision since 52 ky to be 5.1-5.5 mm/y. Similarly, using the minimum age estimate of the T3 terrace abandonment, we deduce a maximum bedrock incision rate of ~5.7-6.1 mm/y since ~21 ky (Fig.10b).

Many studies have used dated strath surfaces to quantify rock uplift rates in the Himalaya (Wesnousky et al., 1999; Lave and Avouac, 2000; Mukul et al., 2007; Thakur et al., 2014). Assuming the channel hypsometry to be constant during the incision period, we may infer

the minimum fluvial incision reflects regional rock uplift caused by movement of rocks over the ramp of the MHT at a rate of ~3.1-3.5 mm/y. This minimum uplift rate estimate is in agreement with long-term exhumation rates of 3.2-3.6 mm/y deduced from the KW (Gavillot et al., 2018). The inferred uplift rate can be translated to a shortening rate by using a simple trigonometric function. Our field findings suggest that the larger ramp on the MHT (MCR-1) have an average near-surface dip of ~60˚. Considering a similar geometry for MCR-2, we obtained a minimum shortening rate of 1.8-2.0 mm/y. On the other hand, considering the minimum ages of T3 terrace abandonment, we obtained maximum uplift rates ~5.5-6.0 mm/y, which would translate into a shortening rate of ~3.2-3.5 mm/y since ~21 ky.

5.5. Our findings in context with the previously-published data

The young AFT-cooling ages by the pioneering work of Kumar et al., (1995) showcased a rapid exhumation of the KW (AFT ages: ~21-3 MaMy) compared to the surroundings (AFT age: 6-12 MaMy). The exhumation rates proposed by Gavillot et al. (2018) are based on using a geothermal gradient of 35-40˚C/km in Dodson's equation assuming a 1-D model (Dodson, 1973). Unfortunately, a Although proper thermal modeling is lacking in this regionof the region is lacking, therefore, regional correlation with the proposed cooling ages and exhumation rates have large uncertainties. However, Lateral lateral similarities of the regional topography and similar thermochronologic age patterns obtained along the Sutlej area, Beas and Dhauladhar Range (Thiede et al., 2017; Thiede et al., 2009; Stübner et al., 2018) have yielded 2-3 mm/y exhumation rates in the range of 2-3 mm/y. Long-term exhumation rates from the NW Himalaya agree well with the findings of Nennewitz et al. (2018). Their study recognized a strong correlation between who correlated the young thermochron ages with high basinwide k_{sn} values suggesting high uplift rates over intermediate to longer timescales. Therefore, the proposed range

of long-term exhumation rates of 3.2-3.6 mm/y determined by Gavillot et al.~~,~~ (2018) agree with the regional data pattern. Although the geomorphic implications on landscape evolution are valid for shorter timescales than the low-T thermochron studies, we must comment that our field observations and analysis support a protracted growth of the LH duplex exposed within the boundaries of the KW. Unless there has been a recent growth of the duplex, the geomorphic signatures would have been subdued. Young low-T thermochron ages (Kumar et al., 1995) had been sampled from the steepened stream reaches, where the SSP is high. Interestingly, exhumation rates obtained from the steepened stretches is ~ten times more than that of the Higher Himalaya in the hanging wall of the duplex. Our estimates of SSP also reflect an increase by ~five times within the steepened stretches.

Deeply-incised channel morphology, steep channel gradients marked by knickpoints at the upstream reaches in and around the KW could be explained by the presence of at least two orogen-parallel mid-crustal ramps on the MHT (Fig.~~4b~~8b). ~~Existence~~ The existence of two mid-crustal ramps ~~has~~ have already been suggested ~~in the balanced cross-section published~~ by Gavillot et al., (2018) (Fig.S2). However, the internal structural orientation of the LH duplex published by Gavillot et al., (2018) (~~fig~~Fig. S2) differ considerably from our field observations (Fig.2, Fig.8b~~Supplement 1, part 2~~). ~~We observe~~Our morphometric analysis and field observation indicate pronounced deformation at the core of the KW suggesting that this is related to active faulting or internal folding at the base of the steepened stretch of K1 ~~(fFig. S16)~~. The ramp of the fault-zone mentioned above triggers the rapid exhumation of the hanging wall. It causes high relief, steep channel gradients and higher basinwide steepness indices over the ramp (Fig.~~4a~~7). Similar ramps have been proposed on the MBT beneath the Dhauladhar Range (Thiede et al., 2017) and in the east of the NW Himalaya (Caldwell et al., 2013; Mahesh et al.,

2015; Stübner et al., 2018; Yadav et al., 2019). We don't have any direct field evidence of surface-breaking faults, which could be linked to the MCR-2. However, a rapid fluvial incision along the western margin of KW and an increase in morphometric parameter values (k_{sn}, channel gradient, topographic relief, etc.) probably justify the existence of MCR-2.

Our findings from the Kishtwar region of the NW Himalaya establish the importance of morphometric parameters in the assessment of intermediate timescales of 10^4-10^6 years. We can resolve variations in the tectonic imprint on landscape evolution by analyzing the topography with high-resolution DEM. Earlier studies used to process larger areas, but the resolution of those data and findings is coarse (Nennewitz et al., 2018).

Models explaining the spatial distribution of the high uplift zone in the interiors of the Himalaya favor the existence of a mid-crustal ramp, which has variable dimension, geometry, and distance from the mountain front along-strike of the Himalayan orogeny (Robert et al., 2009). Our data support the idea of mid-crustal ramps beneath the Higher Himalayan domain (Nennewitz et al., 2018) and we predict that the seismic hypocenters are clustered in the vicinity of the ramp of MHT and within the LHD and are linked to the ongoing growth of the duplex. Our results verify the previously-suggested models that there exist two orogen-parallel small ramps beneath the Kishtwar Window instead of one (Gavillot et al., 2018). However, we must also comment that the previous model, as well as the balanced cross-section, lack detailing and the thermochron data (Kumar et al., 1995) is sparse. Therefore, field observation and the detailed morphometric analysis using high-resolution DEM help to measure the spatial extent of deformation. We ~~are able to~~can resolve the high-relief Kishtwar Window and the surroundings into two major steep orogen-parallel belts/ zones (Fig. 4a). While the larger one is an active high-angle fault-ramp emerging from the MHT and causing sustained uplift in the core of the duplex,

the smaller one lies along the western margin of the KW. We suggest that this has two major implications. One, we have evidence for ongoing internal deformation of duplex, and that entire window is still ~~growing~~ tectonically-active – and therefore this could be a potential source future seismic activity. ~~Two, o~~Our finding contradicts with the existence of a single major ramp in the interiors of the Himalaya, as described from other sectors of the Himalaya (Gahalaut and Kalpna, 2001; Elliot et al., 2016; Thiede et al., 2017).

Nennewitz et al., (2018) have proposed that the million-year-timescale shortening achieved in the interior of the Himalaya near the Sutlej-Beas area in the eastern Himachal Pradesh is caused by accentuated rock uplift over a ramp at a mid-crustal depth of ~ 8-25 km on the MHT. In contrast, studies from the Dhauladhar Range in the north-western Himalaya hints the presence of deep-seated crustal ramp on the MBT and yielded a shortening rate of 3±0.5 mm/y across the MBT over the last 8 My and absence of mid-crustal ramp (Deeken et al., 2011; Thiede et al., 2017). The work by Gavillot et al. (2018) favors the existence of at least two mid-crustal ramps beneath the KW (Supplementary Fig.S2). Their suggestion is in agreement with very young AFT cooling ages (1-3 Ma) (Kumar et al., 1995) in the window (Fig.1a) and the findings of this study. These studies altogether point out the along-strike variation in the location of the rapidly-uplifting crustal ramp with respect to the southern Himalayan front. The crustal ramp in the nearby Kangra recess is located beneath the Dhauladhar Range at the main Himalayan front, whereas, in the Himalayan transects situated towards the east and west of Kangra recess, the ramps are located ~100km inside from the MBT. Topographic relief and basinwide mean k_{sn} distribution (Fig.5) hint towards the existence of a lateral ramp in between the Kangra and the Jammu-Kashmir Himalayan transects. However, at this moment, we have no

conclusive data in support of this claim. ~~This portrays along-strike variations in the geometry of the basal decollement (MHT) in the Himalaya, in agreement with earlier findings.~~

6. Conclusions

Our field observation and the characteristics of terrain morphology match well with the spatial pattern of previously-published thermochronological data and unanimously indicate that the Kishtwar Window is undergoing active and focused uplift and exhumation at present, during intermediate timescales, and in geological past since at least the late Miocene. By compiling ~~all the~~our new results and published records, we favor the following conclusions:

1. The Chenab maintains an over-steepened bedrock channel and a low channel width irrespective of any lithological variations across the KW and beyond, suggesting ongoing rapid fluvial incision.
2. Our field observations, morphometric analysis, and rock strength measurements document that at least two of these major knickzones on the trunk stream are non-lithologic and preferably can be related to differential uplift of the rock units. The incision potential in the steepened stretches ~4-5 times higher than the surroundings.
3. The differential uplift is most-likely related to variations in the geometry of the basal decollement and out-of-sequence surface-breaking fault/s. Our results favor the presence of at least two mid-crustal ramps beneath the Kishtwar Window and the surroundings, as compared to a single crustal ramp proposed from interiors of the nearby sectors of the NW Himalaya.

4. The larger of the proposed crustal ramps emerge as an active high-angle ramp at the core of the Lesser Himalayan Duplex and causes sustained faulting and uplift of the hanging wall.

5. Luminescence chronology of the transiently-stored sediments along the Chenab River suggests that the valley had been overfilled with deposits of fluvioglacial origin as well as with hillslope debris flow. Massive sediment aggradation during ~130-80 ky led to drainage re-organization and bedrock incision, leaving behind a set of strath surfaces.

~~4.~~6. The late Quaternary bedrock incision rates on the mid-crustal ramp beneath the western margin of the KW are high 3.1-3.6 mm/y. We argue that this rapid fluvial incision can potentially be linked to the accommodation of crustal shortening along a mid-crustal ramp of the basal decollement of the Himalaya. Our results indicate a minimum shortening rate of ~1.8-2.1 mm/y being accommodated along the N-S traverse of the Chenab River.

~~To summarize, our new study reinforces the importance of detailed field observation and morphometric analysis in understanding the neotectonic framework of the interiors of the Himalaya.~~ Our study refutes the long-standing hypothesis of nearly 100% accommodation of crustal shortening within the Sub-Himalaya since late Pleistocene-Holocene time and provides new insights on the structural styles and ongoing out-of-sequence deformation in the Himalayan interiors.

Acknowledgments

This study is funded by the DST INSPIRE faculty fellowship program by the Department of Science and Technology, India (grant #DST/INSPIRE/04/2017/003278), and IIT Gandhinagar post-doctoral research fund (IP/IITGN/ES/SD/201718-01). Thiede is supported by German Science Foundation (grant # DFG TH 1317-8 and 9). We thank M.K.Jaiswal and M.Rawat for providing the XRF elemental analysis. We thank Shambhu Das, Avi Das, Niklas Schaaf, Akashsingh Rajput and Chamel Singh for their assistance during fieldwork. We also thank Soumyajit Mukherjee, Rahul Kaushal and Shantamoy Guha for scientific inputs and comments on this manuscript.

References

~~Ahnert, F. (1970). Functional relationships between denudation, relief, and uplift in large, mid-latitude drainage basins. American Journal of Science, 268(3), 243-263.~~

Aitken, M. J. (1992). Optical dating. Quaternary Science Reviews, 11(1-2), 127-131.

Bagnold, R. A. (1966). An approach to the sediment transport problem from general physics. US government printing office.

Bailey, R. M., & Arnold, L. J. (2006). Statistical modelling of single grain quartz De distributions and an assessment of procedures for estimating burial dose. *Quaternary Science Reviews*, *25*(19-20), 2475-2502.

Bhatia, T. R., & Bhatia, S. K. (1973). Sedimentology of the slate belt of Ramban-Banihal area, Kashmir Himalaya. Himalayan Geology, 3, 116-134.

Bollinger, L., Henry, P., & Avouac, J. P. (2006). Mountain building in the Nepal Himalaya: Thermal and kinematic model. *Earth and Planetary Science Letters*, *244*(1-2), 58-71.

Bookhagen, B., & Burbank, D. W. (2006). Topography, relief, and TRMM-derived rainfall variations along the Himalaya. Geophysical Research Letters, 33(8).

~~Bookhagen, B., Fleitmann, D., Nishiizumi, K., Strecker, M. R., & Thiede, R. C. (2006). Holocene monsoonal dynamics and fluvial terrace formation in the northwest Himalaya, India. *Geology*, *34*(7), 601-604.~~

Brozovic, N., & Burbank, D. W. (2000). Dynamic fluvial systems and gravel progradation in the Himalayan foreland. GSA Bulletin, 112(3), 394-412.

Burbank, D. W., Leland, J., Fielding, E., Anderson, R. S., Brozovic, N., Reid, M. R., & Duncan, C. (1996). Bedrock incision, rock uplift and threshold hillslopes in the north-western Himalayas. *Nature*, *379*(6565), 505.

Burgess, W. P., Yin, A., Dubey, C. S., Shen, Z. K., &Kelty, T. K. (2012). Holocene shortening across the Main Frontal Thrust zone in the eastern Himalaya. Earth and Planetary Science Letters, 357, 152-167.

Buylaert, J.P., Murray, A.S., Gebhardt, A.C., Sohbati, R., Ohlendorf, C., Thiel, C., Wastegård, S., Zolitschka, B. and Team, T.P.S., 2013. Luminescence dating of the PASADO core 5022-1D from Laguna Potrok Aike (Argentina) using IRSL signals from feldspar. *Quaternary Science Reviews*, *71*, pp.70-80.

Caldwell, W. B., Klemperer, S. L., Lawrence, J. F., and Rai, S. S., 2013, Characterizing the Main Himalayan Thrust in the Garhwal Himalaya, India with receiver function CCP stacking: Earth and Planetary Science Letters, v. 367, p. 15-27.

Chauhan, N., & Singhvi, A. (2011). Distribution in SAR palaeodoses due to spatial heterogeniety of natural beta dose. *Geochronometria*, *38*(3), 190-198.

~~Cortés-Aranda, J., Vassallo, R., Jomard, H., Pousse-Beltrán, L., Astudillo, L., Mugnier, J. L., Jouanne, F., Malik, M., & Carcaillet, J. (2018). Late quaternary out-of-sequence deformation in the innermost Kangra Reentrant, NW Himalaya of India: Seismic potential appraisal from 10Be dated fluvial terraces. Journal of Asian Earth Sciences, 158, 140-152.~~

Cunningham, A. C., & Wallinga, J. (2012). Realizing the potential of fluvial archives using robust OSL chronologies. *Quaternary Geochronology*, *12*, 98-106.

DeCelles, P. G., Robinson, D. M., Quade, J., Ojha, T. P., Garzione, C. N., Copeland, P., and Upreti, B. N., 2001, Stratigraphy, structure, and tectonic evolution of the Himalayan fold-thrust belt in western Nepal: Tectonics, v. 20, no. 4, p. 487-509.

Deeken, A., Thiede, R. C., Sobel, E. R., Hourigan, J. K., & Strecker, M. R. (2011). Exhumational variability within the Himalaya of northwest India. Earth Planetry Science Letters, 305(1-2), 103–114. https://doi.org/10.1016/j.epsl.2011.02.045

Dey, S., Kaushal, R. K., & Jain, V. (2019). Spatiotemporal variability of neotectonic activity along the Southern Himalayan front: A geomorphic perspective. Journal of Geodynamics, 129, 237-246.

Dey, S., Thiede, R. C., Schildgen, T. F., Wittmann, H., Bookhagen, B., Scherler, D., & Strecker, M. R. (2016). Holocene internal shortening within the northwest Sub-Himalaya: Out-of-sequence faulting of the Jwalamukhi Thrust, India. Tectonics, 35(11), 2677-2697.

DiPietro, J. A., & Pogue, K. R. (2004). Tectonostratigraphic subdivisions of the Himalaya: A view from the west. Tectonics, 23(5).

Dodson, M. H. (1973). Closure temperature in cooling geochronological and petrological systems. Contributions to Mineralogy and Petrology, 40(3), 259-274.

~~Duvall, A., Kirby, E., & Burbank, D. (2004). Tectonic and lithologic controls on bedrock channel profiles and processes in coastal California. Journal of Geophysical Research: Earth Surface, 109(F3).~~

Elliott, J. R., Jolivet, R., González, P. J., Avouac, J. P., Hollingsworth, J., Searle, M. P., & Stevens, V. L. (2016). Himalayan megathrust geometry and relation to topography revealed by the Gorkha earthquake. *Nature Geoscience*, *9*(2), 174.

Eugster, P., Scherler, D., Thiede, R. C., Codilean, A. T., and Strecker, M. R., (2016). Rapid Last Glacial Maximum deglaciation in the Indian Himalaya coeval with midlatitude glaciers: New insights from 10Be-dating of ice-polished bedrock surfaces in the Chandra Valley, NW Himalaya: Geophysical Research Letters, v. 43, no. 4, p. 1589-1597.

Finnegan, N. J., Roe, G., Montgomery, D. R., &Hallet, B. (2005). Controls on the channel width of rivers: Implications for modeling fluvial incision of bedrock. *Geology*, *33*(3), 229-232.

Flint, J. J. (1974). Stream gradient as a function of order, magnitude, and discharge. Water Resources Research, 10(5), 969-973.

Forte, A.M. and Whipple, K.X. (2019). The Topographic Analysis Toolkit (TAK) for Topotoolbox. Earth Surface Dynamics, 7, 87-95.

Gahalaut, V. K., & Kalpna. (2001). Himalayan mid-crustal ramp. *Current Science*, 1641-1646.

951 Gavillot, Y. G. (2014). Active tectonics of the Kashmir Himalaya (NW India) and earthquake
952 potential on folds, out-of-sequence thrusts, and duplexes.

953 Gavillot, Y., Meigs, A. J., Sousa, F. J., Stockli, D., Yule, D., & Malik, M. (2018). Late Cenozoic
954 Foreland-to-Hinterland Low-Temperature Exhumation History of the Kashmir
955 Himalaya. Tectonics.

956 Gavillot, Y., Meigs, A., Yule, Y., Heermance, R., Rittenour, T., Madugo, C., & Malik, M.
957 (2016). Shortening rate and Holocene surface rupture on the Riasi fault system in the Kashmir
958 Himalaya: Active thrusting within the Northwest Himalayan orogenic wedge. Geological Society
959 of America Bulletin, 128(7-8), 1070–1094. https://doi.org/10.1130/B31281.1

960 Hack, J. T. (1973). Stream-profile analysis and stream-gradient index. Journal of Research of the
961 us Geological Survey, 1(4), 421-429.

962 Harvey, J. E., Burbank, D. W., & Bookhagen, B. (2015). Along-strike changes in Himalayan
963 thrust geometry: Topographic and tectonic discontinuities in western Nepal. Lithosphere, 7(5),
964 511-518.

965 Herman, F., Copeland, P., Avouac, J.P., Bollinger, L., Mahéo, G., Le Fort, P., Rai, S., Foster, D.,
966 Pêcher, A., Stüwe, K. and Henry, P., 2010. Exhumation, crustal deformation, and thermal
967 structure of the Nepal Himalaya derived from the inversion of thermochronological and
968 thermobarometric data and modeling of the topography. *Journal of Geophysical Research: Solid*
969 *Earth*, *115*(B6).

970 Hirschmiller, J., Grujic, D., Bookhagen, B., Coutand, I., Huyghe, P., Mugnier, J.-L., and Ojha,
971 T., 2014, What controls the growth of the Himalayan foreland fold-and-thrust belt?: Geology, v.
972 42, no. 3, p. 247-250.

Huntley, D. J., & Lamothe, M. (2001). Ubiquity of anomalous fading in K-feldspars and the measurement and correction for it in optical dating. *Canadian Journal of Earth Sciences*, *38*(7), 1093-1106.

Kaushal, R. K., Singh, V., Mukul, M., & Jain, V. (2017). Identification of deformation variability and active structures using geomorphic markers in the Nahan salient, NW Himalaya, India. *Quaternary International*, *462*, 194-210.

Kothyari, G. C., & Juyal, N. (2013). Implications of fossil valleys and associated epigenetic gorges in parts of Central Himalaya. *Current Science*, 383-388.

Kumar, A., Lal, N., Jain, A. K., &Sorkhabi, R. B. (1995). Late Cenozoic–Quaternary thermo-tectonic history of Higher Himalayan Crystalline (HHC) in Kishtwar–Padar–Zanskar region, NW Himalaya: Evidence from fission-track ages. Journal of the Geological Society of India, 45(4), 375–391.

Kundu, B., Yadav, R. K., Bali, B. S., Chowdhury, S., &Gahalaut, V. K. (2014). Oblique convergence and slip partitioning in the NW Himalaya: implications from GPS measurements. Tectonics, 33(10), 2013-2024.

Lavé, J., & Avouac, J. P. (2000). Active folding of fluvial terraces across the Siwaliks Hills, Himalayas of central Nepal. Journal of Geophysical Research: Solid Earth, 105(B3), 5735-5770.

Lavé, J., & Avouac, J. P. (2001). Fluvial incision and tectonic uplift across the Himalayas of central Nepal. Journal of Geophysical Research: Solid Earth, 106(B11), 26561-26591.

Mahesh, P., Gupta, S., Saikia, U., and Rai, S. S., 2015, Seismotectonics and crustal stress field in the Kumaon-Garhwal Himalaya: Tectonophysics, v. 655, p. 124-138.

994 Malik, J. N., & Mohanty, C. (2007). Active tectonic influence on the evolution of drainage and
995 landscape: geomorphic signatures from frontal and hinterland areas along the Northwestern
996 Himalaya, India. *Journal of Asian Earth Sciences*, *29*(5-6), 604-618.

997 Miller, J. R. (1991). The influence of bedrock geology on knickpoint development and channel-
998 bed degradation along downcutting streams in south-central Indiana. The Journal of
999 Geology, 99(4), 591-605.

1000 Mitra, G., Bhattacharyya, K., & Mukul, M. (2010). The lesser Himalayan duplex in Sikkim:
1001 implications for variations in Himalayan shortening. *Journal of the Geological Society of*
1002 *India*, *75*(1), 289-301.

1003 Montgomery, D. R., & Brandon, M. T. (2002). Topographic controls on erosion rates in
1004 tectonically active mountain ranges. Earth and Planetary Science Letters, 201(3-4), 481-489.

1005 Mukherjee S. (2015) A review on out-of-sequence deformation in the Himalaya. In: Mukherjee
1006 S, Carosi R, van der Beek P, Mukherjee BK, Robinson D (Eds) Tectonics of the
1007 Himalaya. Geological Society, London. Special Publications 412, 67-109.

1008 Mukul, M., Jaiswal, M., & Singhvi, A. K. (2007). Timing of recent out-of-sequence active
1009 deformation in the frontal Himalayan wedge: Insights from the Darjiling sub-Himalaya,
1010 India. *Geology*, *35*(11), 999-1002.

1011 ~~Mukul, M., Jade, S., Bhattacharyya, A. K., &Bhusan, K. (2010). Crustal shortening in~~
1012 ~~convergent orogens: Insights from global positioning system (GPS) measurements in northeast~~
1013 ~~India. Journal of the Geological Society of India, 75(1), 302-312.~~

1014 Nábělek, J., Hetényi, G., Vergne, J., Sapkota, S., Kafle, B., Jiang, M., Su, H., Chen, J., & Huang,
1015 B. S. (2009). Underplating in the Himalaya-Tibet collision zone revealed by the Hi-CLIMB
1016 experiment. Science, 325(5946), 1371-1374.

1017 Nadim, F., Kjekstad, O., Peduzzi, P., Herold, C., &Jaedicke, C. (2006). Global landslide and
1018 avalanche hotspots. Landslides, 3(2), 159-173.

1019 Nennewitz, M., Thiede, R. C., & Bookhagen, B. (2018). Fault activity, tectonic segmentation,
1020 and deformation pattern of the western Himalaya on Ma timescales inferred from landscape
1021 morphology. Lithosphere, 10(5), 632-640.

1022 Ni, J., and M. Barazangi (1984), Seismotectonics of the Himalayan collision zone: Geometry of
1023 the underthrusting Indian plate beneath the Himalaya, J. Geophys. Res., 89, 1147 – 1163.

1024 Niedzielski, T., Migoń, P., & Placek, A. (2009). A minimum sample size required from Schmidt
1025 hammer measurements. *Earth Surface Processes and Landforms: The Journal of the British*
1026 *Geomorphological Research Group*, *34*(13), 1713-1725.

1027 Norin, E. (1926). The relief chronology of the Chenab valley. Geografiska Annaler, 8(4), 284-
1028 300.

1029 Olley, J., Caitcheon, G., & Murray, A. (1998). The distribution of apparent dose as determined
1030 by optically stimulated luminescence in small aliquots of fluvial quartz: implications for dating
1031 young sediments. *Quaternary Science Reviews*, *17*(11), 1033-1040.

1032 Ouimet, W. B., Whipple, K. X., Crosby, B. T., Johnson, J. P., & Schildgen, T. F. (2008).
1033 Epigenetic gorges in fluvial landscapes. *Earth Surface Processes and Landforms: The Journal of*
1034 *the British Geomorphological Research Group*, *33*(13), 1993-2009.

Paul, H., Priestley, K., Powali, D., Sharma, S., Mitra, S., &Wanchoo, S. (2018). Signatures of the existence of frontal and lateral ramp structures near the Kishtwar Window of the Jammu and Kashmir Himalaya: Evidence from microseismicity and source mechanisms. *Geochemistry, Geophysics, Geosystems, 19*(9),3097-3114.

Phartiyal, B., Sharma, A., Srivastava, P., & Ray, Y. (2009). Chronology of relict lake deposits in the Spiti River, NW Trans Himalaya: Implications to Late Pleistocene Holocene climate-tectonic perturbations. *Geomorphology*, *108*(3-4), 264-272.

Powers, P. M., Lillie, R. J., & Yeats, R. S. (1998). Structure and shortening of the Kangra and Dehra Dun reentrants, sub-Himalaya, India. Geological Society of America Bulletin, 110(8), 1010-1027.

Preusser, F. (2003). IRSL dating of K-rich feldspars using the SAR protocol: comparison with independent age control. *Ancient tL*, *21*(1), 17-23.

Raiverman, V. (1983). Basin geometry, Cenozoic sedimentation and hydrocarbon prospects in north-western Himalaya and Indo-Gangetic plains. Petroleum Asia Journal: Petroliferous basins of India, 6(4), 67-92.

Robert, X., Van Der Beek, P., Braun, J., Perry, C., Dubille, M., & Mugnier, J. L. (2009). Assessing Quaternary reactivation of the Main Central thrust zone (central Nepal Himalaya): New thermochronologic data and numerical modeling. *Geology*, *37*(8), 731-734.

Roberts, H. M. (2007). Assessing the effectiveness of the double-SAR protocol in isolating a luminescence signal dominated by quartz. *Radiation measurements*, *42*(10), 1627-1636.

1055 Robinson, D. M., & Martin, A. J. (2014). Reconstructing the Greater Indian margin: A balanced
1056 cross section in central Nepal focusing on the Lesser Himalayan duplex. *Tectonics*, *33*(11), 2143-
1057 2168.

1058 Royden, L., & Taylor Perron, J. (2013). Solutions of the stream power equation and application
1059 to the evolution of ~~river~~ River longitudinal profiles. *Journal of Geophysical Research: Earth*
1060 *Surface*, *118*(2), 497-518.

1061 Scherler, D., Bookhagen, B., Wulf, H., Preusser, F., & Strecker, M. R. (2015). Increased late
1062 Pleistocene erosion rates during fluvial aggradation in the Garhwal Himalaya, northern
1063 India. *Earth and Planetary Science Letters*, *428*, 255-266.

1064 Schwanghart, W., &Scherler, D. (2014). TopoToolbox 2–MATLAB-based software for
1065 topographic analysis and modeling in Earth surface sciences. Earth Surface Dynamics, 2(1), 1-7.

1066 Searle, M. P., Noble, S. R., Cottle, J. M., Waters, D. J., Mitchell, A. H. G., Hlaing, T.,
1067 &Horstwood, M. S. A. (2007). Tectonic evolution of the Mogok metamorphic belt, Burma
1068 (Myanmar) constrained by U-Th-Pb dating of metamorphic and magmatic
1069 rocks. Tectonics, 26(3).

1070 Seeber, L., &Gornitz, V. (1983). River profiles along the Himalayan arc as indicators of active
1071 tectonics. *Tectonophysics*, *92*(4), 335-367.

1072 Snyder, N. P., Whipple, K. X., Tucker, G. E., &Merritts, D. J. (2000). Landscape response to
1073 tectonic forcing: Digital elevation model analysis of stream profiles in the Mendocino triple
1074 junction region, northern California. Geological Society of America Bulletin, 112(8), 1250-1263.

1075 Steck, A. (2003). Geology of the NW Indian Himalaya. EclogaeGeolHelv, 96, 147-196.

Stevens, V. L., & Avouac, J. P. (2015). Interseismic coupling on the main Himalayan thrust. Geophysical Research Letters, 42(14), 5828-5837.

~~Strahler, A. N. (1952). Hypsometric (area-altitude) analysis of erosional topography. Geological Society of America Bulletin, 63(11), 1117-1142.~~

Stübner, K., Grujic, D., Dunkl, I., Thiede, R., & Eugster, P. (2018). Pliocene episodic exhumation and the significance of the Munsiari thrust in the north-western Himalaya. *Earth and Planetary Science Letters*, *481*, 273-283.

Thakur, V. C. (Ed.). (1992). Geology of western Himalaya (Vol. 19). Pergamon Press.

Thakur, V. C., Joshi, M., Sahoo, D., Suresh, N., Jayangondapermal, R., & Singh, A. (2014). Partitioning of convergence in Northwest Sub-Himalaya: estimation of late Quaternary uplift and convergence rates across the Kangra reentrant, North India. International Journal of Earth Sciences, 103(4), 1037-1056.

Thiede, R., Robert, X., Stübner, K., Dey, S., &Faruhn, J. (2017). Sustained out-of-sequence shortening along a tectonically active segment of the Main Boundary thrust: The Dhauladhar Range in the north-western Himalaya. Lithosphere, 9(5), 715-725.

Thiede, R. C., Bookhagen, B., Arrowsmith, J. R., Sobel, E. R., & Strecker, M. R. (2004). Climatic control on rapid exhumation along the southern Himalayan Front. Earth and Planetary Science Letters, 222(3-4), 791–806. https://doi.org/10.1016/j.epsl.2004.03.015

Turowski, J. M., Lague, D., and Hovius, N. (2009). Response of bedrock channel width to tectonic forcing: Insights from a numerical model, theoretical considerations, and comparison with field data. *Journal of Geophysical Research: Earth Surface*, *114*(F3).

Vassallo, R., Mugnier, J. L., Vignon, V., Malik, M. A., Jayangondaperumal, R., Srivastava, P., and Carcaillet, J. (2015). Distribution of the late-Quaternary deformation in north-western Himalaya. Earth and Planetary Science Letters, 411, 241-252.

Wadia, D. N. (1934). The Cambrian-Trias sequence of north-western Kashmir (parts of Muzaffarabad and Baramula districts). Records of the Geological Survey of India, 68(2), 121-176.

Webb, A. A. G., Yin, A., Harrison, T. M., Célérier, J., Gehrels, G. E., Manning, C. E., & Grove, M. (2011). Cenozoic tectonic history of the Himachal Himalaya (north-western India) and its constraints on the formation mechanism of the Himalayan orogen. *Geosphere*, *7*(4), 1013-1061.

Wesnousky, S. G., Kumar, S., Mohindra, R., & Thakur, V. C. (1999). Uplift and convergence along the Himalayan Frontal Thrust of India. Tectonics, 18(6), 967-976.

Whipple, K. X., & Tucker, G. E. (1999). Dynamics of the stream-power river incision model: Implications for height limits of mountain ranges, landscape response timescales, and research needs. Journal of Geophysical Research: Solid Earth, 104(B8), 17661-17674.

Whipple, K. X., DiBiase, R. A., & Crosby, B. T. (2013). Bedrock rivers. In Treatise on geomorphology. Elsevier Inc..

Wallinga, J., Murray, A. S., Duller, G. A., & Törnqvist, T. E. (2001). Testing optically stimulated luminescence dating of sand-sized quartz and feldspar from fluvial deposits. *Earth and Planetary Science Letters*, *193*(3-4), 617-630.

Wobus, C. W., Hodges, K. V., & Whipple, K. X. (2003). Has focused denudation sustained active thrusting at the Himalayan topographic front?. *Geology*, *31*(10), 861-864.

~~Wobus, C., Heimsath, A., Whipple, K., & Hodges, K. (2005). Active out-of-sequence thrust~~ faulting in the central Nepalese Himalaya. Nature, 434(7036), 1008.

Wobus, C., Whipple, K. X., Kirby, E., Snyder, N., Johnson, J., Spyropolou, K., Crosby, B., Sheehan, D & Willett, S. D. (2006). Tectonics from topography: Procedures, promise, and pitfalls. Special papers-geological society of America, 398, 55.

Yadav, R. K., Gahalaut, V. K., Bansal, A. K., Sati, S., Catherine, J., Gautam, P., Kumar, K., and Rana, N., 2019, Strong seismic coupling underneath Garhwal–Kumaun region, NW Himalaya, India: Earth and Planetary Science Letters, v. 506, p. 8-14.

Yin, A., & Harrison, T. M. (2000). Geologic evolution of the Himalayan-Tibetan orogen. Annual Review of Earth and Planetary Sciences, 28(1), 211-280.

Figure captions

Figure 1: (a) An overview geological map of the western sector of the Indian Himalaya showing major lithology (modified after Steck, 2003 and Gavillot et al., 2018) and existing structures (Vassalo et al., 2015; Gavillot et al., 2018). The tectonic Kishtwar Window (KW) is surrounded by exposure of MCT, locally known as the Kishtwar Thrust (KT), and exposes the Lesser Himalayan duplex. The Lesser Himalayan duplex (LH duplex) forms a west-verging asymmetric anticline. The present-day glacial extent is mapped as per the GLIMS-database. Apatite fission-track (AFT) ages are adapted from Kumar et al., (1995). (b) A schematic cross-section of the NW Himalaya showing the general architecture of the Himalayan orogenic wedge (modified after Webb et al., 2011; Deeken et al., 2011; Gavillot et al., 2018). Note that, beneath the LH

Duplex in KW, Gavillot et al., (2018) proposed the existence of at least two crustal ramps (MCR-1 and MCR-2) on the MHT.

Figure 2: Lithological units and structural orientations observed in the Chenab valley. (a) Steeply-dipping HHCS units near the western margin of the KW. (b) Highly-deformed migmatites at the base of the KT. (c) Sub-vertical quartzite slabs exposed in the frontal horses of the LH Duplex. (d) Highly-deformed granite gneisses at the core of the KW, the hanging wall rocks of the proposed surface-breaking fault (Fig. 8b). (e) A close-up view of the folded and fractured gneiss. (f) Steeply-dipping units of granite gneiss outcropping upstream from the fault-zone. (g) Further upstream from the fault-zone, the bedrocks are gentler in the eastern edge of the KW.

Figure 3: Geomorphic features observed along the Chenab River. (a) 'U-shaped' valley profile at the eastern margin of the KW suggests glacial occupancy in the past. The present-day River incises through the transient sediment storage. Photograph was taken near the town of Padder (cf. Fig.1a). (b) The Chenab River is steep and maintains a narrow channel width through the core of the KW. (c) Fluvial incision observed along the N-S traverse of the Chenab River. Photograph was taken from south of the Kishtwar town. The Kishtwar surface is underlain by ~150-170m thick sediment cover overlying the tilted Higher Himalayan bedrock. The River incised ~240m bedrock in this section. (d) Epigenetic gorge formed along the Chenab River in its' N-S traverse through the HHCS. The town of Drabshalla is built on the hillslope deposits. (e) Chenab River maintained very narrow channel (width: ~20-25 m) through moderately-strong HHCS rocks, suggesting tectonic imprint on topography. (f) Formation of knickpoint at the confluence of the tributary with the trunk stream implying a transient topographic condition. (g) Three levels of strath surfaces observed below the Kishtwar surface. The strath levels are marked as T1

(~280m), T2 (~170m) and T3 (~120m). OSL dating of fluvial sediments lying above the T3 surface yield a minimum depositional age of ~21.6±2.6 ky.

Figure 4: (a) Lithological distribution near the western margin of the KW. Luminescence sample (OSL and IRSL) locations and respective depositional ages (in ky) are shown. Every sample except K16 and K17, are taken above strath level T1. K16 and K17 are taken from above the T3 level. Note that, the ages reported in italics are minimum age estimates. (b) A field photograph from the village Janwas, south of the town of Kishtwar, showing the aggraded sediments lying above the Higher Himalayan tilted bedrock units. (c) IRSL ages (in ky) from the fluvioglacial sediments and OSL age (in ky) from the hillslope debris units suggest the valley aggradation probably started at the transition of the glacial to interglacial phase ~120-130 ky and continued till ~80 ky ago. (d) A close-up view (red rectangle in fig.4c) of the tilted fluvioglacial sediment layers showing alternate conglomerate and medium-coarse sand layers. (e) A ~3m thick fine sand layer within the hillslope debris yield depositional age of ~86±5 ky. Fieldphoto was taken near the village of Pochal, northwest of the town of Kishtwar.

Figure 5: Regional variations in (a) topography, (b) topographic relief (moving window of ~4 km) (c) TRMM-derived rainfall (after Bookhagen and Burbank, 2006), and (d) Basinwide Normalized steepness indices (ksn value) of the region shown dashed box in Figure 1a. (e) Swath profiles (swath window: 50 km) along the line AB (cf. Fig.5a) demonstrate the orogen-perpendicular variations in elevation, rainfall and ksn value. KW is characterized by high elevation, high relief and high steepness, but low rainfall. This suggests that tectonics control uplift and shape of topography not climate.

Figure 6: Longitudinal profile of the Chenab River show major changes in channel gradient associated with knickpoints in the upstream. We classified knickpoints on the basis of their

genesis. The substrate lithology along the River is shown. Knickpoints caused by glacial occupancy (G1, G2 and G3) are adapted from Eugster et al., (2016), who reconstructed the timing of maximum glaciation and extent of glacial cover in source region of Chenab River basin during the last glacial maximum. These knickpoints highlight the importance of glacial erosion in the high-elevation sectors, especially in the northern tributaries of the Chenab River (For present-day glacial extent cf. Fig.1a). Further in this study, we focused on the area marked by red rectangle.

Figure 7: Along-river variations in (a) channel-elevation, (b) channel width, (c) channel gradient, (d) Normalized steepness index and (e) rock-strength of non-fractured bedrock units (R value taken by rebound hammer) till 165 km upstream from the MBT (point A, cf. Fig.1a). The mean R-value$\pm\sigma$ for each rock type has been plotted against their spatial extent. We identified two distinct zones (K1 and K2) of high channel gradient and steepness index which maintain low channel width despite variable rock strength of the substrate. Knickpoint K3 may have been generated by the formation of epigenetic gorge along the N-S traverse of the Chenab River (cf. Fig.3c). Knickpoints L1 and L2 mark the transition of soft-to-hard bedrock substrate.

Figure 8: (a) Detailed structural data from the study area showing structural and lithological variations (modified after Steck, 2003; Gavillot et al., 2018). (b) A conceptual drawing of the internal deformation of the LH duplex showing the existing structural variations of the MHT and possible locations of mid-crustal ramps. We assume that two steep stream segment (in the vicinity of knick-zones K1 and K2 – see Fig. 6) refer to ramp segments within the MHT trace. The pervasively folded and fractured LH units at the base of the ramp (cf. Fig. 2e) possibly indicate a surface-breaking fault within the LH duplex. Sustained uplift of the hanging wall of the proposed fault is expressed by the higher topographic relief, narrowing of the channel and

river steepening on the hanging wall. Structural variations on the hanging wall impart differential uplift, marked by a quasistatic knickpoint K1 at the transition from the flat to the ramp of the fault. 3-km-wide topographic swath profiles are drawn across the steep stream segments K1 (fig.8c) and K2 (fig.8d). The orthogonal profile projection method has been used in the case of K2 (cf. fig.7) to identify the width of the steep segment.

Figure 9: A satellite image of the northern Kishtwar town showing the present-day flow-path of the Chenab River. Hillslope debris originated from the steep frontal horses of the LH duplex (white quartzite rocks) and was deposited over fluvioglacial and glacio-lacustrine sediments and Higher Himalaya schists bedrock exposed below in the Kishtwar valley. Massive hillslope sediment flux impeded the paleo-drainage system leaving behind the paleo-valley of the tributary, the Maru River. Our interpretation of the paleo-drainage is marked in white dashed line. (a) A view of the Kishtwar surface from the western margin of the KW showing present-day gorge of the Chenab River and its tributary. The wind-gap (paleo-valley) of the tributary is visible. (b) Thick clay-silt deposit in the wind-gap suggests abandonment of river-flow. The OSL sample is saturated and hence only denotes the minimum age of valley abandonment/ hillslope debris flow. (c) Overview picture of the frontal horses of the LH duplex and the direction of debris flow towards the Kishtwar town. (d) Angular, poorly-sorted clasts and boulders observed at the base of the debris flow unit near village of Pochal, north of the Kishtwar town. As only east of the KT-boundary the white quartzites of LH are exposed in vicinity of the Kishtwar Town (see satellite image) – only the eastern valley flank can have collapsed in the past.

Figure 10: (a) A topographic and geomorphic profile across the Chenab valley drawn over the Kishtwar Town. The valley aggradation by fluvioglacial and hillslope debris sediments was succeeded by fluvial incision which penetrated through the unconsolidated sediments of

thickness ~140-150m and incised Higher Himalayan bedrock by ~280±5 m, leaving behind at least three recognizable strath surfaces with a thin late Pleistocene sediment cover. The three surfaces are at 280±5 m (T1), ~170 m (T2) and ~120±5 m (T3) heights with respect to the present-day river height. We assume that the present day bedrock gorge has been carved since deposition of the glacio-lacustrine sediment deposits (~100-130 ky) and the hillslope debris (~90-80 ky) onto former fluvial strath surface of Higher Himalayan Bedrock. The width of the fluvial strath surface where the Kishtwar Town is located indicates that the river network had been dammed earlier too. (b) Graphical representation of mean bedrock incision rates since 80 ky. Age constraints for T3 are shown in Fig. 4a. We propose a minimum and a maximum bedrock incision rate of 3.1-3.5 mm/y and 5.2-5.6 mm/y, respectively. Rapid bedrock incision along the N-S traverse of the Chenab River may imply sustained exhumation over the proposed mid-crustal ramp of the MHT.

Table captions:

Table 1: Morphometric parameters for calculation of discharge-normalized specific stream power (SSP) in the study area, highlighting the changes in SSP through the steepened stretches. Increase in the SSP by 4-5 times through the steepened stretches reflects higher potential for fluvial erosion, balancing the differential uplift of the terrain.

Table 2: Details of sample locations, dose rate estimation parameters, Equivalent dose estimation and depositional ages of OSL-IRSL samples procured from the Kishtwar region.

Figures for manuscript #esurf_2020_37 (Dey et al.)

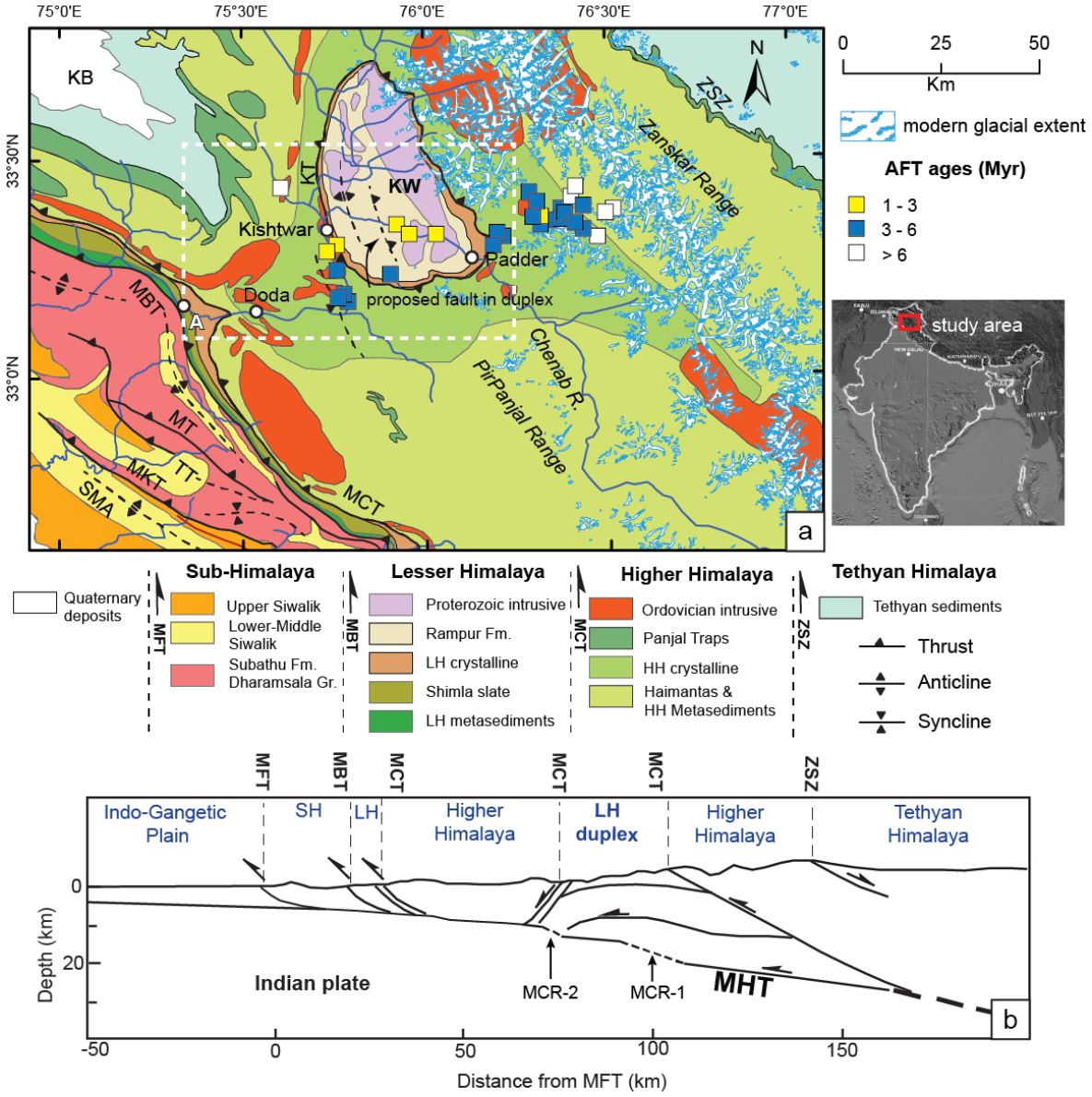

Figure 1: (a) An overview geological map of the western sector of the Indian Himalaya showing major lithology (modified after Steck, 2003 and Gavillot et al., 2018) and existing structures (Vassalo et al., 2015; Gavillot et al., 2018). The tectonic Kishtwar Window (KW) is surrounded by exposure of MCT, locally known as the Kishtwar Thrust (KT), and exposes the Lesser Himalayan duplex. The Lesser Himalayan duplex (LH duplex) forms a west-verging asymmetric anticline. The present-day glacial extent is mapped as per the GLIMS-database. Apatite fission-track (AFT) ages are adapted from Kumar et al., (1995). (b) A schematic cross-section of the NW Himalaya showing the general architecture of the Himalayan orogenic wedge (modified after Webb et al., 2011; Deeken et al., 2011; Gavillot et al., 2018). Note that, beneath the LH Duplex in KW, Gavillot et al., (2018) proposed the existence of at least two crustal ramps (MCR-1 and MCR-2) on the MHT.

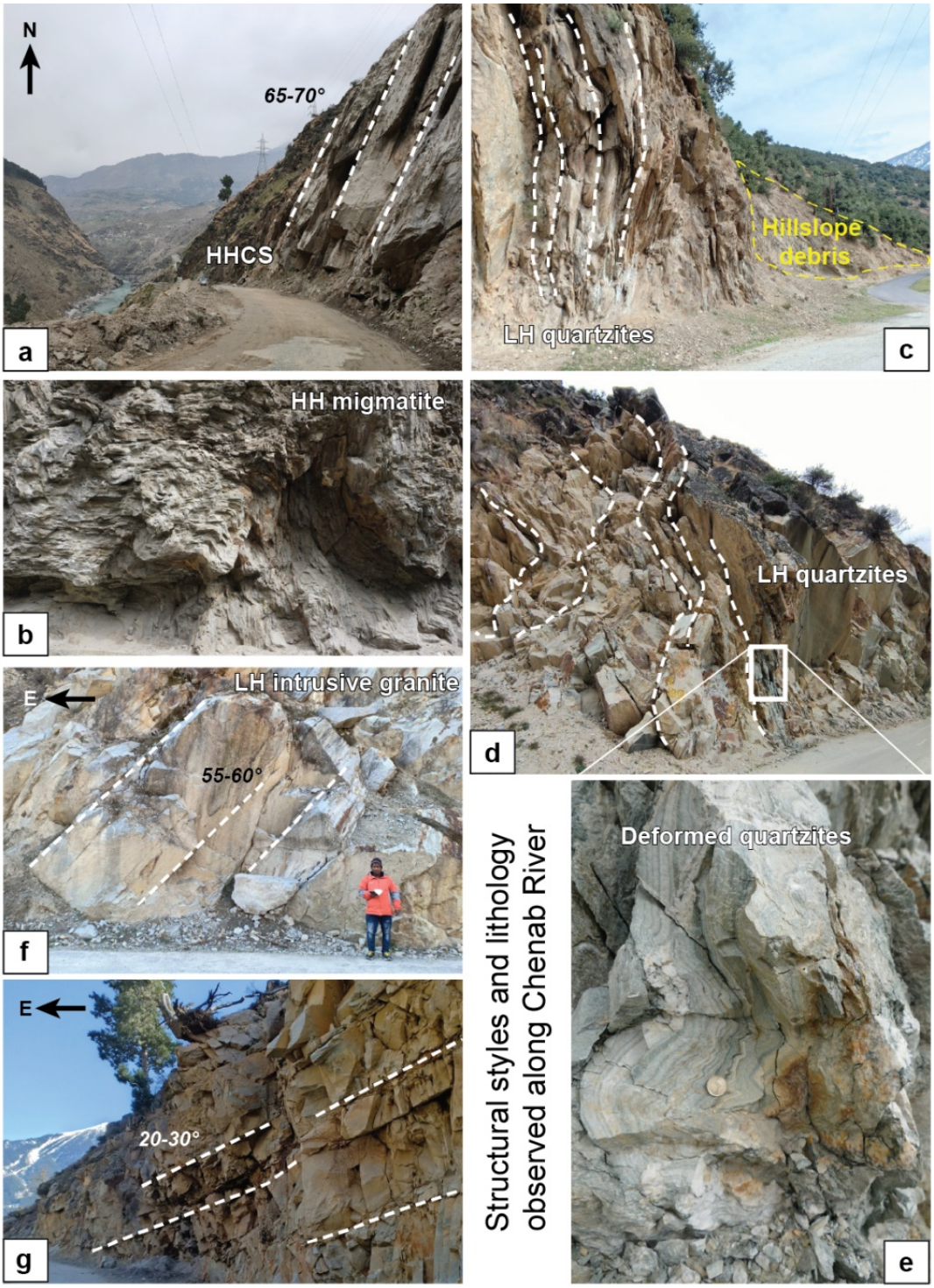

Figure 2: Lithological units and structural orientations observed in the Chenab valley. (a) Steeply-dipping HHCS units near the western margin of the KW. (b) Highly-deformed migmatites at the base of the KT. (c) Sub-vertical quartzite slabs exposed in the frontal horses of the LH Duplex. (d) Highly-deformed granite gneisses at the core of the KW, the hanging wall rocks of the proposed surface-breaking fault (Fig. 8b). (e) A close-up view of the folded and fractured gneiss. (f) Steeply-dipping units of granite gneiss outcropping upstream from the fault-zone. (g) Further upstream from the fault-zone, the bedrocks are gentler in the eastern edge of the KW.

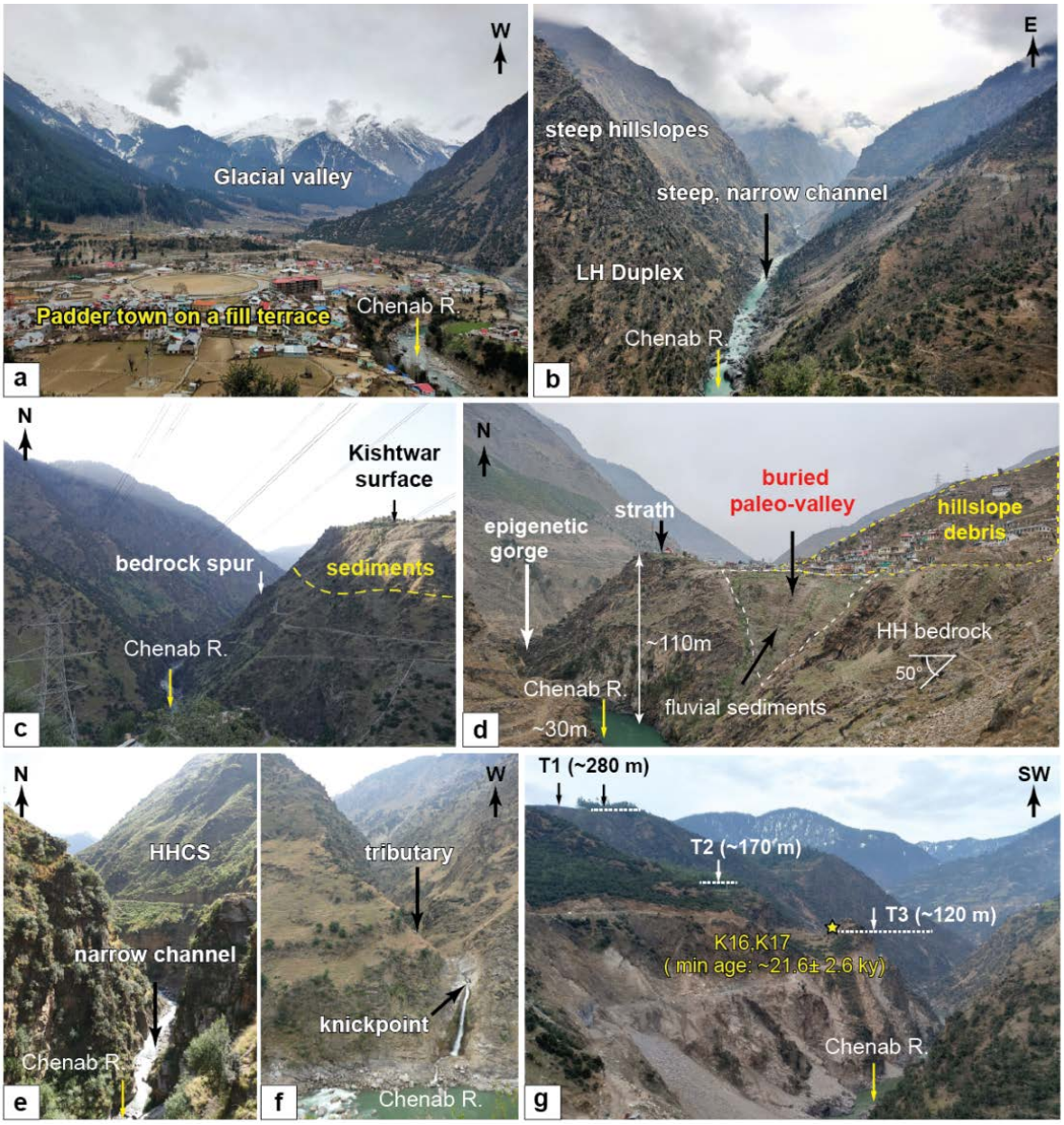

Figure 3: Geomorphic features observed along the Chenab River. (a) 'U-shaped' valley profile at the eastern margin of the KW suggests glacial occupancy in the past. The present-day River incises through the transient sediment storage. Photograph was taken near the town of Padder (cf. Fig.1a). (b) The Chenab River is steep and maintains a narrow channel width through the core of the KW. (c) Fluvial incision observed along the N-S traverse of the Chenab River. Photograph was taken from south of the Kishtwar town. The Kishtwar surface is underlain by ~150-170m thick sediment cover overlying the tilted Higher Himalayan bedrock. The River incised ~240m bedrock in this section. (d) Epigenetic gorge formed along the Chenab River in its' N-S traverse through the HHCS. The town of Drabshalla is built on the hillslope deposits. (e) Chenab River maintained very narrow channel (width: ~20-25 m) through moderately-strong HHCS rocks, suggesting tectonic imprint on topography. (f) Formation of knickpoint at the confluence of the tributary with the trunk stream implying a transient topographic condition. (g) Three levels of strath surfaces observed below the Kishtwar surface. The strath levels are marked as T1 (~280m), T2 (~170m) and T3 (~120m). OSL dating of fluvial sediments lying above the T3 surface yield a minimum depositional age of ~21.6±2.6 ky.

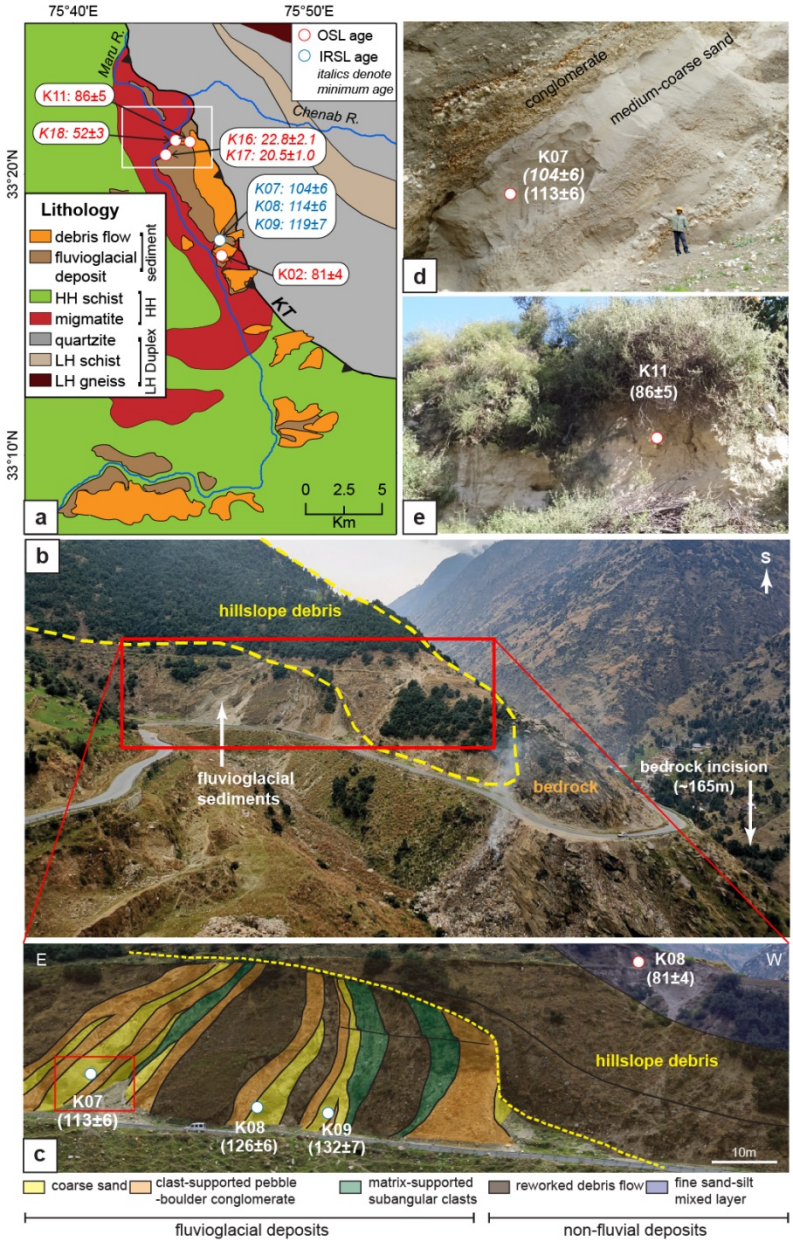

Figure 4: (a) Lithological distribution near the western margin of the KW. Luminescence sample (OSL and IRSL) locations and respective depositional ages (in ky) are shown. Every ample except K16 and K17 are taken above strath level T1. K16 and K17 are taken from above the T3 level. Note that, the ages reported in italics are minimum age estimates. (b) A field photograph from the village Janwas, south of the town of Kishtwar, showing the aggraded sediments lying above the Higher Himalayan tilted bedrock units. (c) IRSL ages (in ky) from the fluvioglacial sediments and OSL age (in ky) from the hillslope debris units suggest the valley aggradation probably started at the transition of the glacial to interglacial phase ~120-130 ky and continued till ~80 ky ago. (d) A close-up view (red rectangle in fig.4c) of the tilted fluvioglacial sediment layers showing alternate conglomerate and medium-coarse sand layers. (e) A ~3m thick fine sand layer within the hillslope debris yield

depositional age of ~86±5 ky. Picture taken near the village Pochal, northwest of the town of Kishtwar.

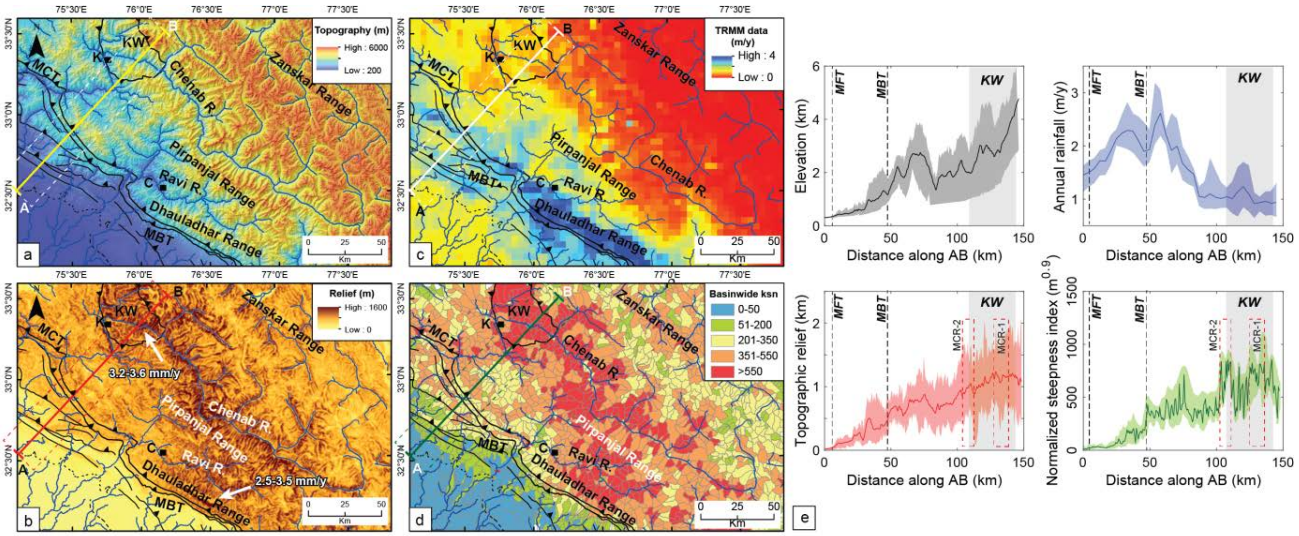

Figure 5: Regional variations in (a) topography, (b) topographic relief (moving window of ~4 km) (c) TRMM-derived rainfall (after Bookhagen and Burbank, 2006), and (d) Basinwide Normalized steepness indices (ksn value) of the region shown dashed box in Figure 1a. (e) Swath profiles (swath window: 50 km) along the line AB (cf. Fig.5a) demonstrate the orogen-perpendicular variations in elevation, rainfall and ksn value. KW is characterized by high elevation, high relief and high steepness, but low rainfall. This suggests that tectonics control uplift and shape of topography not climate.

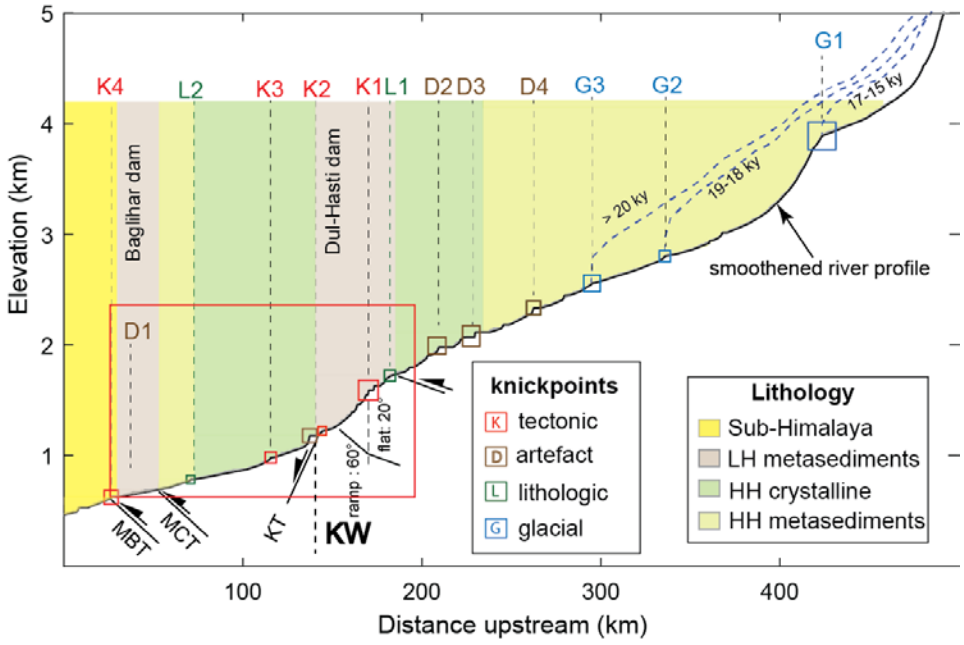

Figure 6: Longitudinal profile of the Chenab River show major changes in channel gradient associated with knickpoints in the upstream. We classified knickpoints on the basis of their genesis. The substrate lithology along the River is shown. Knickpoints caused by glacial occupancy (G1, G2 and G3) are adapted from Eugster et al., (2016), who reconstructed the timing of maximum glaciation and extent of glacial cover in source region of Chenab River basin during the last glacial maximum. These knickpoints highlight the importance of glacial erosion in the high-elevation sectors, especially in the northern tributaries of the Chenab River (For present-day glacial extent cf. Fig.1a). Further in this study, we focused on the area marked by red rectangle.

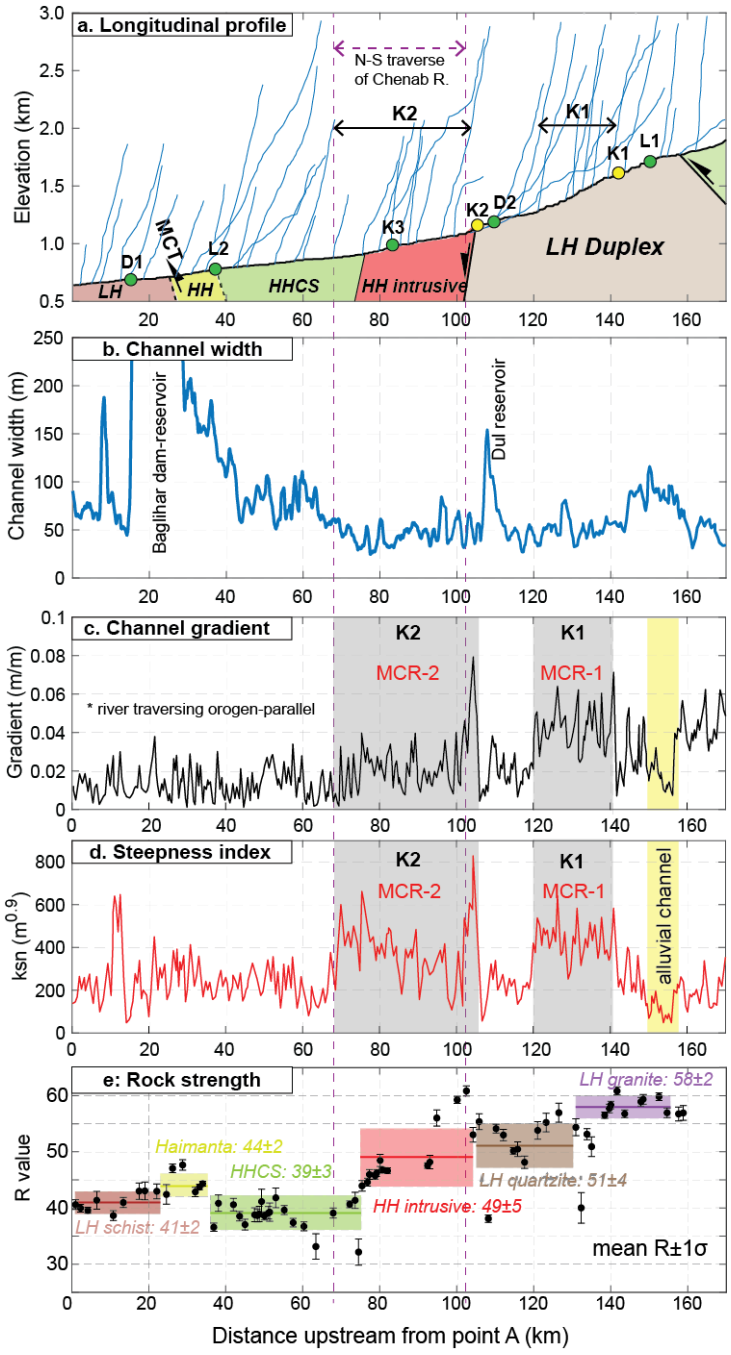

Figure 7: Along-river variations in (a) channel-elevation, (b) channel width, (c) channel gradient, (d) Normalized steepness index, and (e) rock-strength of non-fractured bedrock units (R-value taken by rebound hammer) till 165 km upstream from the MBT (point A, cf. Fig.1a). The mean R-value±σ for each rock type has been plotted against their spatial extent. We identified two distinct zones (K1 and K2) of high channel gradient and steepness index, which maintain low channel width despite the variable rock strength of the substrate. Knickpoint K3 may have been generated by the formation of the epigenetic gorge along the N-S traverse of the Chenab River (cf. Fig.3c). Knickpoints L1 and L2 mark the transition of a soft-to-hard bedrock substrate.

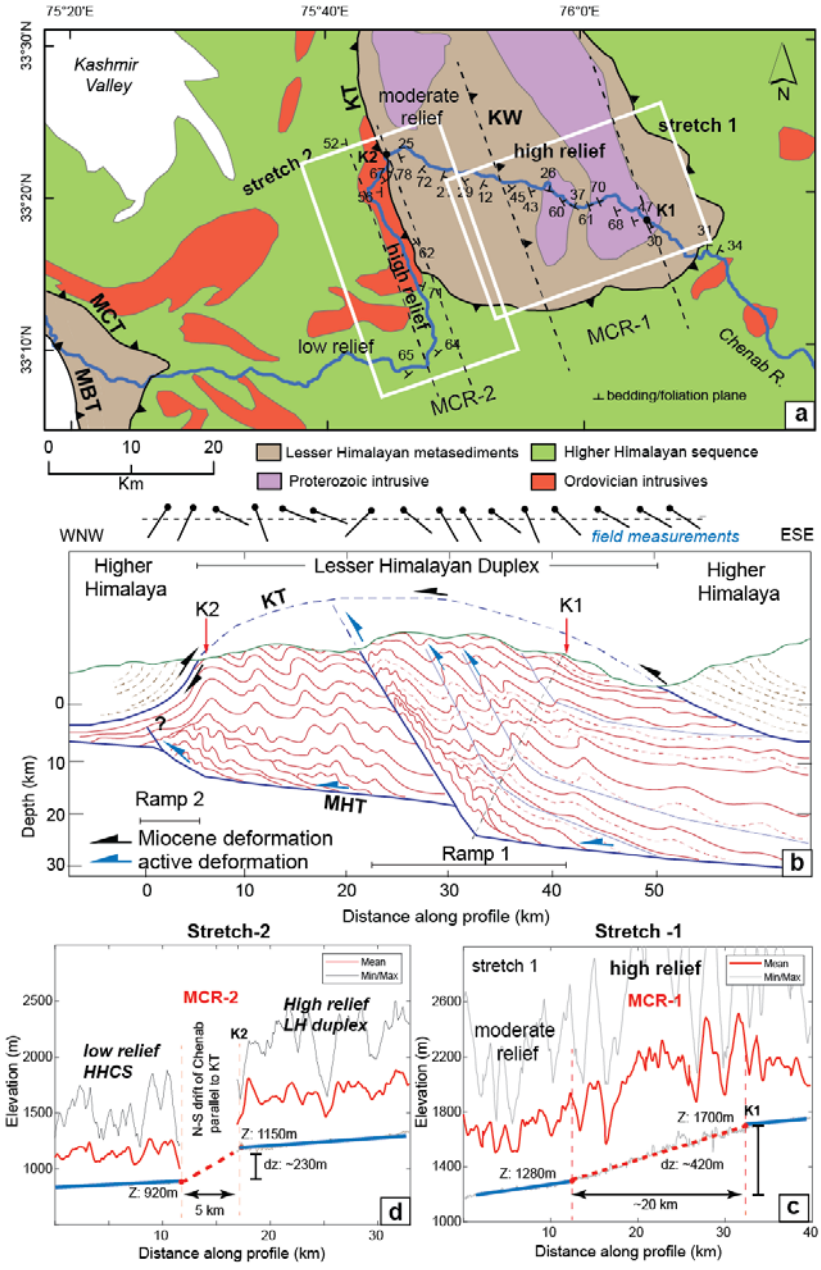

Figure 8: (a) Detailed structural data from the study area showing structural and lithological variations (modified after Steck, 2003; Gavillot et al., 2018). (b) A conceptual drawing of the internal

deformation of the LH duplex showing the existing structural variations of the MHT and possible locations of mid-crustal ramps. We assume that two steep stream segment (in the vicinity of knick-zones K1 and K2 – see Fig. 6) refer to ramp segments within the MHT trace. The pervasively folded and fractured LH units at the base of the ramp (cf. Fig. 2e) possibly indicate a surface-breaking fault within the LH duplex. Sustained uplift of the hanging wall of the proposed fault is expressed by the higher topographic relief, narrowing of the channel and River steepening on the hanging wall. Structural variations on the hanging wall impart differential uplift, marked by a quasistatic knickpoint K1 at the transition from the flat to the ramp of the fault. 3-km-wide topographic swath profiles are drawn across the steep stream segments K1 (fig.8c) and K2 (fig.8d). The orthogonal profile projection method has been used in the case of K2 (cf. fig.7) to identify the width of the steep segment.

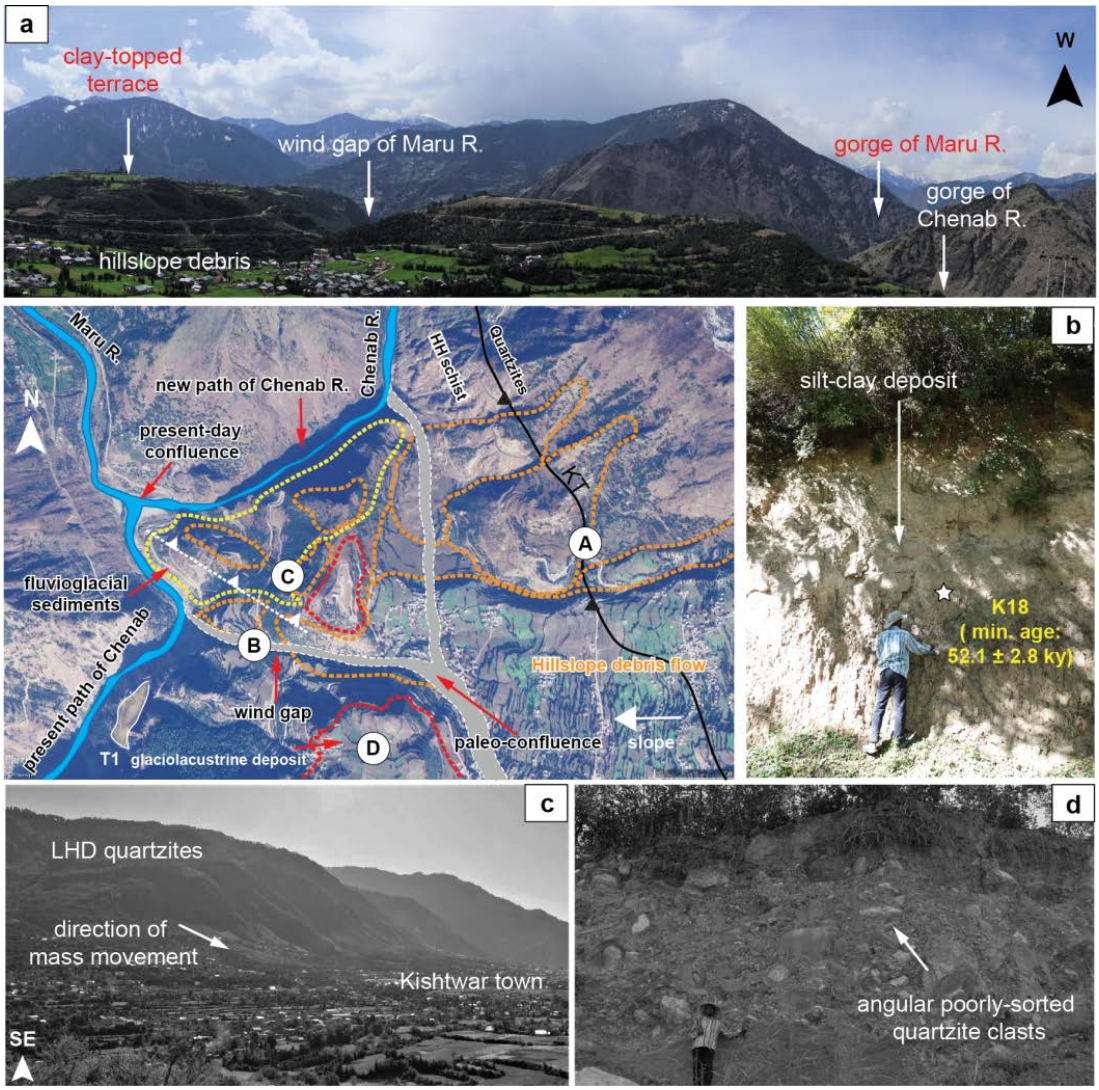

Figure 9: A satellite image of the northern Kishtwar town showing the present-day flow-path of the Chenab River. Hillslope debris originated from the steep frontal horses of the LH duplex (white

quartzite rocks) and was deposited over fluvioglacial and glaciolacustrine sediments and Higher Himalaya schists bedrock exposed below in the Kishtwar valley. Massive hillslope sediment flux impeded the paleo-drainage system leaving behind the paleo-valley of the tributary, the Maru River. Our interpretation of the paleo-drainage is marked in a white dashed line. (a) A view of the Kishtwar surface from the western margin of the KW showing present-day gorge of the Chenab River and its tributary. The wind-gap (paleo-valley) of the tributary is visible. (b) Thick clay-silt deposit in the wind-gap suggests abandonment of river-flow. The OSL sample is saturated and hence only denotes the minimum age of valley abandonment/ hillslope debris flow. (c) Overview picture of the frontal horses of the LH duplex and the direction of debris flow towards the Kishtwar town. (d) Angular, poorly-sorted clasts and boulders were observed at the base of the debris flow unit near the village of Pochal, north of the Kishtwar town. The white quartzites of LH are exposed in the vicinity of the Kishtwar Town (see satellite image) – only the eastern valley flank can have collapsed in the past.

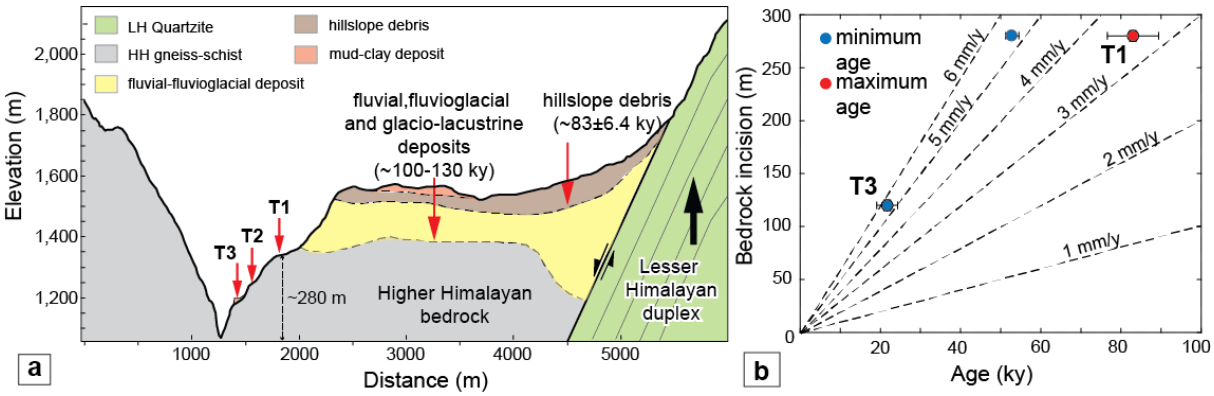

Figure 10: (a) A topographic and geomorphic profile across the Chenab valley drawn over the Kishtwar Town. The valley aggradation by fluvioglacial and hillslope debris sediments was succeeded by a fluvial incision which penetrated through the unconsolidated sediments of thickness ~140-150m and incised Higher Himalayan bedrock by ~280±5 m, leaving behind at least three recognizable strath surfaces with a thin late Pleistocene sediment cover. The three strath surfaces are at 280±5 m (T1), ~170 m (T2), and ~120±5 m (T3) heights from the present-day River. We assume that the present-day bedrock gorge has been carved since the deposition of the glaciolacustrine sediment deposits (~100-130 ky) and the hillslope debris (~90-80 ky) onto former fluvial strath surface of Higher Himalayan Bedrock. The width of the fluvial strath surface where the Kishtwar Town is located indicates that the river network had been dammed earlier too. (b) Graphical representation of mean bedrock incision rates since 80 ky. Age constraints for T3 are shown in Fig. 4a. We propose a minimum and a maximum bedrock incision rate of 3.1-3.5 mm/y and 5.2-5.6 mm/y, respectively.

Rapid bedrock incision along the N-S traverse of the Chenab River may imply sustained exhumation over the proposed mid-crustal ramp of the MHT.

Tables

Parameter	flat 1	ramp 1	% change	ratio ramp 1:flat 1	flat 2	ramp 2	% change	ratio ramp 2:flat 2
average channel gradient (m/m)	0.006	0.021	250.00	3.5	0.01	0.046	360	4.60
average channel width (m)	70	45	-35.71	0.6	55	42	-24	0.76
*Specific stream power (SSP)	0.000086	0.000467	444.44	5.4	0.000182	0.001095	502	6.02

* SSP calculated by assuming equal-discharge (Q)

Table 1: Calculations of change in specific stream power (SSP) values across the ramp and the flat segments beneath the LH Duplex. We used a uniform discharge for SSP calculation.

Sample type	Sample name	Lat (°)	Long (°)	U (ppm)	Th (ppm)	K (%)	water (%)	Dose rate (Gy/ky)	De (Gy)	OD (%)	Age (ky)	fading correction	Corrected age (ky)
using central age model													
OSL	K02	33.29607	75.77619	3.8	7.2	0.46	6.1	1.74±0.02	141±8	19.5	81.1±4.6		
OSL	K11	33.3535	75.74649	3.1	12.7	2.41	6	3.97±0.09	341±19	16.8	85.7±5.1		
IRSL	K07	33.2778	75.76922	3.3	13.8	2.31	5.3	4.67±0.22	489±29	16.8	104.5±5.9	0.89	113±6
IRSL	K08	33.2778	75.76922	3.5	16.9	1.97	5.6	4.61±0.23	528±38	20.5	114.4±6.3		
IRSL	K09	33.2778	75.76922	3.3	12.2	1.98	4.8	4.29±0.20	510±42	18.1	119.2±6.8	1.11	132±7
using minimum age model													
OSL	K16	33.34873	75.73324	3.5	16.8	2.03	7.5	3.95±0.1	90±8	40	22.8±2.1		
OSL	K17	33.34873	75.73324	3.4	18	2.17	10.5	3.96±0.11	81±3.5	46	20.5±1.0		
saturated sample													
OSL	K18	33.35176	75.74325	3.3	18.7	2.61	4.5	4.36±0.13	227±14		52.1±2.8		

Table 2: Sample locations, elemental concentrations, dose rates, equivalent doses and age estimations for sand samples from Kishtwar valley.

Supplement for the manuscript titled

‘Structural variations in basal decollement, internal deformation of the Lesser Himalayan Duplex and rapid fluvial incision modulate landscape morphology in NW Himalayan interiors’

Saptarshi Dey[1], Rasmus Thiede[2], Arindam Biswas[3], Naveen Chauhan[4], Pritha Chakravarti[1] and Vikrant Jain[1]

[1]*Earth Science Discipline, IIT Gandhinagar, Gandhinagar-382355, India.*

[2]*Institute of Geosciences, Christian Albrechts University of Kiel, Kiel-24118, Germany.*

[3] *Department of Applied Geology, IIT-ISM Dhanbad, Jharkhand-826004, India.*

4 Atomic Molecular and Optical Physics Division, Physical Research Laboratory, Ahmedabad.

Corresponding author: Saptarshi Dey; saptarshi.dey@iitgn.ac.in

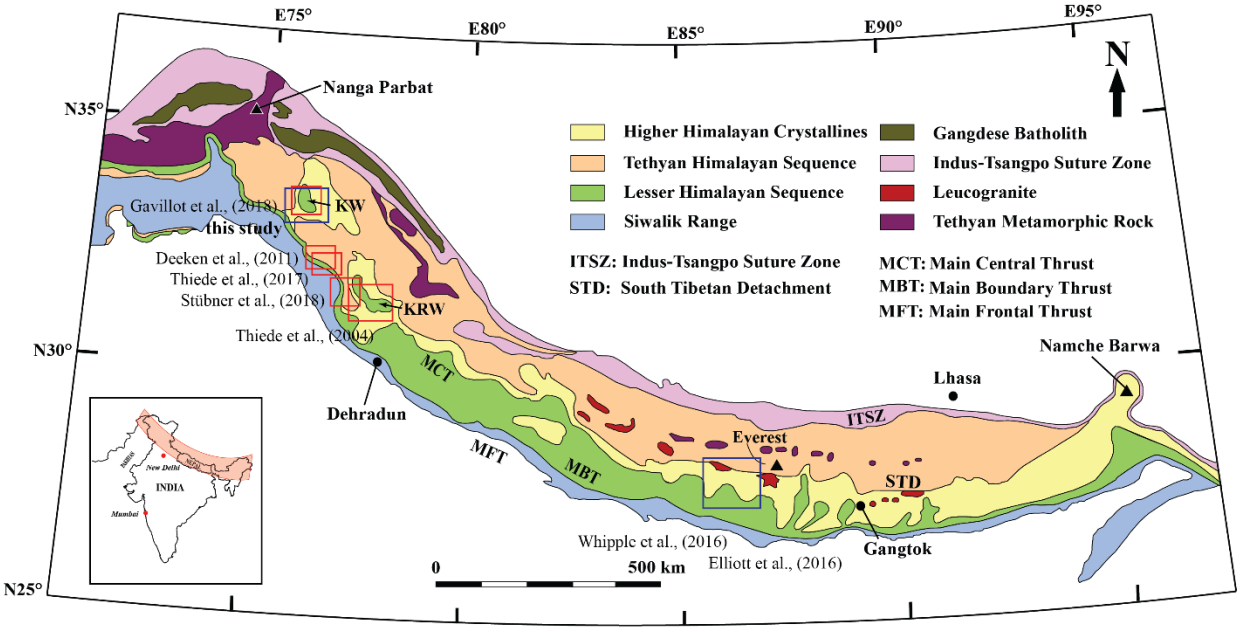

Fig. S1: A generalized geological map of the Himalayan orogen (modified after Yin and Harrison, 2000; DiPietro and Pogue, 2004) showing the spatial distribution of major morphotectonic sectors. Locations of

crucial low-T thermochronology studies in the NW Himalaya are shown (Thiede et al., 2004; Deeken et al., 2011; Thiede et al., 2017; Stuebner et al., 2018; Gavillot et al., 2018).

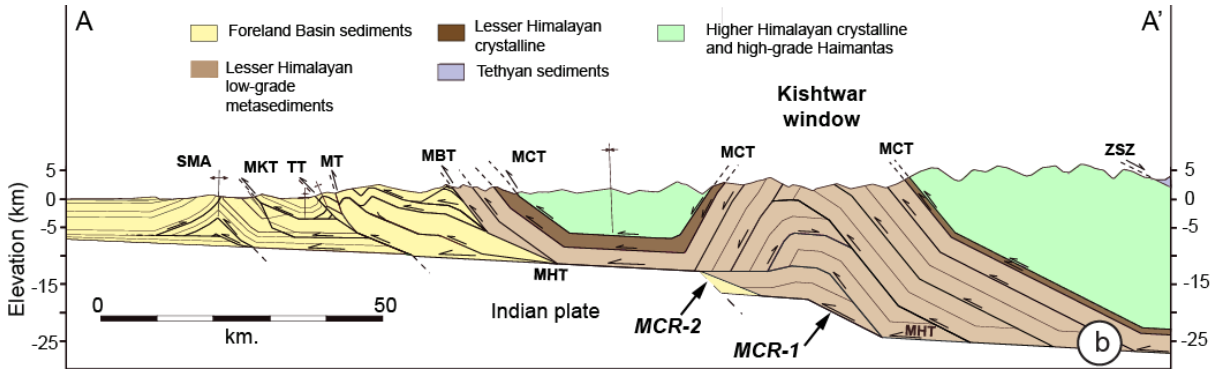

Fig. S2: Balanced cross-section across the Jammu-Kishtwar sector of the NW Himalaya (modified after Gavillot et al., 2018), showing model-predicted structural variations of the Himalayan orogenic wedge. Important to note the two small mid-crustal ramps (MCR-1 and MCR-2) emerging from the MHT, lying beneath the Lesser Himalayan duplex. They propose a higher exhumation rate of the LH duplex (3.2-3.6 mm/a) since Quaternary.

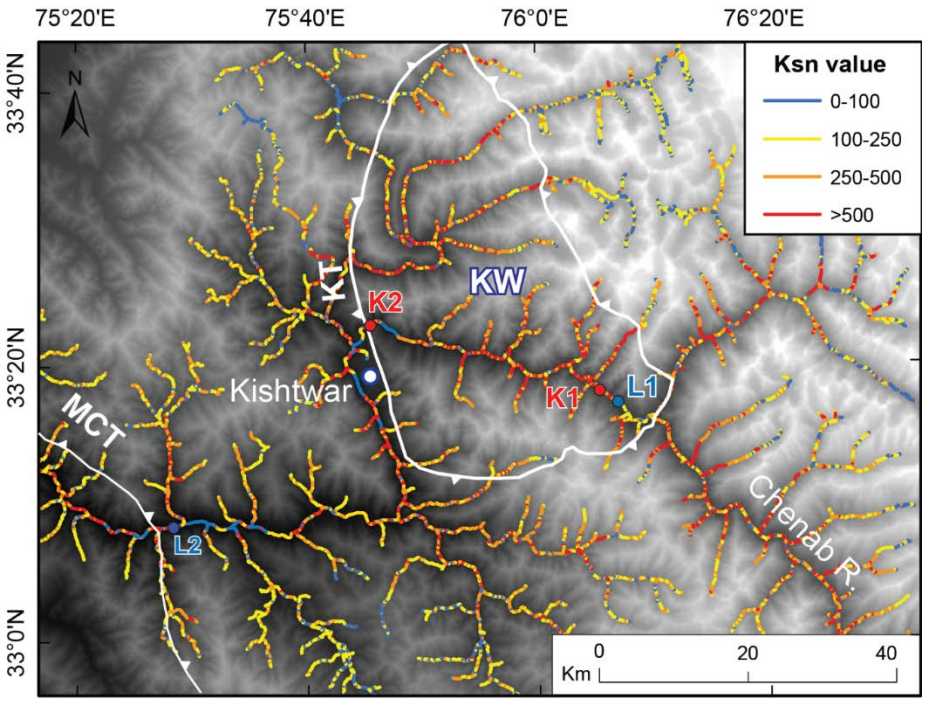

Fig. S3: Stream-specific normalized steepness indices map of the study area with major knickpoints on the trunk stream of Chenab watershed. The average ksn values within the KW and the N-S traverse of Chenab is > 300 (matching well with basinwide averaged ksn values suggested by Nennewitz et al., (2019).

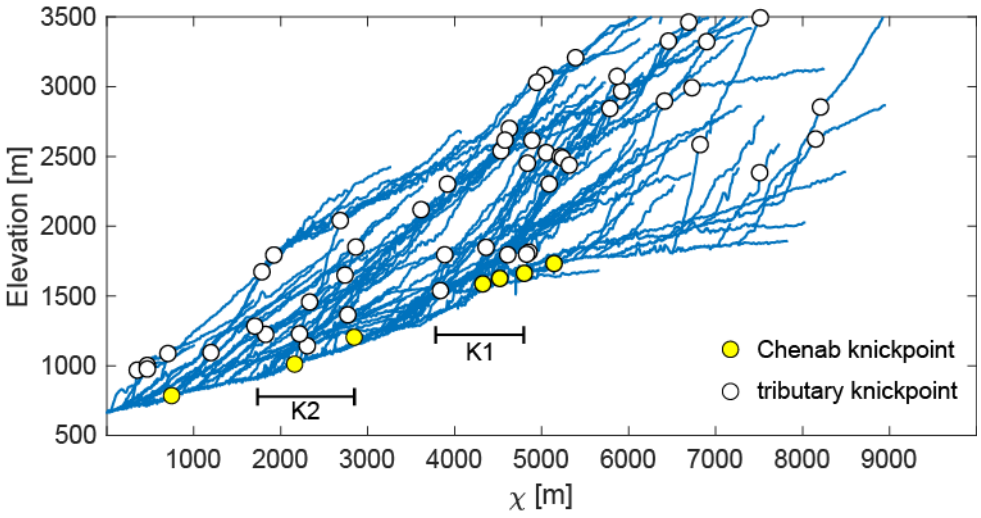

Fig.S4: Chi vs. elevation plot of the Chenab drainage system showing major knickpoints.

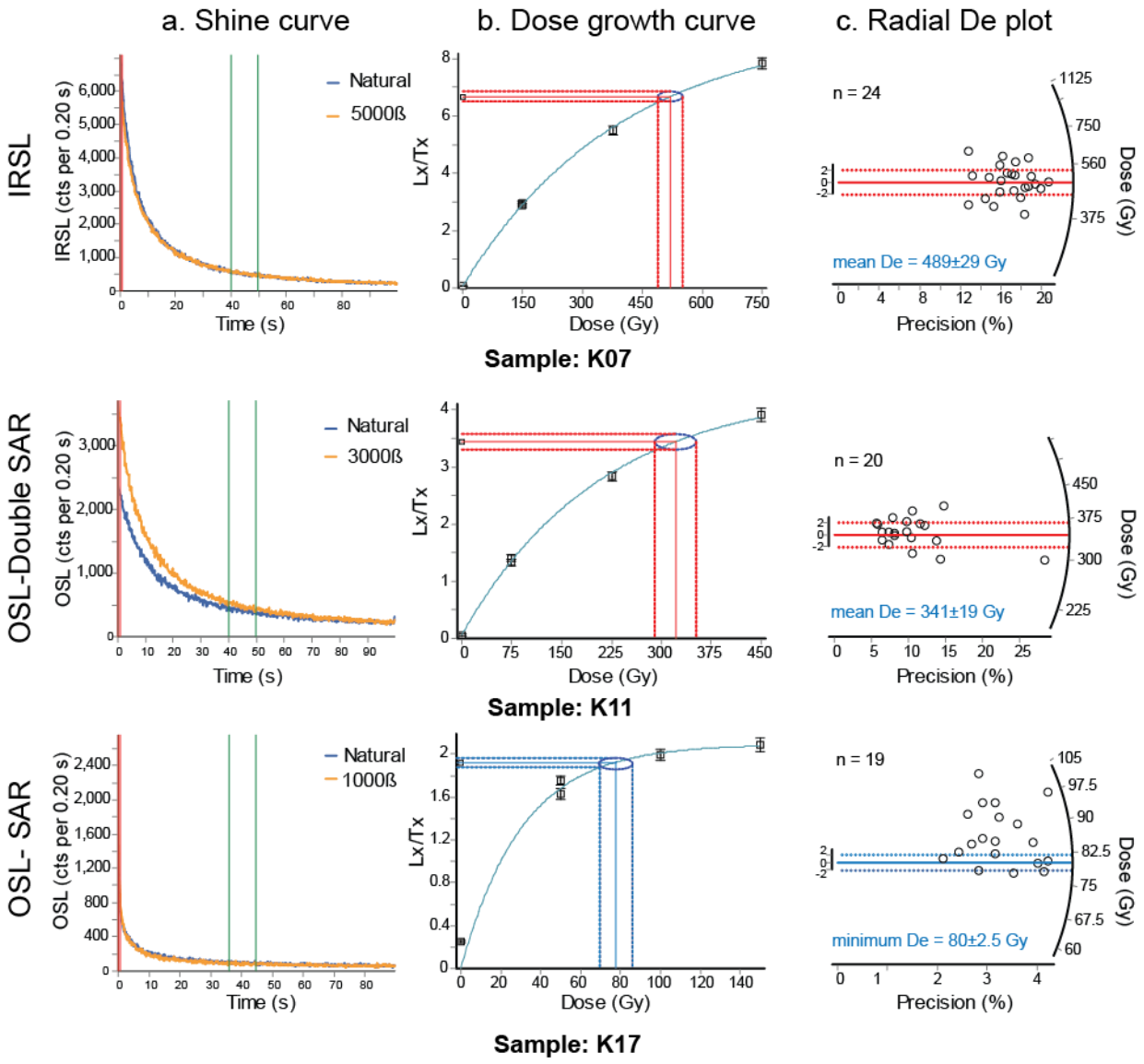

31

32 Figure S4: (a) Shine curve, (b) dose growth curve, and (c) radial De estimation plot for the three different

33 luminescence dating protocols used in this study.

34

Supplementary Table ST1:

Site	latitude	longitude	rock type	Dist. (km)	R1	R2	R3	R4	R5	R6	R7	R8	R9	R10	R11	R12	Mean_R	stdev_R	lithology_meanR	lithology_R_sigma
1	33.1842	75.3047	LH MS	1	39.9	39.3	40.6	40.3	42.3	41.5	40	40.7	40.9				40.6	0.8	41.1	1.9
2	33.1664	75.3123	LH MS	2.3	40	40.2	40	39	39.2	40.3	39.2	40.9	41	41.2			40.0	0.7		
3	33.1604	75.3253	LH MS	4.2	39.8	39	39.5	40.2	39.1	40.2	40.4	38.9	39.2	39.4	39.6		39.6	0.5		
4	33.1497	75.3485	LH MS	6.5	41.3	41.5	40.5	43.8	43.4	38.9	39.2	41.8	42				41.4	1.6		
5	33.139	75.3671	LH MS	10.8	40.1	37.8	37.7	37.2	39	38.8	39.2	39	39.1	38.5			38.7	0.9		
6	33.1343	75.3797	LH MS	13.4	42	40.6	40.2	39.6	39.9	42.2	41.4	41.8	41.1	41.6			41.0	0.9		
7	33.1317	75.4039	LH MS	17.5	43.1	43.5	40.2	40.9	43.9	45	44.1	43.4	42.9				43.0	1.4		
8	33.1266	75.417	LH MS	19	44	43.8	45.2	43.7	42	40.2	40.8	43.3	44.4	44.6			43.0	1.6		
9	33.1287	75.4281	LH MS	22.1	43.1	43.2	44.5	44	44.7	40.3	41.6	42.3	43	42.9			43.0	1.3		
10	33.134	75.4411	Haimanta	24.6	45	44.3	44.4	41.5	40.8	40	43.4	43.2	42	40.1	40.5	44	42.4	1.7	44.5	2.2
11	33.1306	75.4547	Haimanta	26.2	47.2	47	45.5	48.2	47.9	46.6	47	47.1					47.1	0.8		
12	33.1373	75.4619	Haimanta	28.8	47.7	48	49.1	48.2	49	46.2	46.6	46.7	47.3	47.8			47.7	0.9		
13	33.1372	75.4747	Haimanta	32.1	43.4	42	42.9	44.1	42	43.1	43.6	43.3	43.2	43	41		42.9	0.8		
14	33.1352	75.4843	Haimanta	33.2	43.5	43.7	44	43.3	43.3	44.4	44.5	44	42.8	43.9			43.7	0.5		
15	33.1398	75.4995	Haimanta	34	44.1	44.5	45	44.5	44.3	44.8	43.6	43.8	44.4				44.3	0.4		
16	33.1404	75.5219	HHCS	36.9	36.6	36.9	35.3	35.9	36.6	37	37.3	36.8	38	37.1	35.6	36	36.6	0.7	38.9	2.4
17	33.1316	75.5482	HHCS	38.1	41.1	41.2	42.6	40	40.4	41.3	42.8	38	42.3	38.7	40.9		40.8	1.4		
18	33.1362	75.5618	HHCS	42	40.8	40.3	42.3	39	39.4	40.9	42.2	42	39.6	40	40.1		40.6	1.1		

19	33.1361	75.5857	HHCS	43.6	38.8	39	39.2	39.9	37.2	37.9	39.9	38.3	38	37.9	38		38.6	0.8		
20	33.132	75.6025	HHCS	45	35.9	36	36.2	35.8	37.2	36.9	38	36.8	39	37.5	37.2	38.2	37.1	1.0		
21	33.1211	75.6232	HHCS	47.5	39	39.8	39	38.9	37.1	40.4	40.1	37.3	38	36.9	40.3		38.8	1.2		
22	33.1217	75.6399	HHCS	48.2	39.5	38.9	39	39.8	40.2	37.1	40.4	38.4	37.9	37	38.1	37.5	38.7	1.1		
23	33.1304	75.656	HHCS	48.7	42.1	40	39.8	37.5	37.8	37.8	38.6	39	38.4	37.3	39.9		38.9	1.4		
24	33.1498	75.6753	HHCS	49.3	40.4	40.2	41.1	41.3	45	40.7	38.4	40.2	43.7	44	37.6		41.1	2.2		
25	33.1471	75.6649	HHCS	50	37.7	38	38.9	37.8	39.2	39.1	38.8	39	39.9	37.7			38.6	0.7		
26	33.1489	75.7136	HHCS	51.1	40.7	40.7	40	38.8	39.1	39.1	39.7	39.2	40	37.8	37.4	37.3	39.2	1.1		
27	33.1527	75.7408	HHCS	51.4	40.5	40.3	39.8	36.9	37	42.3	40.3	40	37.2	38.7	39		39.3	1.6		
28	33.1352	75.759	HHCS	53	42.4	42.2	40.6	45.7	40.2	39.2	39.9	42.1	43	43.2	41.5		41.8	1.7		
29	33.149	75.8031	HHCS	55.2	39.6	39.9	39.2	39	38.3	40.6	41.1	39.9	38.6	39.8	40		39.6	0.8		
30	33.1611	75.8064	HHCS	57.5	38	36.8	37	37.2	38.9	36.6	36.4	37.2	37	38.2	38.1		37.4	0.7		
31	33.1832	75.8146	HHCS	60.3	37.6	36.9	37	35.8	36	37.2	38.1	36.7	35.4	36.7			36.7	0.8		
32	33.1913	75.8107	HHCS	63.4	36	34.4	35.8	32.3	35	30.1	28.9	33.1	32.2	31.5	35.3		33.1	2.3		
33	33.2068	75.8036	HHCS	67.9	39.3	39.2	37.9	37.3	40	38.4	38.6	39.8	40.1	39.6	39.9		39.1	0.9		
34	33.2256	75.8014	HHCS	72.2	39.9	40.6	40.3	39.8	39.8	41.3	41.5	40.8	41	41.1	41.2		40.7	0.6		
35	33.2304	75.7918	HHCS	73.6	44.7	40.1	40.2	40.2	41.1	41.3	40.4	43.2	42.6	40.4	40.9		41.4	1.4		
36	33.2405	75.7895	HH mg	74.5	37.7	34.2	30.4	30.6	32.2	30.9	31.1	30	34.1	30.4			32.2	2.3	48.9	6.7
37	33.2493	75.7824	HH mg	75.4	44	44.9	43.9	43.8	44.2	45.7	45.2	43.1	43	42.6	43	44	43.9	1.0		
38	33.2614	75.7753	HH mg	76.8	43.7	44	45.3	45.2	44.8	44.3	44.9	45	45.5	44.8	43.1	45.2	44.6	0.7		
39	33.2674	75.7746	HH mg	77.3	45.5	45.3	46.2	45.2	44.9	45.3	48	46.2	46.3	46.8			46.0	0.9		
40	33.2728	75.7698	HH mg	78.8	45.3	45.4	47	46.7	45.9	45.3	46	45.6	45.1	45	46		45.8	0.6		

41	33.2829	75.7699	HH mg	79.2	48	46.6	45.9	46	45.7	46	45.8	46.3	45.9	46.3	46	46.2	0.6		
42	33.2897	75.7644	HH mg	80.1	45.9	47.8	48	49.2	49.4	48.5	49.5	47.3	48.9	49.5	49.2	48.5	1.1		
43	33.2918	75.754	HH mg	80.6	46.9	46.5	47.2	47.2	46.9	47.4	47.1	46	46.2	45.9	47.1	46.8	0.5		
44	33.3316	75.7271	HH mg	82	47	47.2	46.6	46.9	46.2	47.4	46.5	47.2	46	45.9	46.2	46.6	0.5		
45	33.3443	75.7296	HH mg	92.4	47	47.2	48.2	48.1	47.7	47	48.2	46.9	47.3	48		47.6	0.5		
46	33.3578	75.7225	HH mg	93	50.1	50	48.8	48.8	46.4	48	47.2	46.9	47.3	48.2		48.2	1.2		
47	33.3383	75.7256	HH mg	94.8	58.3	56.9	55	57.2	52.6	55.6	55.9	56	56.3	57.2	55.2	56.0	1.4		
48	33.3497	75.7329	HH mg	100.1	60.5	58.9	60.1	59.2	59	60	58.3	58.8	58.9	59	59.1	59.3	0.6		
49	33.3227	75.743	HH mg	102.5	62.9	60.7	61	61.5	60.3	60.5	59.9	60.2	60.3	59.9	62	60.8	0.9		
50	33.3577	75.7345	HH mg	104.2	50.6	54.7	53.9	53.8	54	50.8	52	53.9	54	52.5	53.2	53.0	1.3		
51	33.3603	75.749	HH mg	105.8	56.2	56	55.9	54.3	51.9	56.8	57	55.5	56	53.8	55.7	55.4	1.4		
52	33.3737	75.7539	LH schist	108.2	37.9	36.9	37.8	39.3	38.2	38	38.2	37.7	39.2	38		38.1	0.7		
53	33.377	75.7759	LH qt	110.2	54.9	53.4	54	54.4	52.5	53.2	55	54.7	54.1	55	54.2	54.1	0.8	51.6	4.8
54	33.3708	75.7879	LH qt	112.1	51	51.9	53.3	54.2	54.5	52.9	52.8	52.5	53.8	53		53.0	1.0		
55	33.3586	75.8062	LH qt	114.7	49.9	50.3	50.5	49.5	51	51	50.2	49.2	50.3	49.8		50.2	0.6		
56	33.3578	75.8286	LH qt	115.8	50.5	52.1	50.4	50.9	48.4	47.9	52	51.1	50.5	50.9		50.5	1.3		
57	33.353	75.8478	LH qt	117.6	48.7	48.9	50	49.4	47.3	47	47.1	48.4	48.2	46.5		48.2	1.1		
58	33.3535	75.8654	LH qt	121	50.5	54.1	55	53.2	55.9	52.1	54.8	54.1	53.1	55.4		53.8	1.6		
59	33.3412	75.8917	LH qt	123.2	57.2	53.1	53.2	56	55.7	52.7	57.1	54.3	56.6	56.3		55.2	1.6		
60	33.3438	75.9054	LH qt	126.5	57.8	56.9	57.1	53.3	59	55	57.2	58.8	57.5			57.0	1.7		
61	33.3437	75.9238	LH qt	130.9	52.9	53	55.3	54.6	55	52.4	57.7	53.3	55.2	54.3		54.4	1.5		
62	33.3349	75.9373	LH qt	132.3	40.3	45.2	37.3	37	38.3	44	39.2	41	41.1	36.9		40.0	2.7		

63	33.3381	75.9574	LH gr	133.8	53.6	53	54.5	54.1	52.8	52.5	53.3	53.9	50.8	52.9			53.1	1.0	55.4	3.0
64	33.3272	75.9669	LH gr	135	49.9	48.8	49.1	53	50.7	48.3	50.8	53.5	50.6	52.4	53.1		50.9	1.8		
65	33.3183	75.9932	LH gr	138.4	55.8	55.7	57.1	57.3	57	56.7	56.4	55.9	56	56.9	57		56.5	0.6		
66	33.3228	76.0164	LH gr	139.6	56.1	56.8	57	57.4	57.3	58.7	58	58.1	57.9	58.5	58.7	58	57.7	0.8		
67	33.3293	76.0406	LH gr	140	58	58.1	58.9	60.1	57.8	57.9	58	58.5	58.2	57.9			58.3	0.7		
68	33.3164	76.0556	LH qt	141.6	62.6	61.1	60.7	61.1	60.5	60.2	59.7	60.5	61.2	60.7			60.8	0.7		
69	33.3123	76.07	LH qt	143.6	56.6	56.9	57	56.4	56.6	57.5	55.2	56.8	56.7	58			56.8	0.7		
70	33.3055	76.0779	LH gr	147.8	59	59.3	57.8	58.8	60.1	59.2	58.9	59.7	59	57.3			58.9	0.8	58.1	1.6
71	33.2967	76.0874	LH gr	148.4	59.9	59.3	59.8	57.8	58	58.6	59.9	60.5	59.9	59.8			59.4	0.9		
72	33.2925	76.1009	LH gr	152.5	60.3	60.2	61.2	60	58.9	59.2	59.2	59.9	60.1	59.1			59.8	0.7		
73	33.2783	76.1112	LH gr	154.6	58.6	56.9	56.8	57	57.5	58.2	56	56.6	55.9	56			57.0	0.9		
74	33.2628	76.119	LH gr	157.6	59	56.7	55	55.4	55.9	57.2	57.5	57	58.3	55.5			56.8	1.2		
75	33.2586	76.1389	LH gr	158.8	58.2	57.7	57.7	55.9	56	58.2	58.4	55	55.2				56.9	1.3		

Table ST1: Details of site-specific R-values collected using rock-rebound hammer. [Abbreviations: LH MS – Lesser Himalayan Metasediments, LH gr – Lesser Himalayan granite, LH qt – Lesser Himalayan quartzite, HHCS – Higher Himalayan crystalline sequence, HH mg – Higher Himalayan migmatites).